USGS
science for a changing world

Incorporation of Fine-Grained Sediment Erodibility Measurements into Sediment Transport Modeling, Capitol Lake, Washington

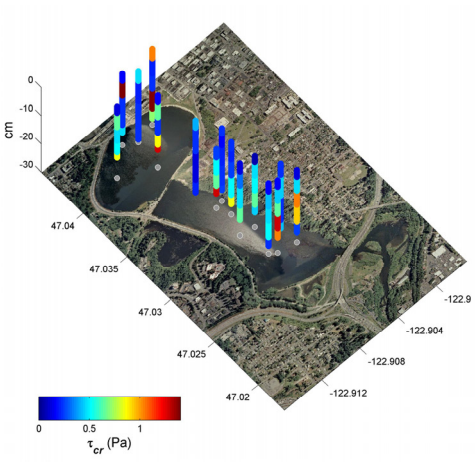

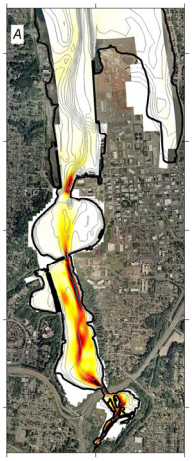

Open-File Report 2008-1340

U.S. Department of the Interior
U.S. Geological Survey

This page intentionally left blank

Incorporation of Fine-Grained Sediment Erodibility Measurements into Sediment Transport Modeling, Capitol Lake, Washington

By Andrew W. Stevens[1], Guy Gelfenbaum[1], Edwin Elias[2,3], and Craig Jones[4]

[1]U.S. Geological Survey, 345 Middlefield Rd. MS999, Menlo Park, California, 94025

[2]U.S. Geological Survey, 400 Natural Bridges Dr., Santa Cruz, California, 95060

[3]Deltares, 185 Rotterdamseweg, Delft, The Netherlands, 2600 MH

[4]Sea Engineering, Inc., 200 Washington St., Santa Cruz, California, 95060

Open-File Report 2008-1340

U.S. Department of the Interior
U.S. Geological Survey

U.S. Department of the Interior
DIRK KEMPTHORNE, Secretary

U.S. Geological Survey
Mark D. Myers, Director

U.S. Geological Survey, Reston, Virginia 2008

For product and ordering information:
World Wide Web: http://www.usgs.gov/pubprod
Telephone: 1-888-ASK-USGS

For more information on the USGS—the Federal source for science about the Earth,
its natural and living resources, natural hazards, and the environment:
World Wide Web: http://www.usgs.gov
Telephone: 1-888-ASK-USGS

Suggested citation:
Stevens, A.W., Gelfenbaum, G., Elias, E., Jones, C. 2008, Incorporation of fine-grained sediment erodibility measurements into sediment transport modeling, Capitol Lake, Washington: U.S. Geological Survey Open-File Report 2008-1340, 72 p.

Contents

Contents iii
Introduction 1
Methods 3
  Selection of Erosion Device 3
  Core Collection 4
  Sedflume Analysis 5
    Measurements of Sediment-Erosion Rates 8
    Determination of Critical Shear Stress 8
    Sediment Properties 8
  Deschutes Estuary Model Overview 9
    Delft3D Sediment Transport 10
Results and Discussion 11
  Field Data 11
    Sediment Properties 11
    Erodibility Measurements 11
  Incorporation of Field Data into Existing Model 17
    Erosion Rate Parameter Calculation 17
    Sediment Parameters for Phase II Simulations 20
  Model Results 25
    Long-Term Morphological Change 25
      Estuary Alternative 26
      Dual-Basin Estuary Alternative 33
      Comparison Between Estuary and Dual-Basin Estuary Alternatives 38
      Predam Removal Dredge and Fill 39
    Comparison between Phase I and Phase II 44
    Sensitivity Analysis 48
Summary and Conclusions 49
Acknowledgments 49
References 49
Appendix A. Sediment Properties and Erodibility Parameters from Sedflume Analysis 52
Appendix B. Grain-size Data from Samples Collected in Lower Budd Inlet 69

Figures

1. Map of southern Puget Sound showing an overview of the study area 2
2. Maps of predam estuary and modern lake bathymetry 3
3. Capitol Lake and environs in 2004 4
4. Map of core locations collected in Capitol Lake 5
5. Photographs of field operation in Captiol Lake 6
6. Photos of the undisturbed surface of two cores collected from Capitol Lake 7

7. Schematic diagram showing the main components of Sedflume.. 7
8. Grain size data from cores 12
9. Dry sediment density from cores. 13
10. Map of critical shear stress measured in cores 14
11. Results from Sedflume analysis for core LP4 showing dry sediment density and critical shear stress 15
12. Relationship between dry sediment density and critical shear stress 15
13. Plots of erosion rate versus applied shear stress for each core 16
14. Bar graphs showing erosion rate for each core at 1.6 Pa applied shear stress 17
15. Example fit of the data to the linear sediment erosion model of Partheniades (1965) 18
16. Simulation results showing maximum predicted shear stress and percent of 3-year simulation that the bottom shear stress exceeds 1.6 Pa 19
17. Map of erosion coefficient, M, measured in cores collected from Capitol Lake. 20
18. Relationship between erosion coefficient and mud content, dry sediment density, and critical shear stress 21
19. Histogram of the log of measured erosion coefficients from samples with sand contents < 40 percent 21
20. Down-core patterns in dry sediment density, critical shear stress, and erosion rate parameter for each core collected from Capitol Lake 22
21. Sand content in bottom sediments showing map of core locations plotted on top of the percent sand in the Phase I model 24
22. Map showing the sand content schematization of bottom sediments in the Phase II model. 24
23. Map showing the proposed restoration alternatives, estuary alternative and dual-basin estuary alternative 25
24. Model domain showing the extent of several regions of interest including South basin, Middle basin, Percival Cove, North basin, Port, Marina, and Budd Inlet 26
25. Long-term simulation results showing initial bathymetry and evolved bathymetry 10 years after dam removal for the estuary alternative 27
26. Yearly patterns of erosion and deposition for the long term simulation of the estuary alternative 28
27. Results of long-term simulation for the estuary alternative 29
28. Cross-estuary transects at three locations showing the local changes in bottom depth over time for the estuary alternative 30
29. Time-series of cumulative erosion and sedimentation for each of the regions of interest in the model for a one-year simulation using medium erodibility parameters of the estuary alternative 31
30. Maps showing the evolution of sediment grain size through time for the estuary alternative 32

31. Long-term simulation results showing initial bathymetry evolved bathymetry 10 years after dam removal for the dual-basin estuary alternative 33
32. Yearly patterns of erosion and deposition for the long term simulation of the dual-basin estuary alternative. 34
33. Results of long-term simulation of the dual-basin estuary alternative 35
34. Cross-estuary transects at three locations showing the local changes in bottom depth over time for the dual-basin estuary alternative 36
35. Maps showing the evolution of sediment grain size through time for the dual-basin estuary alternative 37
36. Comparison of predam bathymetry and modern lake bathymetry with evolved bathymetry for the estuary and dual-basin estuary alternatives after 10 year morphological simulations 38
37. Comparison of the depth distributions between the predam estuary, modern lake, estuary alternative, and dual-basin estuary alternative 39
38. Time-series of cumulative erosion and sedimentation comparing the volume change in each of the regions between the estuary alternative and dual-basin estuary alternative 40
39. Predam removal dredge and fill showing proposed dredge and fill areas 41
40. Results of 3-year simulation for the estuary alternative with dredging prior to dam removal 42
41. Results of 3-year simulation for the dual-basin estuary alternative with dredging prior to dam removal 43
42. Cumulative volume change ($\times 10^4$ m^3) after 3 year for the estuary alternative comparing Phase II medium erodibility values (with and without dredging prior to dam removal) and the Phase I lower and higher erodibility values. 44
43. Cumulative volume change ($\times 10^4$ m^3) after 3 year for the dual-basin estuary alternative comparing Phase II medium erodibility values (with and without dredging prior to dam removal) and the Phase I lower and higher erodibility values 45
44. Maps showing erosion and sedimentation for simulations S0-S6 after 3 years for the estuary alternative 46
45. Cumulative volume change ($\times 10^4$ m^3) after 3 years in simulations S0 through S6 47
46. Cumulative volume change ($\times 10^4$ m^3) after 3 years for the estuary alternative in simulations P1 through P14 comparing various combination of low, medium, and high erodibility parameters 48
A1. Data for core HP1 from Sedflume analysis 54
A2. Data for core HP2 from Sedflume analysis 55
A3. Data for core HP3 from Sedflume analysis 56
A4. Data for core HP4 from Sedflume analysis 57
A5. Data for core HP5 from Sedflume analysis 58
A6. Data for core HP6 from Sedflume analysis 59
A7. Data for core HP7 from Sedflume analysis 60

A8. Data for core HP8 from Sedflume analysis 61
A9. Data for core HP9 from Sedflume analysis 62
A10. Data for core LP4 from Sedflume analysis 63
A11. Data for core LP5 from Sedflume analysis 64
A12. Data for core MP1 from Sedflume analysis 65
A13. Data for core MP2 from Sedflume analysis 66
A14. Data for core MP3 from Sedflume analysis 67
A15. Data for core MP4 from Sedflume analysis 68
B1. Locations of grab samples collected from lower Budd Inlet 70
B2. Sediment grain size distribution (weight percent) for samples B1 through B14 71
B3. Sediment grain size distribution (weight percent) for samples B15 through B21 72

Tables

1. Locations of cores collected in Capitol Lake, Washington 5
2. Erodibility parameters calculated from field data. 22
3. Probability of occurrence estimated by using a Bayes network for each possible combination of the three erodibility parameters 23
4. Sediment volume change ($\times 10^4$ m^3) for the estuary alternative in each region of interest over 10 years using medium values for each of the erodibility parameters 26
5. Sediment volume change ($\times 10^4$ m^3) for the dual-basin estuary alternative in each region of interest over 10 years using medium values for each of the erodibility parameters 33
6. Sediment volume change ($\times 10^4$ m^3) after 3 years comparing the sediment accumulation that occurs in the Port and Marina areas with and without dredging prior to dam removal for both restoration alternatives 41
7. Values of the erodibility parameters used for the sensitivity analysis in Phase I of hydrodynamic and sediment transport modeling study (George and others, 2006). 44
8. Erodibility parameters used in for Simulations S0 through S6 to investigate the difference in estimated volume changes between Phase I and Phase II. 45
A1. List of sediment properties and erodibility parameters for each core analyzed with Sedflume 52
B1. List of sample identification numbers, locations, date collected, percent gravel, percent sand, percent silt, percent clay, and mean grain size for each grab sample collected from lower Budd Inlet 69

Incorporation of Fine-Grained Sediment Erodibility Measurements into Sediment Transport Modeling, Capitol Lake, Washington

By Andrew W. Stevens, Guy Gelfenbaum, Edwin Elias, and Craig Jones

Introduction

Capitol Lake was created in 1951 with the construction of a concrete dam and control gate that prevented salt-water intrusion into the newly formed lake and regulated flow of the Deschutes River into southern Puget Sound (fig. 1). Physical processes associated with the former tidally dominated estuary were altered, and the dam structure itself likely caused an increase in retention of sediment flowing into the lake from the Deschutes River. Several efforts to manage sediment accumulation in the lake, including dredging and the construction of sediment traps upriver, failed to stop the lake from filling with sediment (fig. 2). The Deschutes Estuary Feasibility Study (DEFS) was carried out to evaluate the possibility of removing the dam and restoring estuarine processes as an alternative ongoing lake management.

An important component of DEFS was the creation of a hydrodynamic and sediment transport model of the restored Deschutes Estuary (George and others, 2006). Results from model simulations indicated that estuarine processes would be restored under each of four restoration alternatives, and that over time, the restored estuary would have morphological features similar to the predam estuary. The model also predicted that after dam-removal, a large portion of the sediment eroded from the lake bottom would be deposited near the Port of Olympia and a marina located in lower Budd Inlet seaward of the present dam. The volume of sediment transported downstream was a critical piece of information that managers needed to estimate the total cost of the proposed restoration project. However, the ability of the model to predict the magnitude of sediment transport in general and, in particular, the volume of sediment deposition in the port and marina was limited by a lack of information on the erodibility of fine-grained sediments in Capitol Lake.

Erodibility is the rate at which sediment is resuspended from the seabed when a force from waves or currents is applied. Whereas the erodibility of sand-sized particles can be determined relatively accurately based solely on grain-size (for example, Hjulstrom, 1939), the erodibility of fine-grained sediments (silts and clays) cannot. Fine-grained sediment erodibility depends both on the physical characteristics of the sediment, such as grain-size, water content (Postma, 1967), and mineralogy, as well as several biologically mediated factors (Jumars and Nowell, 1984). Because the site-specific parameters that affect fine-grained sediment erodibility are seldom known and cannot be accurately predicted, direct measurements are needed to characterize local erodibility (Stevens and others, 2007).

The lack of direct sediment erodibility measurements in Capitol Lake prompted George and others (2006) to rely on a range of model-input parameters that describe sediment erodibility taken from the literature (van Rijn, 1993). The range of erodibility parameters used in the model simulations resulted in a factor of 2 difference in the amount of sediment that was

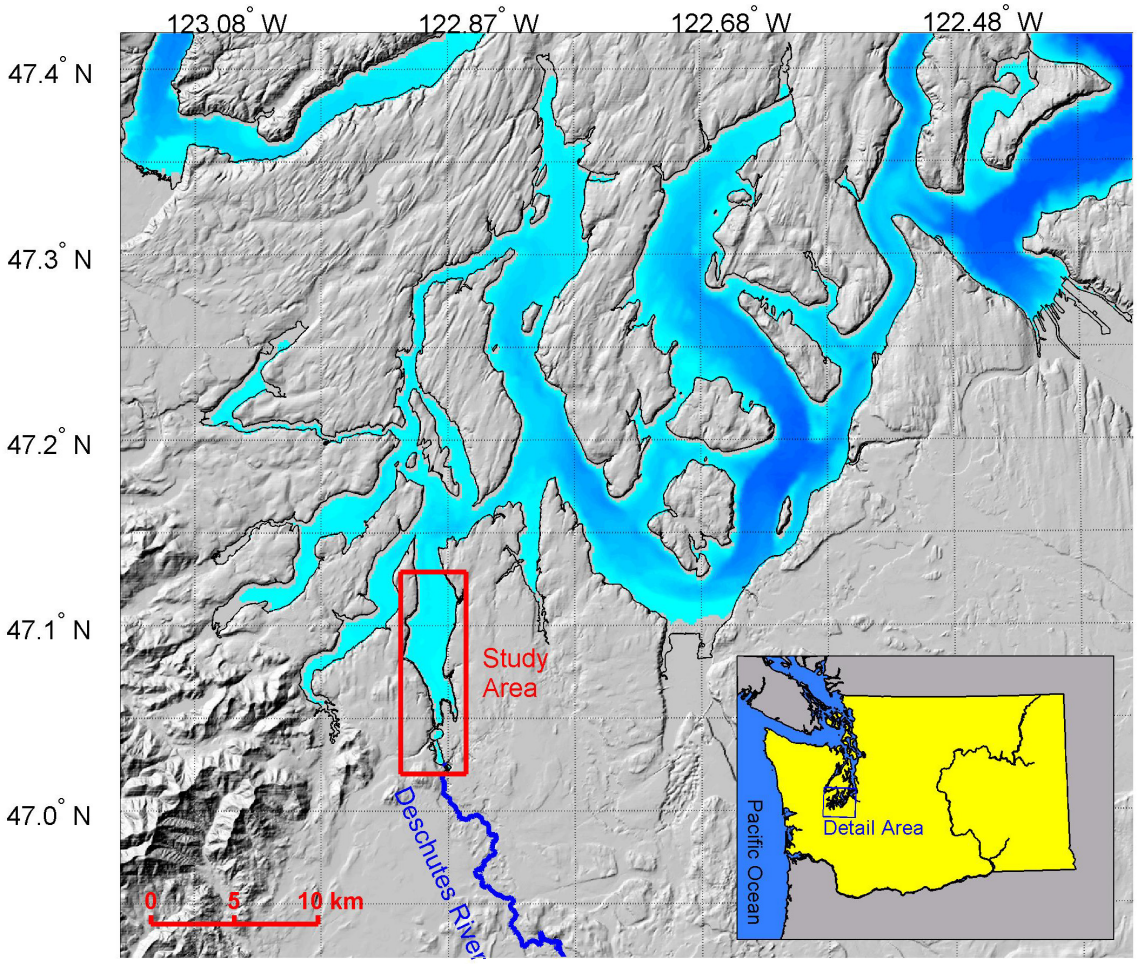

Figure 1. Map of southern Puget Sound, Washington, showing the study area, including Capitol Lake and lower Budd Inlet. The Deschutes River flows into Capitol Lake from the south. See figure 3 for detailed map of Capitol Lake. DEM source is Finlayson (2005).

predicted to accumulate in the port and marina during 10 years after dam removal. In order to constrain the uncertainty in model estimates of sediment transport after dam removal, direct measurements of sediment erodibility were proposed.

A small team from the U.S. Geological Survey (USGS) and Sea Engineering Inc. (SEI) collected cores at several sites throughout Capitol Lake between October 31 and November 1, 2007 (USGS Field Activity B-1-07-WA). The erodibility of sediments in the cores was later determined in the SEI lab with Sedflume, an apparatus for measuring sediment erosion-parameters (McNeil and others, 1996; Roberts and others, 1998). In this report, we present results of the characterization of fine-grained sediment erodibility within Capitol Lake. The erodibility data were incorporated into the previously developed hydrodynamic and sediment transport model (George and others, 2006). Model simulations using the measured erodibility parameters were conducted to provide more robust estimates of the overall magnitudes and spatial patterns of sediment transport resulting from restoration of the Deschutes Estuary. Metadata for this field activity are available at http://walrus.wr.usgs.gov/infobank/b/b107wa/html/b-1-07-wa.meta.html.

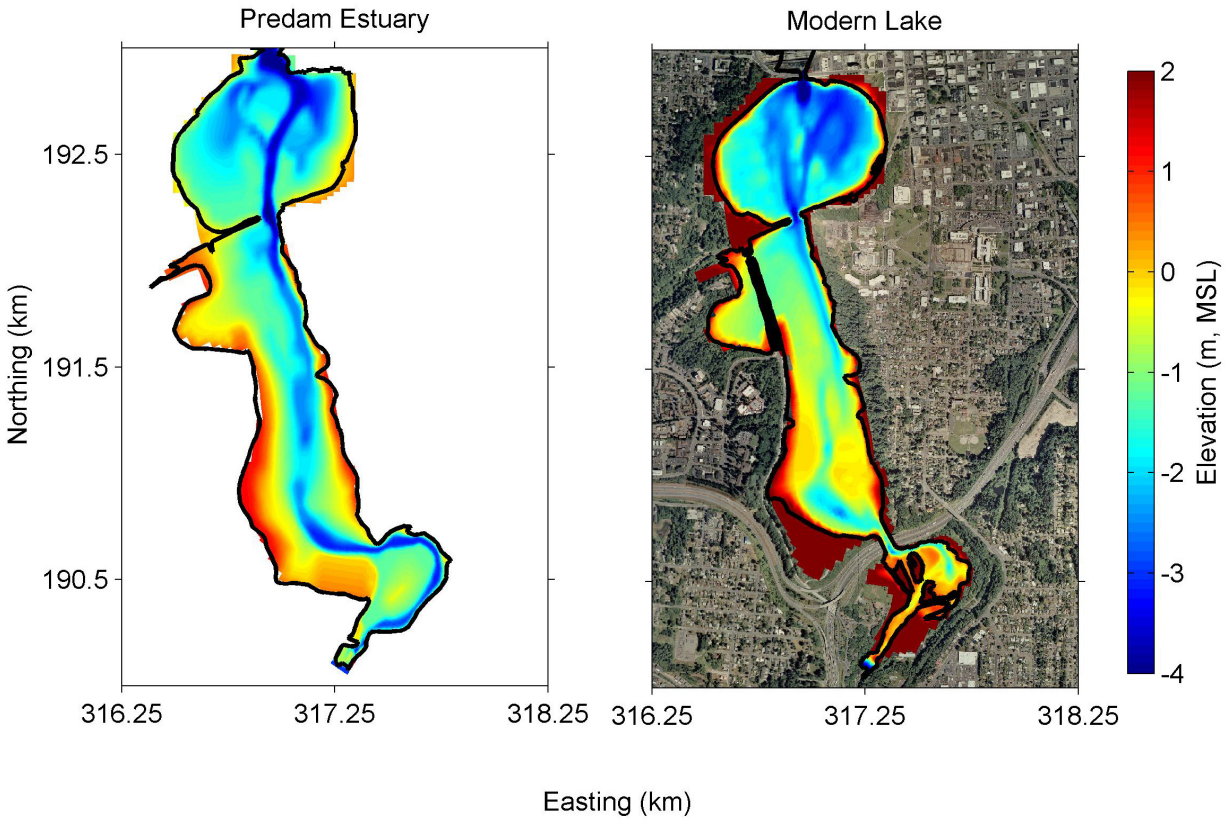

Figure 2. Map of Capitol Lake showing the bathymetry prior to dam construction and present lake bathymetry. Note that sediment accumulation has occurred primarily in the southern part of the lake.

Methods

Selection of Erosion Device

There are several different methods that have been developed to measure sediment erodibility (see Black and Paterson, 1997). Some methods rely on devices that are designed to be deployed in the field and measure sediment erodibility in place, characterizing the erodibility of the upper few millimeters of the sediment surface (for example, Maa and others, 1993). Other methods rely on devices that require sediments to be brought back to a laboratory for analysis and are capable of characterizing erodibility with depth in the sediment (for example, McNeil and others, 1996). The hydrodynamics (Gust and Mueller, 1997) and erosion rates measured with each device are often not easily comparable (Widdows and others, 2007). Each of the available devices has strengths and weaknesses and selection of the most appropriate tool for the situation is an important component of designing a field study (Jepsen, 2006).

Sedflume (McNeil and others, 1996) was selected as the erodibility measurement tool for this study for several reasons. Sedflume is capable of measuring vertical profiles of sediment erodibility. For Capitol Lake, characterizing the erodibility below the surface was important because the model simulations predicted as much as 2 m of erosion after the dam is removed. Therefore, measurements that span only the upper few millimeters of the sediment surface would not be appropriate. Many other devices allow for deposition during an erosion experiment and, therefore, measure net erosion rates. On the other hand, Sedflume measures gross erosion rates

because no deposition occurs or is quantified during erosion experiments. Sedflume is also capable of applying relatively high stresses during the erosion tests compared with other devices. This is important because relatively high stresses are predicted when tidal processes are restored to Capitol Lake.

Core Collection

Capitol Lake is separated into three distinct basins that are connected (fig. 3). In order to characterize local sediment erodibility in Capitol Lake, 15 cores were collected in Middle and North Basins by SEI and USGS personnel (fig. 4) in depths ranging from 0.5 to 3.6 m (Table 1). Core locations were selected based on sediment grain-size information from prior surface-grab samples and on erosion and deposition patterns predicted in initial model results presented in George and others (2006). Core locations were primarily in muddy areas where erosion was predicted to occur after dam removal.

A handheld GPS was used to position a pontoon boat at the designated core location. A pole was attached with clamps to a 10-cm by 15-cm rectangular core barrel (fig. 5). A valve was temporarily affixed to the top of the core tube to provide suction when the core was pulled out of the sediment bed. The core was then lowered into the water and positioned perpendicular to the sediment bed. Pressure was applied by hand until at least 30 cm and no more than 50 cm of the core penetrated into the sediment bed. During core penetration, the valve was open, permitting sediment to enter the core tube as overlying water escaped. While the core was being extracted, the valve was closed to help retain the sediment in the core barrel. Once on deck, the core was immediately inspected visually for length and quality. Undisturbed surface sediment was present in all 15 cores collected (fig. 6). The cores were capped and immediately shipped upright at ambient temperature to the SEI Sedflume Laboratory in Santa Cruz, California. All cores arrived at the Sedflume Laboratory intact with sediment structure and surface preserved.

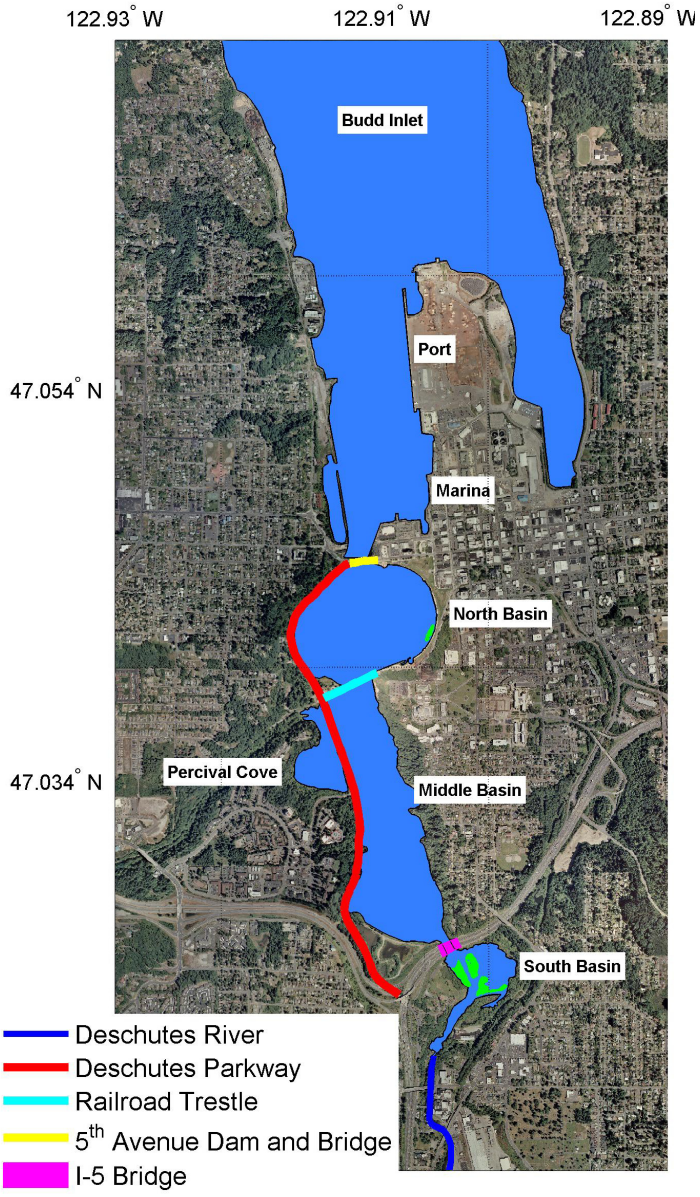

Figure 3. Capitol Lake and environs in 2004. The four distinct basins are South Basin, Middle Basin, Percival Cove, and North Basin. The basins are connected through the labeled features. The Port of Olympia and municipal marina are north of the 5th Avenue Dam and Bridge in lower Budd Inlet. Background photo taken in 2002, courtesy of Thurston, Washington Regional Planning Council.

Table 1. Locations of cores collected in Capitol Lake, Washington.

Core ID	Latitude, degrees north	Longitude, degrees west	Date and time collected	Water depth, in meters	Core length, in centimeters
HP4	47.03537	122.90839	10/31/2007 09:07	3.1	44
HP3	47.04196	122.90689	10/31/2007 09:41	3.6	50
HP2	47.04157	122.90870	10/31/2007 10:05	2.8	53
HP1	47.04042	122.91199	10/31/2007 10:45	2.7	41
HP6	47.03331	122.90811	10/31/2007 11:30	1.6	44
HP7	47.02773	122.90775	10/31/2007 12:06	0.9	52
HP9	47.02696	122.90548	10/31/2007 12:49	<0.5	42
HP8	47.02731	122.90718	10/31/2007 14:37	1.6	51
MP4	47.03011	122.90702	10/31/2007 15:58	1.2	46
MP3	47.03213	122.90762	10/31/2007 16:18	1.5	54
MP1	47.04222	122.90979	11/01/2007 10:15	3.0	42
MP2	47.03896	122.90907	11/01/2007 10:38	3.0	52
LP4	47.03035	122.90834	11/01/2007 11:01	1.1	51
LP5	47.002874	122.90557	11/01/2007 11:18	1.2	53
HP5	47.03349	122.90737	11/01/2007 11:37	3.1	51

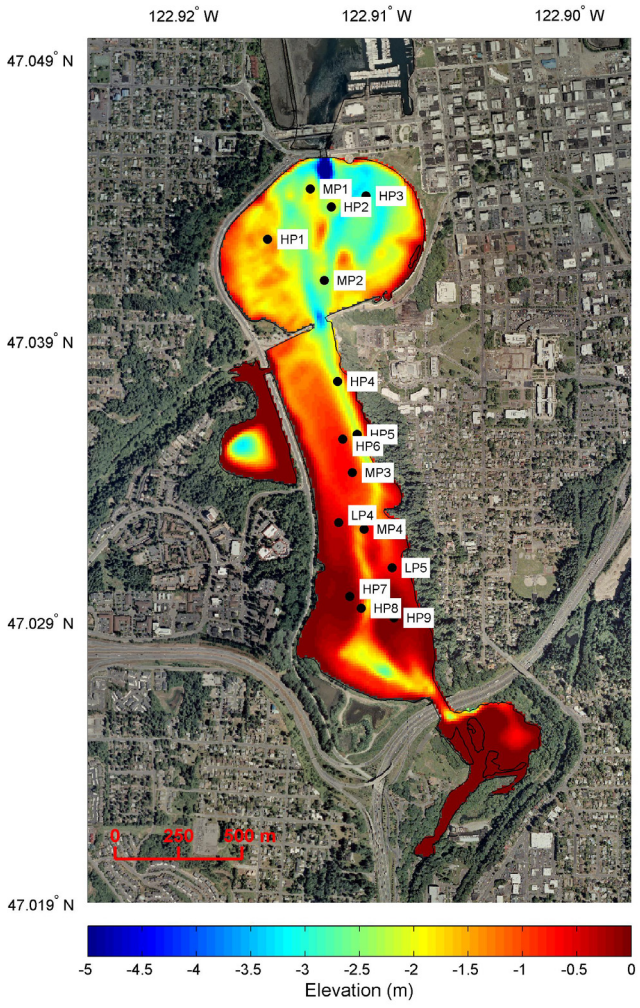

Figure 4. Map of core locations collected in Capitol Lake. Bathymetric data is derived from Eshleman and others, 2006. Vertical datum is NAVD88.

Sedflume Analysis

The cores were analyzed by using Sedflume to characterize the erodibility of fine-grained sediments in Capitol Lake. Sedflume and its application are explained in detail in McNeil and others (1996) and Roberts and others (1998). Sedflume is a straight flume that has a test section with an open bottom through which a core containing sediment can be inserted (fig. 7). Water is pumped through the system from a 500 gallon storage tank. The water passes through a flow converter into the rectangular flume section producing a fully developed, turbulent flow over the test section. A ball valve regulates the flow so that the flow rate into the flume can be precisely controlled.

During Sedflume analysis, a core containing sediment was inserted into the test section. An operator moved the sediment upward by using a piston inside the core that was connected to a hydraulic jack. The sediment within the core was raised to be level with the bottom of the flume-test section. As flowing water was forced over the surface of the

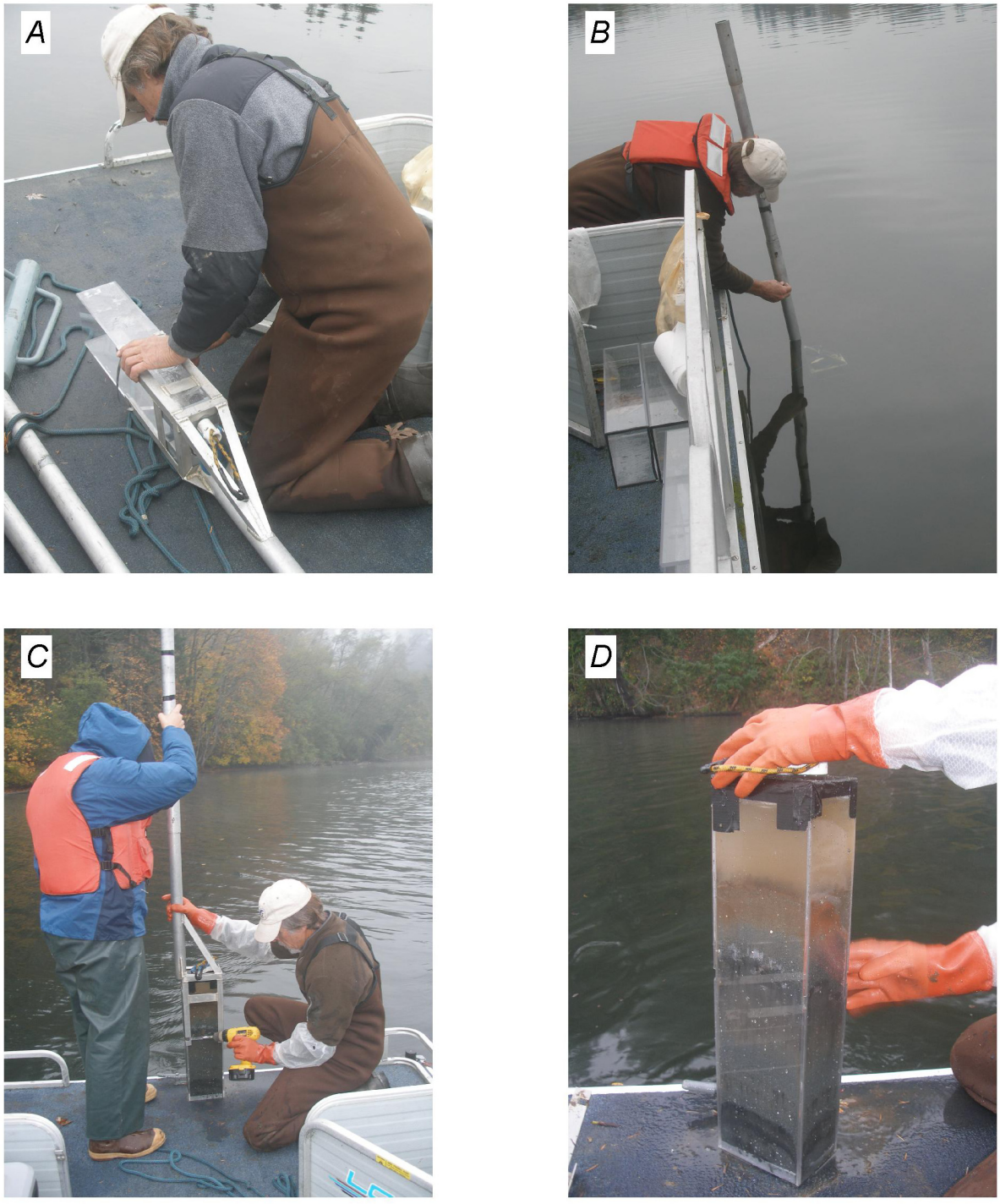

Figure 5. Photographs of field operation collecting cores from Capitol Lake showing, *A*, preparation of the core barrel, *B*, core collection, *C*, core retrieval and, *D*, a collected core.

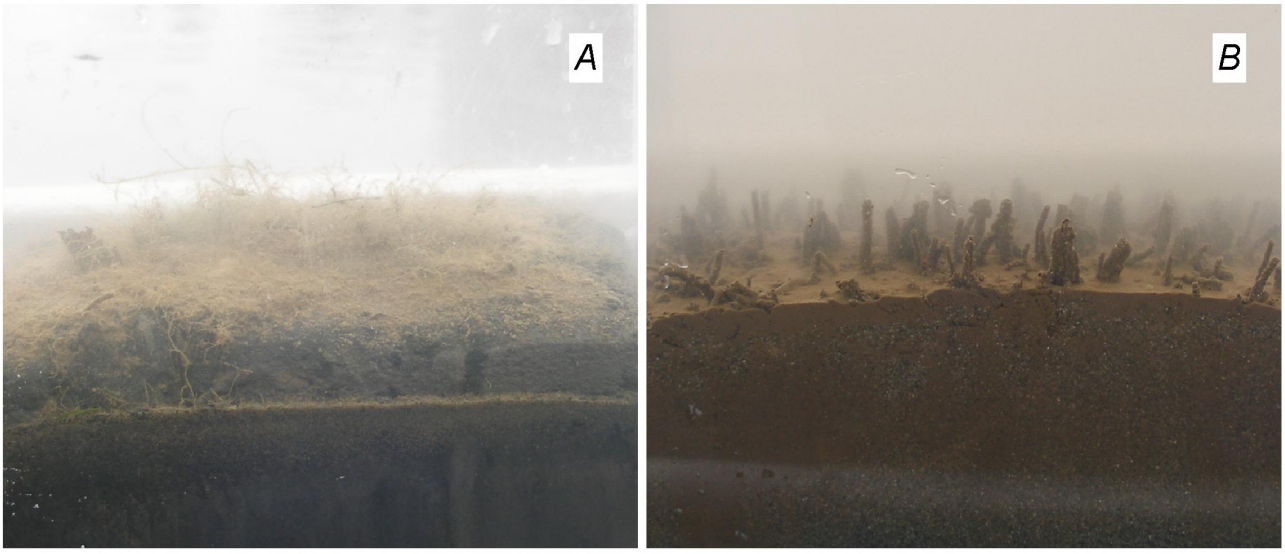

Figure 6. Photos of the undisturbed surface of two cores collected from Capitol Lake showing *A*, algae on the surface of core HP3, and *B*, worm tubes protruding through the surface of core HP4.

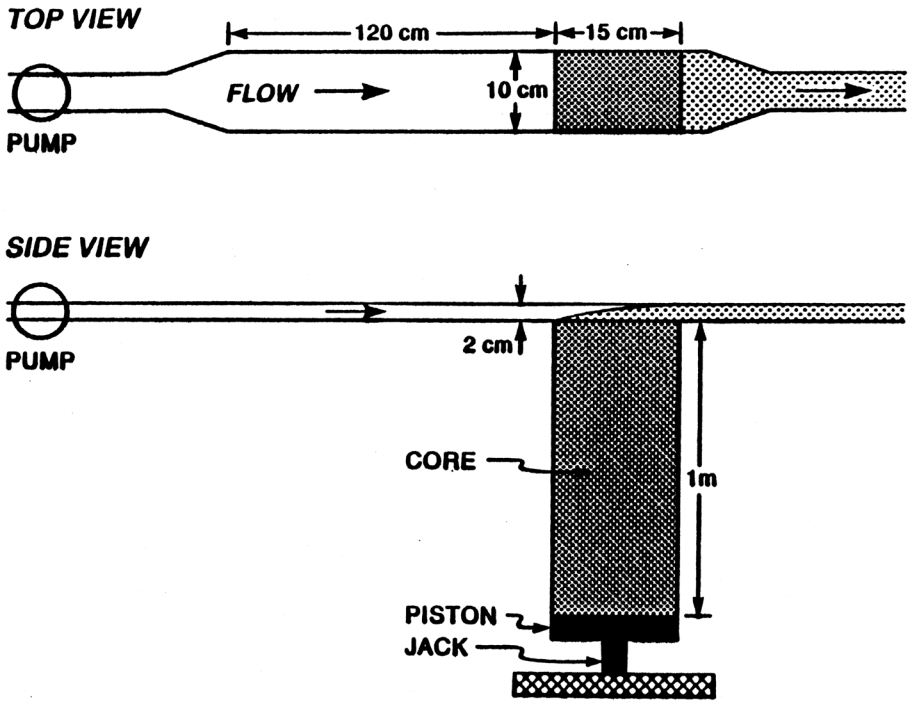

Figure 7. Schematic diagram showing the main components of Sedflume. After McNeil and others (1996).

sediment in the test section, the sediment eroded. The erodibility of sediment in the test section was characterized by two metrics, the erosion rate as a function of shear stress and the critical shear stress. These two metrics were measured on each core collected from Capitol Lake during a series of erosion cycles, described below.

Measurements of Sediment Erosion Rates

A series of erosion cycles were performed on each core. Each cycle consisted of a sequence of step increases in applied shear stress. During each cycle, approximately 5 cm of the core was eroded. To begin an erosion cycle, a core was positioned in the flume, and a low shear stress (typically 0.1 Pa) was applied to the test section. As the sediment in the core eroded, an operator moved the sediment in the core upward to keep the sediment-water interface level with the bottom of the flume. Raw erosion rates were obtained by measuring the core length at different time intervals as shown in Equation 1,

$$Er = \frac{\Delta z}{t}, \qquad (1)$$

where Er is the raw sediment erosion rate (cm s^{-1}), Δz is the measured change in core height (cm), and t is elapsed time (s). After the core eroded a measurable amount (between 1 mm and 2 cm), the applied shear was increased by a factor of 2, and the new erosion rate was recorded. Stress increments of 0.1-3.2 Pa were typically included in each erosion cycle.

Erosion cycles were repeated until all of the sediment had eroded from the core. If after three cycles a particular shear stress showed a rate of less than 10^{-4} cm/s, that stress increment was removed from subsequent cycles. If the erosion rates decreased measurably after many cycles, a higher shear-stress increment was included in subsequent cycles.

The measurement of erosion rates with Sedflume is defined by operator observation and therefore some uncertainty arises by differences between operators (Jepsen, 2006). In an independent study, Roberts and Jepsen (2001) quantified the uncertainty of erosion rates to be ±25 percent based on comparison of different operators on identical sediment samples.

Determination of Critical Shear Stress

The critical shear stress of a sediment bed is defined quantitatively as the shear stress required to initiate a measurable amount of sediment erosion (van Rijn, 1993). The minimum measurable erosion rate for Sedflume studies has been defined as 10^{-4} cm/s. This represents 1 mm of erosion in approximately 15 minutes. The critical shear stress was bracketed by applied shear stresses that were insufficient to erode sediment and the smallest applied shear stress that generated a measurable erosion rate. Linear interpolation between the largest applied stress that did not cause sediment to erode, and the smallest applied shear stress that caused measurable erosion was used to calculate the critical shear stress for each erosion cycle.

Sediment Properties

Subsamples from the cores were collected and analyzed for sediment water content and particle size. Sub samples were collected from the surface of each core and at the end of each erosion cycle. A sample was collected approximately every 5 cm down-core.

Sediment water content in each subsample was determined by using standard gravimetric techniques described in Hakanson and Jansson (2002). Sub samples were placed in preweighed beakers and weighed. The samples were then dried in an oven and weighed dry. The water content was calculated based on the ratio of wet weight to dry weight. Water content was converted to dry sediment density by using the empirical formula of Flemming and Delafontaine (2000),

$$\rho_{sed} = 2.6596369 - 0.0886164\phi + 0.0088041\phi^{1.5} - 0.0002594\phi^{2} \qquad (2)$$

where ρ_{sed} is the dry sediment density (kg m^{-3}), and ϕ is the measured water content (percent).

Sediment dry-density values were used to convert raw erosion rates to mass eroded per unit time per unit area by using,

$$Em = \left(\frac{Er}{100} \right) \times \rho_{sed}, \qquad (3)$$

where Em is the normalized erosion rate (kg m^{-2} s^{-1}) and Er is the raw erosion rate (cm s^{-1}).

Grain-size distributions were determined by using laser-diffraction analysis. Subsamples from the cores were prepared by addition of sodium hexametaphosphate (to deflocculate fine particles) and inserted into a Beckman Coulter LS13320. Each sample was analyzed in three 1-minute intervals, and the results were averaged. This method is valid for particle sizes between 0.04 and 2000 microns. No significant fraction greater than 2000 microns was observed in any of the subsamples collected.

Deschutes Estuary Model Overview

The hydrodynamic and sediment transport model of the restored Deschutes Estuary, developed as part of the Deschutes Estuary Feasibility Study, was described in detail in George and others (2006). The model results presented by George and others (2006) will be hereafter referred to as "Phase I", while the additional simulations that incorporate measured erodibility parameters will be referred to as "Phase II".

In this section, a basic description of the model and boundary conditions is provided. Hydrodynamics and sediment transport were simulated by using Delft3D. Delft3D is a numerical model for calculating water motion, sediment transport and morphological change (Lesser et al., 2004). Our simulations used the two-dimensional (2D), depth-averaged version of Delft3D where the hydrodynamics, including river and tidal flows, density-driven mixing, and shear stress calculations, are performed by solving the unsteady shallow-water equations that consist of the continuity equation, the horizontal-momentum equations, and the transport equation under the shallow water and Boussinesq assumptions. Sediment transport and morphological-change routines are incorporated directly into the hydrodynamic calculations.

In Phase II, sediment transport and morphology simulations were conducted by using the 2D application developed during Phase I (George and others, 2006). The model domain was formed by a curvilinear grid that extends from the mouth of the Deschutes River to outer Budd Inlet, with maximum resolution in the channels of South, Middle and North Basins. Approximately 6000 grid cells allow for computationally efficient long-term (10-year) morphological simulations. The model bathymetry was based on bathymetric and topographic data from surveys conducted in 2004 and 2005 (Eshleman and others, 2006).

Sediment grain-sizes of 2 μm, 31 μm, 200 μm, and 2,000 μm were included in the model to represent clay-, silt-, sand-, and gravel-sediment classes, respectively. The grain-size fractions varied spatially based on available samples throughout the model domain. The thickness of available sediment was set to 10 m in most areas to provide sediment in excess of the erosion that was expected. In areas where no grain-size data were available, or where the data suggested that the area was predominantly gravel, the available sediment thickness was set to zero to prevent erosion.

The model was forced with schematized boundary conditions as the constraints of numerical modeling; the difference between the time step in field data and the model simulation, and the goal of predicting future conditions do not allow direct input of river discharge and calculated sediment concentrations into the model. At the seaward boundary, a simple harmonic (morphologic) tide equal to 1.1 times the M2 component (1.46-m amplitude) was imposed. The southern boundary of the model is the Deschutes River, defined as fluvial forcing with four sediment grain sizes and associated concentrations. River inputs by Percival Creek were assumed to be negligible compared to the Deschutes River. The annual average flow of the Deschutes River is approximately 12 m^3 s^{-1}, but fluctuates widely within a year and from year to year (based on USGS river gauge #12080010, in

Tumwater, Wash.). To simulate event-driven nature of the river, the freshwater discharge was binned into five discharge classes ranging from 13 $m^3 s^{-1}$ to 146 $m^3 s^{-1}$ representing low flow to 5-year flood conditions, respectively. The sediment flux from the river was calculated to be 25,200 m^3 annually based on a rating curve developed by Mih and Orsborn (1974). The concentration of each grain-size class was varied based on the river discharge class.

A technique known as "morphological acceleration" was used to scale the morphological change associated with hydrodynamic forcing (Roelvink, 2006; Lesser et al., 2004) to achieve computationally efficient, long-term (>1 year) morphological simulations. The scaling occurs by multiplying the depositional and erosional fluxes to and from the bed by a dimensionless morphological acceleration factor, or MORFAC, at every computational time-step. The adjusted bed changes are then incorporated into the hydrodynamic calculations. In the Deschutes Estuary Model, the morphological acceleration factor varied with the river discharge class to link the river hydrodynamics and sediment load with tidal hydrodynamics and morphology in the estuary. The MORFAC ranged between 0.78 during the largest river discharge events to 114 during low-flow conditions.

The influence of wind (enhanced turbulence and wind-driven flow) and waves (increased bed shear stresses) were included in the model. Additional forcing included a constant wind field of 5 m/s from the south (based on averaged data from Deerfield Park/Tolmie State Park in Olympia), and a uniform wave field (H1/3 = 10 cm; Ts = 2 sec) over the entire model domain.

Delft3D Sediment Transport

Erosion rates for noncohesive (sandy) and cohesive (muddy) sediment fractions are calculated separately based on different formulations in the Delft3D sediment transport model. Cohesive sediment transport is modeled in Delft3D by using the linear formula given in Partheniades (1965),

$$E = M\left(\frac{\tau_b}{\tau_{cr}} - 1\right), \qquad (4)$$

where E is the erosion rate (kg $m^{-2}s^{-1}$), M is an erosion coefficient (kg $m^{-2}s^{-1}$), τ_b (Pa) is the bottom shear stress, and τ_{cr} (Pa) is the critical shear stress. The term in the parentheses is often referred to as the normalized excess shear stress (dimensionless). This formulation dictates that erosion rates are a linear function of excess shear stress, and the erosion rate remains constant at a given excess stress over time because the critical shear stress is assumed to be constant as sediment erodes. Several more recent studies describe erosion formulations that allow the critical shear stress to vary with depth (for a review, see Sanford and Maa, 2001).

Noncohesive-sediment transport in Delft3D is calculated by using the approach outlined in van Rijn (1993). This approach separates the calculation of bed load and suspended load transports. Suspended sediment transport is computed by the advection-diffusion solver, while bed load is calculated by using a nonlinear empirical relationship (see Van Rijn (1993) for specific transport formulations).

Erosion rates for each sediment fraction are calculated separately and summed to calculate the total transport for each grid cell in the model domain. Thus, the total transport is determined by the proportion of each sediment fraction included in the model. Changes in the proportions of sediment fractions as a result of erosion and deposition are affected by the prescribed thickness of available sediment. For example, suppose a 5-m thick sediment layer is composed of 80 percent sand, 10 percent silt, and 10 percent clay. If 0.5 m of the silt and clay fractions from this layer erode quickly (at equal rates) while the sand fraction does not erode, the resulting bed will be composed of 89 percent sand, 5.5 percent silt, and 5.5 percent clay. If however, the sediment layer was 20-m thick

instead of 5 m, 0.5 m of erosion would result in a bed composed of 82 percent sand, 9 percent silt and 9 percent clay. Therefore, the cumulative erosion and deposition over a simulation is based in part on the prescribed thickness of available sediment.

Sediment-deposition rates for all sediment fractions are based on their settling velocity. The settling velocity of the silt and clay classes was set to 1×10^{-3} m s^{-1} in saline water to parameterize flocculation of the fine fractions in seawater (Hill, 1998).

Results and Discussion

The results and discussion of this report are presented in three sections. The first section describes the laboratory measurements of sediment properties and erodibility made on cores collected from Capitol Lake. The second section explains how the field data were incorporated into the Deschutes Estuary Model. The final section presents and discusses predicted morphological change from model simulations by using the erodibility parameters measured from field samples.

Field Data

Sediment Properties

The sediment grain-size measured in the cores varied horizontally (between cores) and vertically (with depth in a core). The mean grain size ranges from 13 to 578 µm (fig. 8 *A*). The eastern and western sides of North Basin are characterized by fine particle sizes. Near the dam, coarser sediments are observed. Coarse, sandy sediments are observed in Middle Basin near the Burlington-Santa Fe railroad trestle located between Middle and North Basins. The cores in this region have complex stratigraphy with coarser layers overlain by finer deposits near the surface. In the southern part of Middle Basin, the grain size is finer and less variable with depth in the core. Throughout Capitol Lake, the sediment is predominately sand (62.5-2,000 µm) and silt-sized (4-62.5 µm) particles (fig. 8*B*). The proportion of clay-sized (< 4 µm) particles is uniformly low (< 25 percent) for all samples.

The surface grain-size distributions in Capitol Lake are likely controlled by present-day processes. Many of the processes that controlled both the grain-size distributions and morphology of the predam estuary are still active, though altered, in the lake. The river continues to supply new sediment to the lake during flood events. Larger particles are likely transported as bed load in the present channel, while finer particles are suspended throughout the lake. Currents also influence grain-size distributions in the lake. During the sampling period, the dam was partially opened to release water into southern Puget Sound. At that time, strong currents were observed in the constriction between North and Middle Basins. Currents likely maintain the channel geometry in the present lake (fig. 4) and prevent the deposition of fine particles in some locations.

The dry sediment density measured in the cores (fig. 9) varies between 250 and 1,400 kg m^{-3}. The dry density of sediment is positively correlated with the percentage of sand in the sample (fig. 9*B*) as has been found in other studies of sediment properties (for example, Flemming and Delafontaine, 2000). In the absence of major changes in sediment grain size, the dry density of muddy sediments is typically lowest near the sediment-water interface and increases with depth in the sediment due to self-weight consolidation (Been and Sills, 1981). A summary table with the measured sediment properties for each core is given in Appendix A.

Erodibility Measurements

An important factor describing sediment erodibility is the critical shear stress for erosion (τ_{cr}). Critical shear stresses measured on cores from Capitol lake vary between 0.06 and 1.84 Pa (fig. 10). No clear spatial pattern of critical shear stress is observed in the data. However, in several cores the lowest erosion thresholds are near the sediment-water interface while in deeper layers of the core, more stress is required to

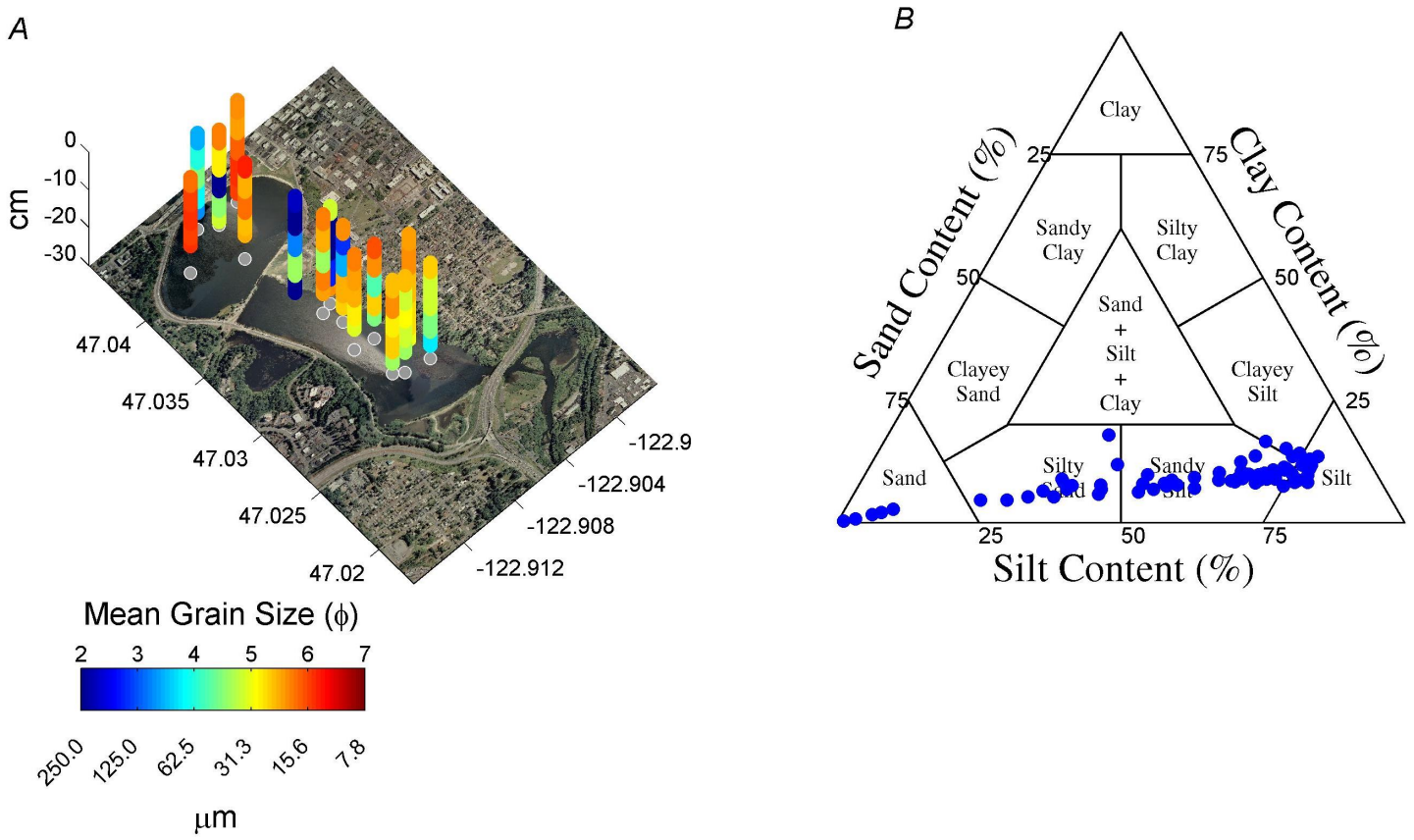

Figure 8. Grain-size data from cores collected in Capitol Lake showing *A*, mean grain size with depth in the core. The z-axis is positive upward, and 0 indicates the sediment-water interface. In *B*, the relative percentages of sand, silt and clay in each of the sub-samples analyzed are given.

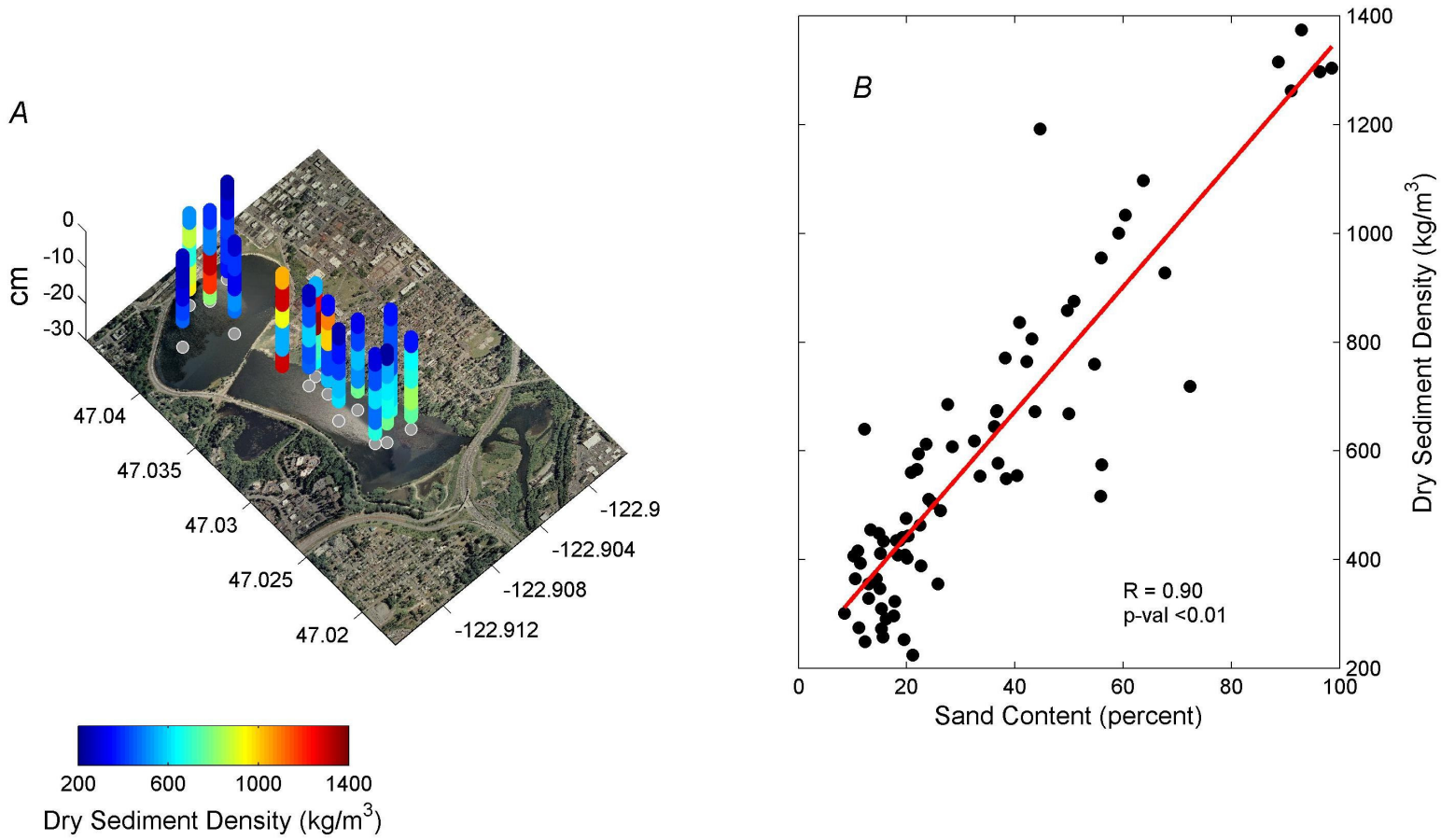

Figure 9. Dry sediment density data from cores collected in Capitol Lake showing *A*, dry sediment density with depth in the core. The z-axis is positive upward, and 0 indicates the sediment-water interface. *B*, Graph showing the relationship between sand content and dry sediment density in Capitol Lake samples.

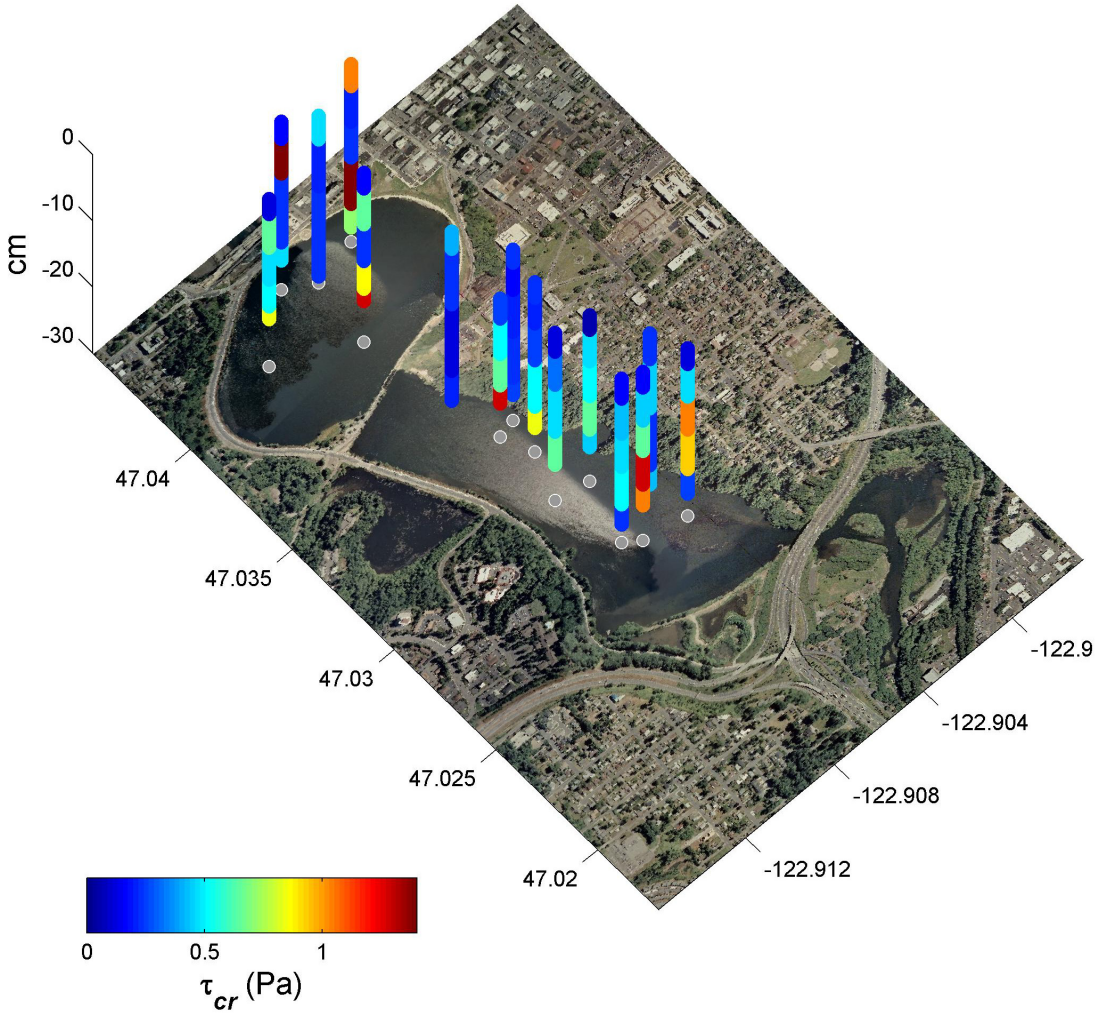

Figure 10. Map of critical shear stress measured in cores collected from Capitol Lake. The z-axis is positive upward and 0 indicates the sediment-water interface. The colors indicate the measured critical shear stress in the cores.

initiate sediment erosion. This is likely due to the presence of more consolidated (higher sediment density) sediments at depth than at the surface of the core (fig. 11; Postma, 1967; Jepsen and others, 1997).

Other studies have found a positive relationship between critical shear stress and sediment density for muddy, estuarine sediments (Postma, 1967; Amos and others, 1997). Indeed, a weak correlation between dry sediment density and critical shear stress is observed (by using a t-test to test the hypothesis of a correlation greater than random chance, n=52, p=0.06) for Capitol Lake samples containing less than 40 percent sand (fig. 12). A simple critical shear stress-dry density relationship in this study is likely masked by different mixtures of sand, silt, and clay-sized particles (for example, van Ledden and others, 2004), as well as biological effects (for example, Stevens and others, 2007).

Erosion rates measured with Sedflume varied from 4×10^{-4} to 1.2 kg/m^2 s^{-1} for shear stresses between 0.1 and 10 Pa (fig. 13). The erosion rates measured in the Capitol Lake cores are typical of muddy depositional sediments measured in other areas with Sedflume (for example, Lick and others, 1997). The erosion-rate data were analyzed for spatial trends by

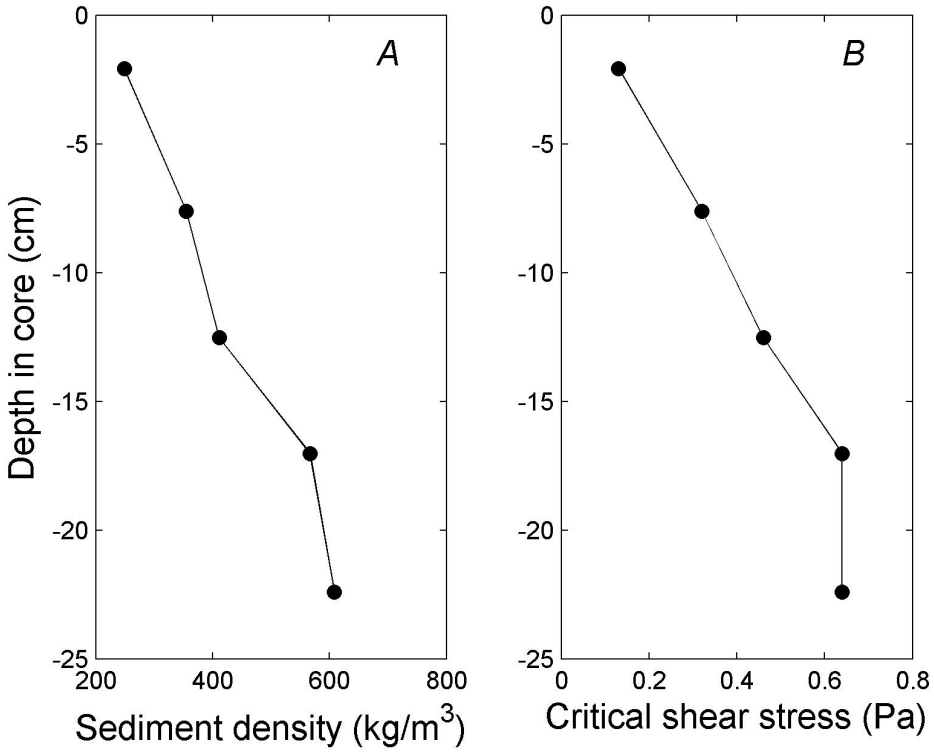

Figure 11. Results from Sedflume analysis for core LP4 showing *A*, dry sediment density, and *B*, critical shear stress versus depth in the core.

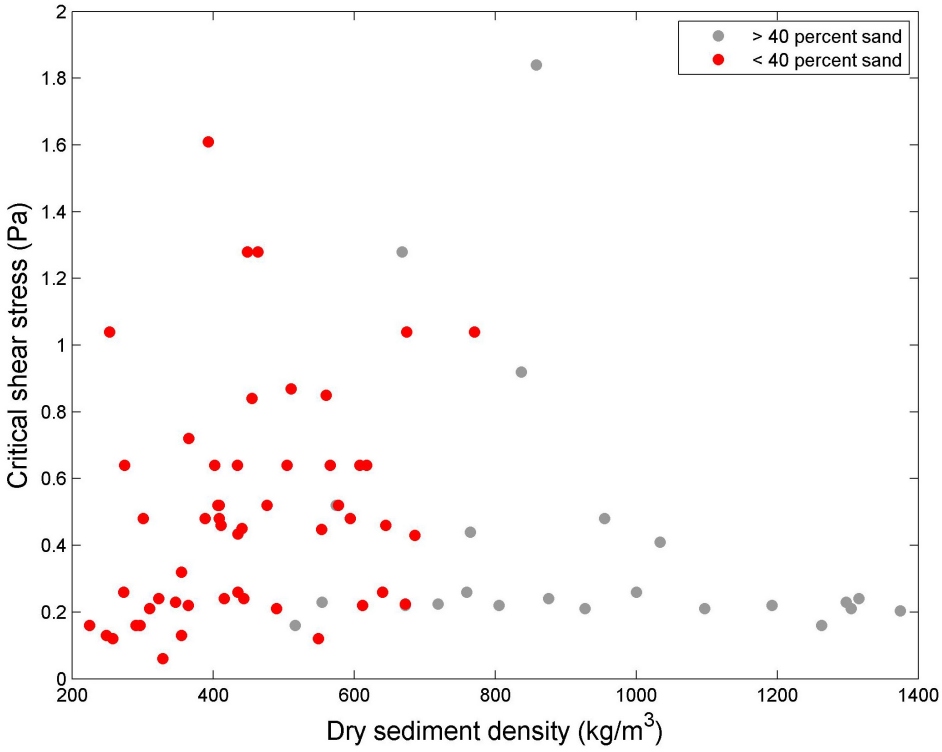

Figure 12. Relationship between dry sediment density and critical shear stress for samples containing >40 percent sand (gray circles) and <40 percent sand (red circles).

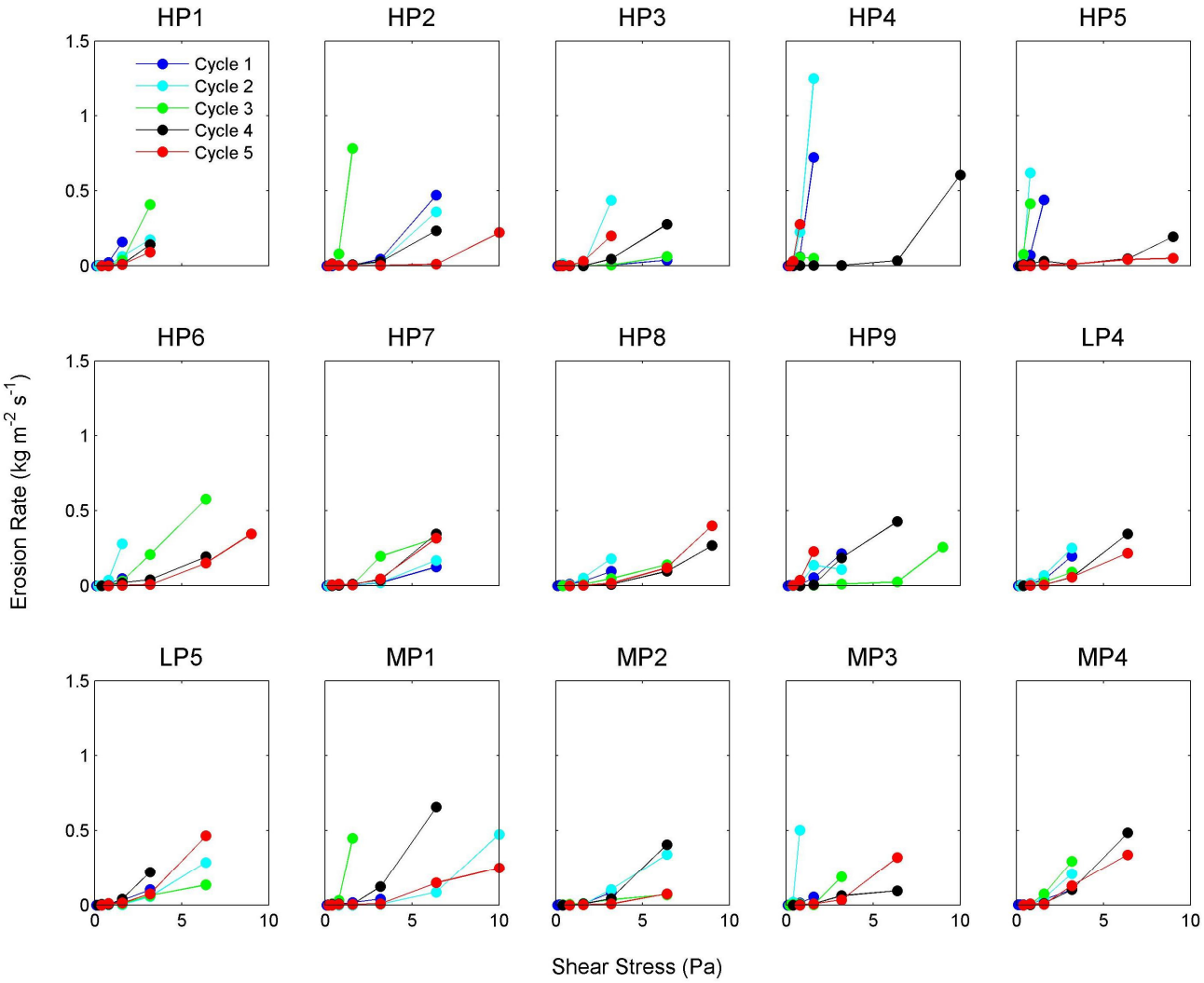

Figure 13. Plots of erosion rate versus applied shear stress for each core sample (HP1 – MP4) analyzed with Sedflume. For each core, five erosion cycles were performed to estimate erodibility parameters with depth in the core. During each cycle, approximately 5 cm of sediment was eroded. See figure 4 for core locations.

comparing erosion rates at a given shear stress (fig. 14). At a shear stress of 1.6 Pa, comparison of the erosion rates for samples with sand content less than 40 percent reveals a complex spatial pattern, both horizontally and with depth in the core. At the surface (Cycle 1), the highest erosion rate is observed in core HP1. However, in the next erosion cycle, at roughly 5-10 cm depth in the core, the highest erosion rates are observed in core HP6. No single core eroded more quickly at 1.6 Pa than any other core throughout all erosion cycles. Overall, the erosion rates are generally higher in the upper 10 cm (Cycles 1 and 2), relative to deeper in the core.

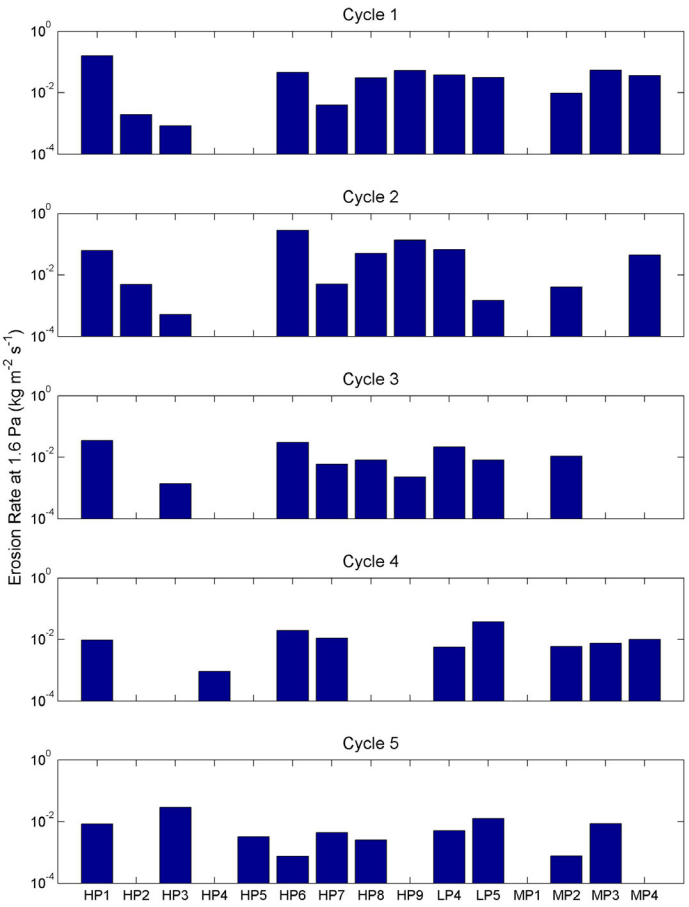

Figure 14. Bar graphs showing erosion rate for each core at 1.6 Pa applied shear stress. From top to bottom, the results from cycle 1 to cycle 5 are shown. Samples with sand contents >40 percent were removed from the plot. Note that the y-axis is a logarithmic scale.

Incorporation of Field Data into Existing Model

The purpose of making the erodibility measurements on Capitol Lake sediments is to characterize erodibility for input into the Deschutes Estuary hydrodynamic and sediment-transport model. This section describes how the measurements from field data are incorporated into the existing model framework. Only clay and silt fractions are considered cohesive and are calculated by using cohesive sediment transport formulations in the Deschutes Estuary Model, while the sand and gravel fractions are noncohesive. No distinction is made between the erodibility of silt and clay fractions; that is, the erodibility parameters (ρ_{sed} , τ_{cr} , M) for each cohesive sediment fraction are identical.

Erosion Rate Parameter Calculation

Three input quantities are required for each cohesive sediment fraction included in the Delft3D model: (1) critical shear stress; (2) erosion rate parameter; (3) and dry sediment density. The critical shear stress and erosion rate coefficient determine the mass of sediment that is eroded as stress is applied to the bed. The dry sediment density relates the eroded and deposited sediment mass to sediment volume. The critical shear stress and dry sediment density are measured directly during analysis of the cores with Sedflume. The erosion rate parameter is calculated by substituting measured erosion rates, critical shear stress, and bottom shear stresses into Equation 4 and solving for the erosion rate parameter. Graphically, when the erosion rate is plotted against excess shear stress, the slope of the line (forced through zero) is the erosion rate parameter, M.

The Sedflume data from Capitol Lake cores generally do not fit the linear Partheniades (1965) model over the entire range of applied excess shear stress. An example of the linear fit to the Sedflume data from one erosion cycle is shown in figure 15. At high excess shear stress,

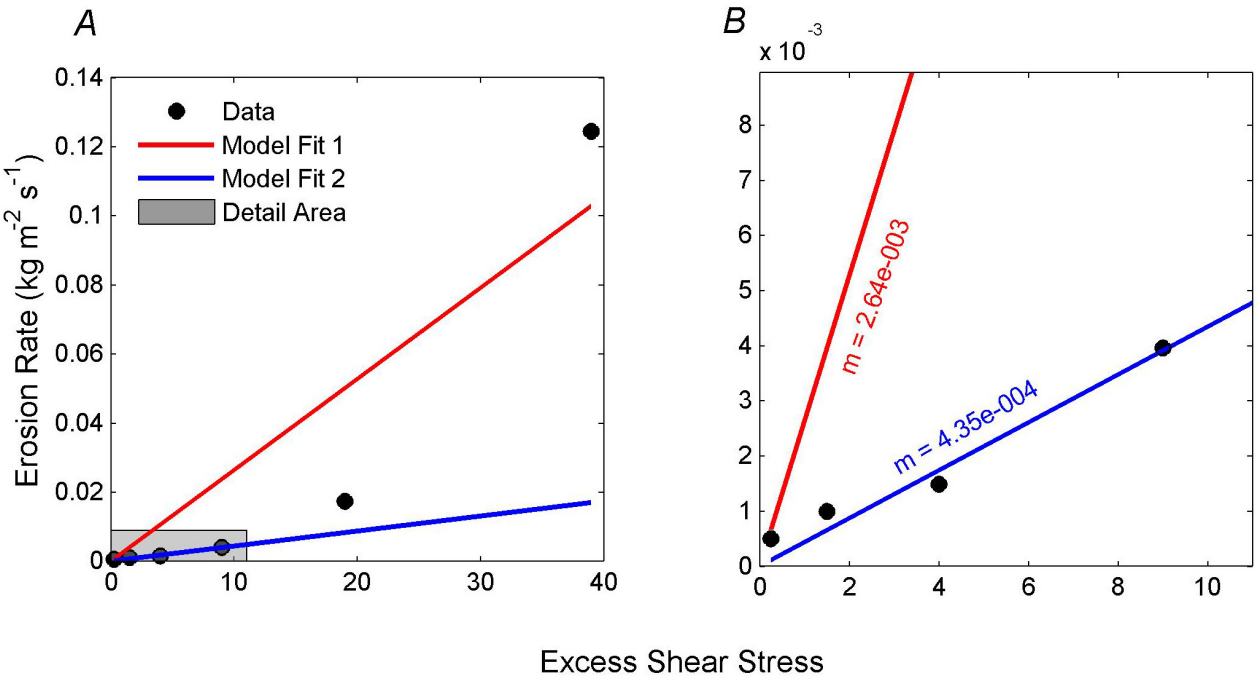

Figure 15. Example fit of the measured erosion rates to the model of Partheniades (1965) showing A, a poor fit over the entire range of excess shear stress, and B, a better fit to the linear model if the data are limited to the lower range of excess shear stress.

a power law relationship (for example, Roberts and others, 1998) would more accurately fit the field data. The linear model tends to over predict the erosion rates at low excess shear stress and under predict the erosion rate at higher excess shear stress. However, if the data are limited to points with relatively low excess shear stress, the data can be fit with a linear model (blue line, fig. 15*B*). Changing the sediment transport model for mud to allow for a nonlinear formulation was not possible for this study. Instead, we fit the data in the range of smaller excess stress with a linear model. Operationally, we eliminated data points where the applied shear stress was greater than 1.6 Pa from the model fit. For this example, the critical shear stress was 0.13 Pa. Therefore the cut-off value of 1.6 Pa was equivalent to disregarding samples with a normalized excess shear stress greater than 11.3.

The elimination of the portion of the laboratory data with high excess shear stress is well justified. Although the Phase I model simulations predict a maximum shear stress approaching 10 Pa in the channel during high river flow, the bottom shear stress in shallow areas where muddy deposits occur is generally low (fig. 16*A*). During a 3-year model simulation, the bottom shear stress is predicted to exceed 1.6 Pa less than 2 percent of the time (fig. 16*B*) for shallow, muddy areas. Thus, limiting the data used to calculate the erosion rate parameter would not have a large effect on predicting the magnitude of sediment transport in areas where muddy deposits exist. In the channel where bottom shear stresses are predicted to be high, the sediment deposits are sandy, and the fine-grained sediment transport formulations do not apply.

The erosion coefficient was calculated for each erosion cycle by least-squares regression in samples with sand contents less than 40 percent. Samples with higher sand contents are disregarded from the calculations because erosion rates for sand-sized sediment fractions in the model were calculated by using noncohesive sediment transport formulations that do not

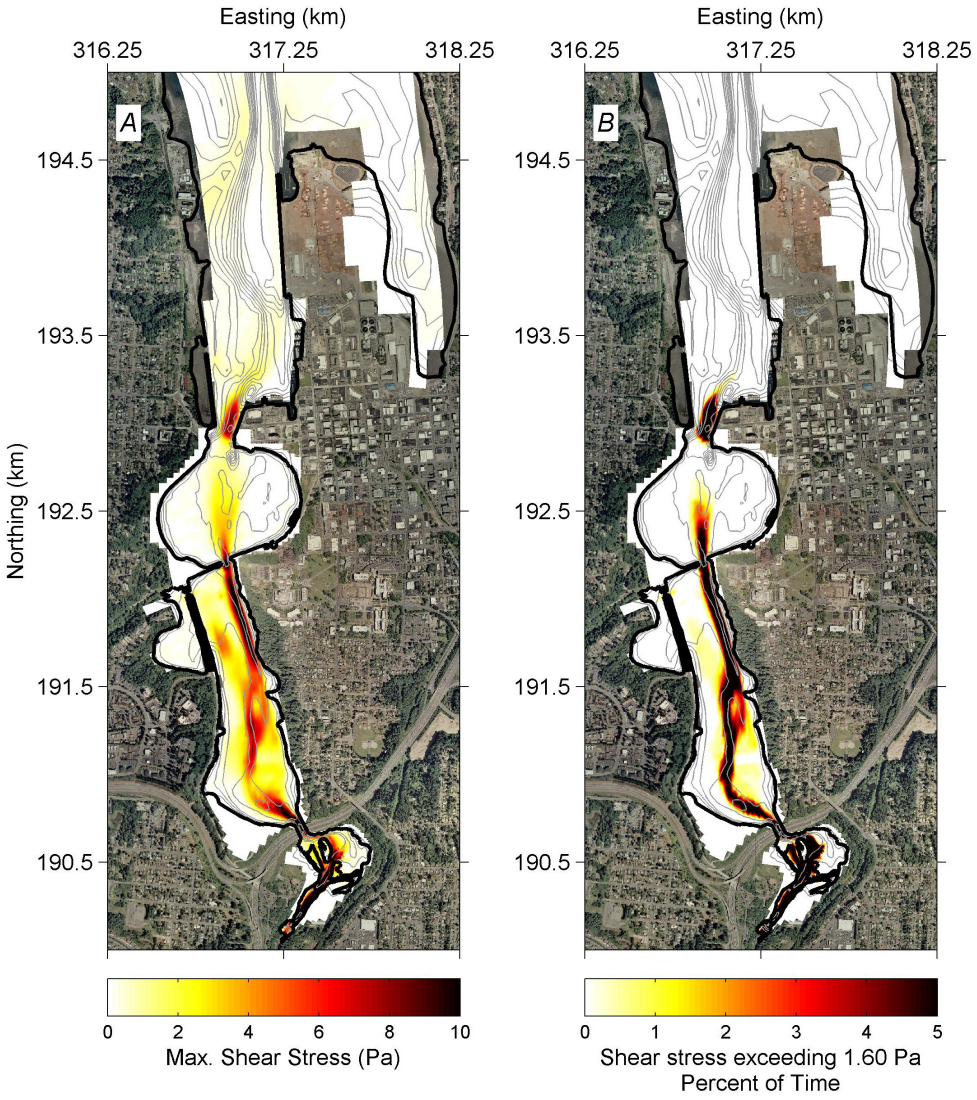

Figure 16. Simulation results showing, *A*, maximum predicted shear stress, and *B*, percent of 3-year simulation that the bottom shear stress exceeded 1.6 Pa.

require field-measured erodibility values. The cutoff for sand content was not arbitrary, but was chosen based on a classification system (van Ledden and others, 2004) that suggests that for Capitol Lake sediment, has a clay to silt ratio of approximately 15:100 (fig. 8), the bed behaves cohesively when the sand content is less than approximately 40 percent. Sediment with sand content greater than 40 percent is, likewise, expected to behave noncohesively.

In Capitol Lake, the erosion coefficient varied by several orders of magnitude between 1.2×10^{-4} and 5.1×10^{-2} kg m^{-2} s^{-1} (fig. 17). The spatial pattern of the measured erosion coefficient is complex. No statistically significant relationship exists between the erosion coefficient and sediment dry density or grain size (fig. 18). A summary table with the measured erodibility parameters for each core is provided in Appendix A.

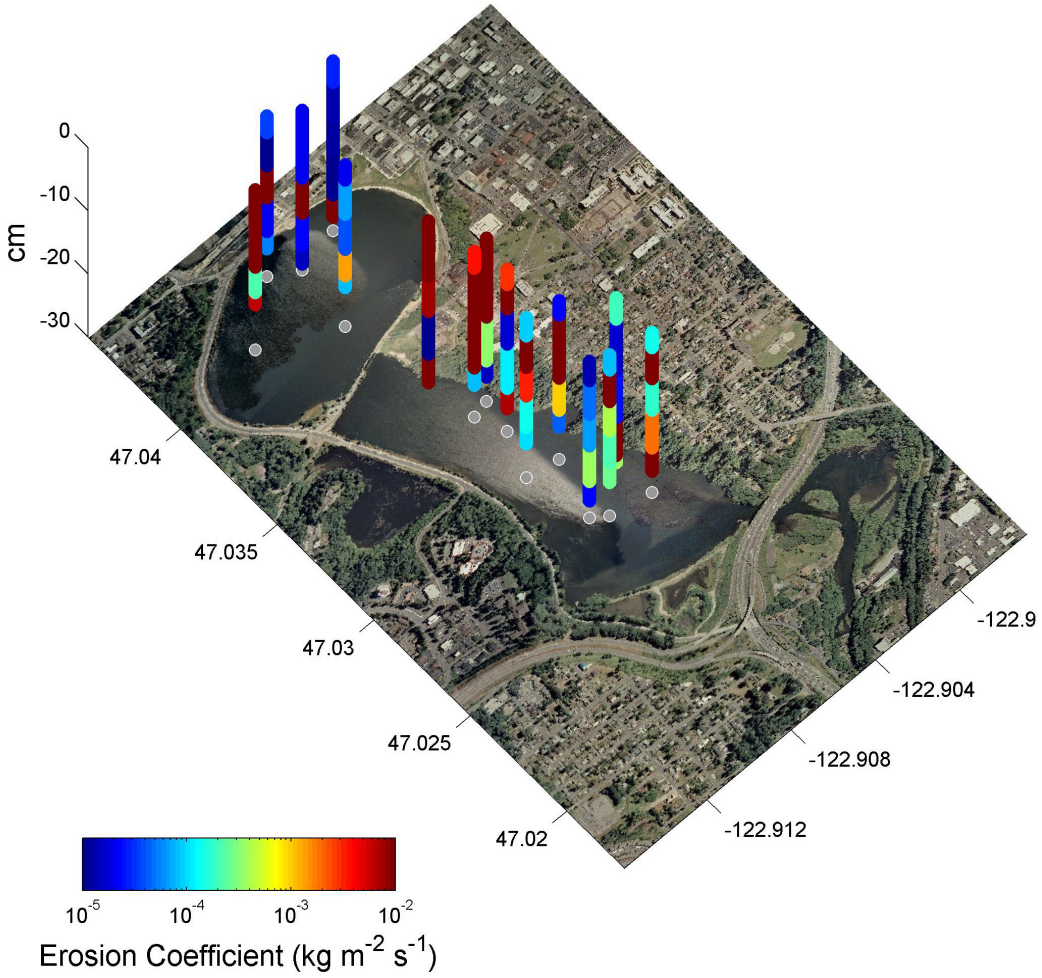

Figure 17. Map of erosion coefficient, *M*, measured in cores collected from Capitol Lake. The z-axis is positive upward, and 0 indicates the sediment-water interface. The colors indicate the measured erosion rate coefficient in the core samples. Note: the color scale is logarithmic.

The measured values of the erosion coefficient (fig. 19) are up to several orders of magnitude higher than the values given in van Rijn (1993) and used by George and others (2006) in the Phase I simulations. van Rijn (1993) does not report the original sources of the erosion rate parameter, nor whether they were obtained by field or laboratory measurements. Possible reasons for the discrepancy between previously reported values of the erosion coefficient and the results of this study include the measurement methodology (Gust and Muller, 1997; Tolhurst and others, 2000), and the role that waves play in mud resuspension (Blom and Aalderink, 1998).

Sediment Parameters for Phase II Simulations

The previous sections describe the measurements of erodibility and sediment properties made on cores collected in Capitol Lake and how the measurements are related to the fine-grained sediment transport formulation used in Delft3D (Delft Hydraulics, 2006). This section describes how the results from the field data are input into the model. The process of preparing the data for input into the model is based in part by limitations imposed by the present formulation of the model. One such

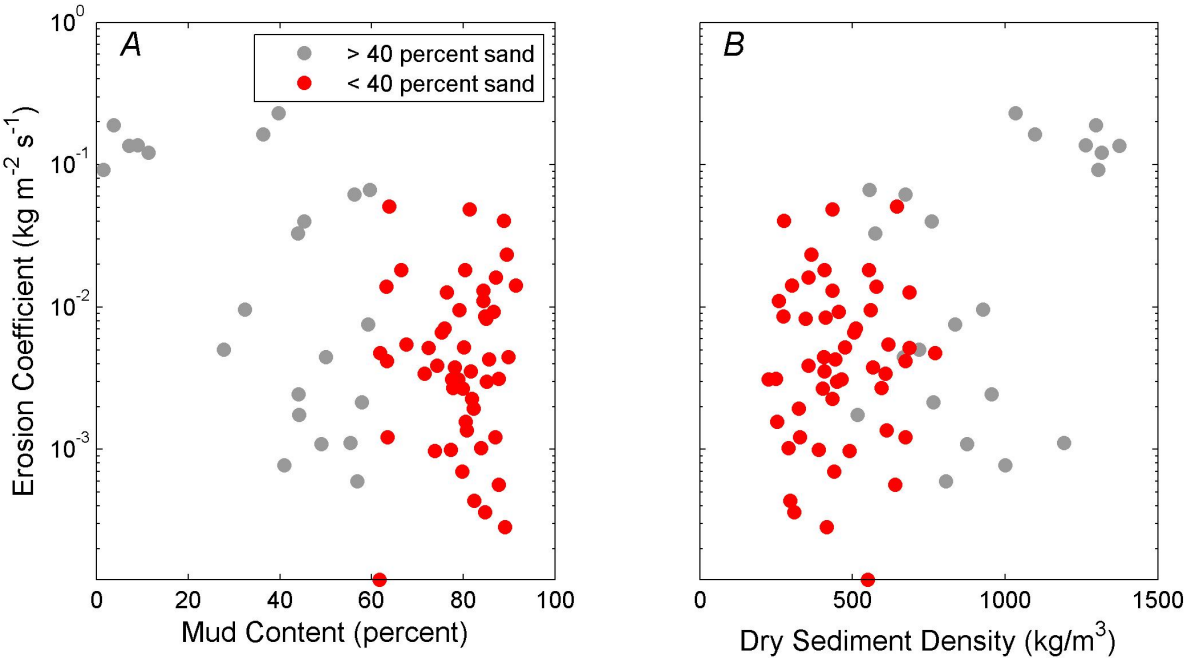

Figure 18. Relationship between the erosion coefficient and *A*, mud content and, *B*, dry sediment density.

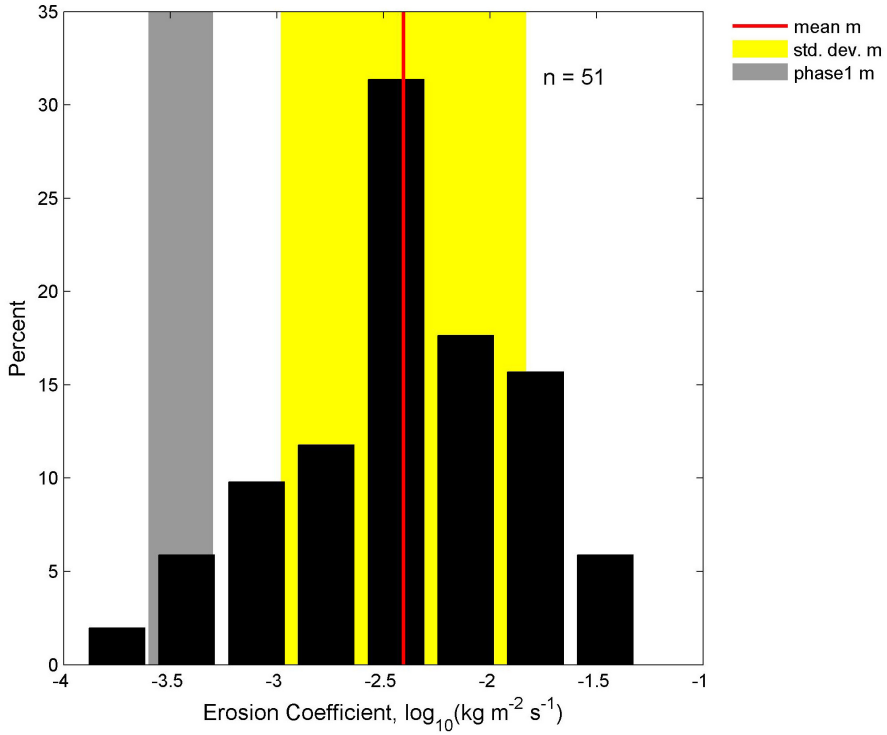

Figure 19. Histogram of the log of measured erosion coefficients from samples with sand contents <40 percent. The mean erosion coefficient and standard deviation are shown with a red line and yellow bar, respectively. The range of erosion coefficients used in Phase I (gray bar) is shown for comparison.

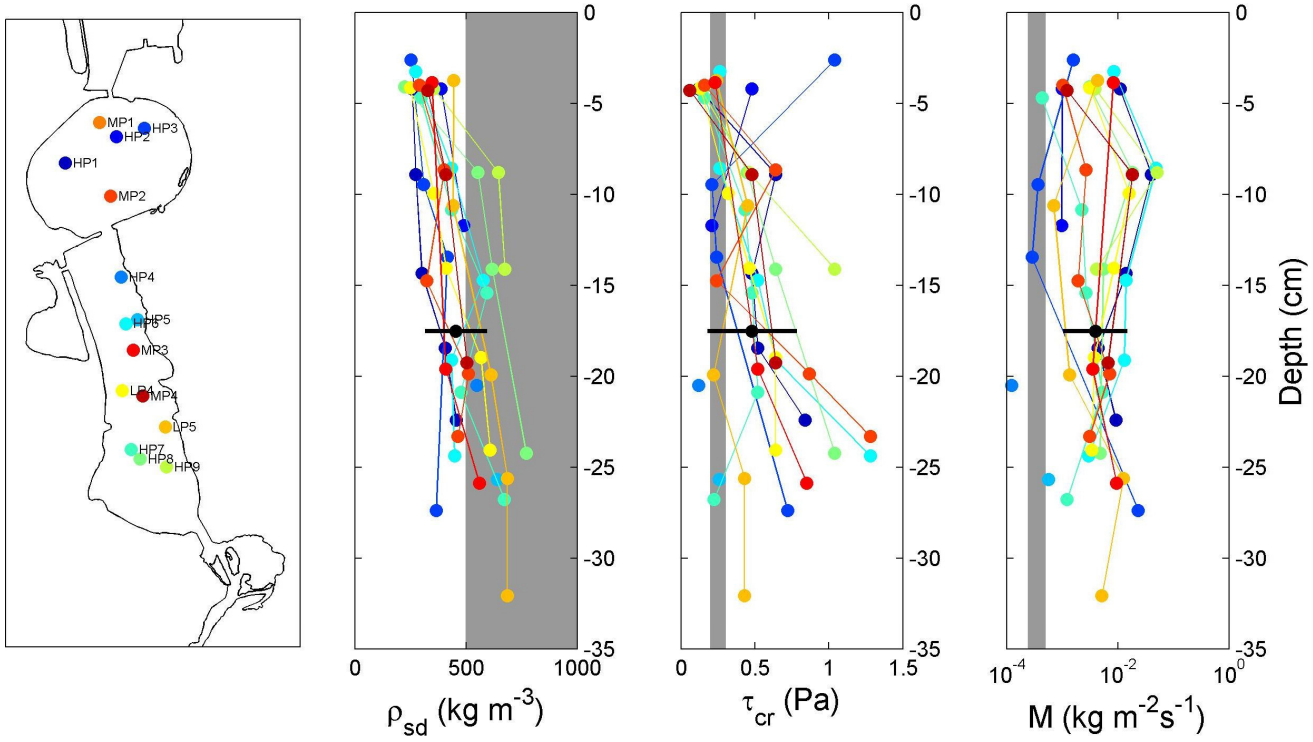

Figure 20. Down-core patterns in dry sediment density, critical shear stress, and erosion rate parameter for each core collected from Capitol Lake. Samples with > 40 percent sand content were removed from the plot. The gray bars show the range of values used in Phase I model simulations.

limitation is that, unlike sediment grain size, the erodibility parameters cannot vary spatially throughout the model domain. Rather, a single value for each erosion parameter must be selected for each fine-grained sediment fraction included in the model.

Field data from muddy areas of Capitol Lake suggest that dry sediment density, critical shear stress and erosion coefficient vary spatially both between cores and with depth in a core (fig. 20). Therefore, the variability in the erodibility parameters is statistically characterized by the mean value of all of the observed erodibility parameters ±1 standard deviation (black lines, fig. 20, Table 2). All depth intervals were used to calculate the statistics. The mean and standard deviation is calculated based only on samples with sand contents less than 40 percent (n=51).

Table 2. Erodibility parameters calculated from field data. The high and low values represent the mean value plus or minus 1 standard deviation for each parameter, respectively.

Parameter	Low	Medium	High
Dry sediment density (kg m^{-3})	316	455	594
Critical shear stress (Pa)	0.18	0.48	0.78
Erosion rate parameter (kg m^{-2} s^{-1})	0.001	0.00393	0.0147

With the exception of the dry sediment density, the standard deviation of measured erodibility parameters is larger than the range of values used in George and others (2006) in Phase I (gray areas, fig. 20). That is, the observed range in erodibility parameters using field data from Capitol Lake is greater than the range of values selected from the literature. The mean dry sediment density is slightly smaller than the lower value of sediment density used in Phase I. The mean measured critical shear stress is higher than the upper end value used in Phase I. The mean erosion rate parameter is an order of magnitude higher than was used in Phase I.

In order to evaluate the sensitivity of the model to the observed variations in sediment erodibility values, several combinations of low, medium, and high values for each erodibility parameter are used in 3-year simulations. The most-likely combinations of the three parameters (table 3) were chosen based on analysis of field data with a Bayes network (for example, Spiegelhalter and others, 1993) by using the computer program Netica. The Bayes network uses probabilistic inference to determine the relationships between each of the erodibility parameters and calculates the probability of occurrence based on the field data for each of the 27 possible combinations. The Bayes network analysis suggests that the most-likely combination of erodibility parameters occurs with a medium bulk density (455 kg m^{-3}), a medium critical shear stress (0.48 Pa), and a medium erosion rate parameter (3.93×10^{-3} kg m^{-2} s^{-1}). The most-likely scenario of medium values for each of the erodibility parameters is used for long-term morphological simulations. Other combinations of erodibility parameters are used to evaluate the sensitivity of the model to variations in the erodibility parameters. Several of the combinations are unlikely to occur according to the field data and the Bayes network and are not used as input into the model.

Finally, an additional modification to the original Phase I model is suggested as a result of field data collected in Phase II. The percentage of sand relative to mud in the cores is higher than in the Phase I model (fig. 21). The difference between the mean sand content in the cores and in the original model is as high as 55 percent and is largest in the main channel. A grab sampler was used to collect bottom sediments (Eshleman and others, 2006) for grain-size measurements that were used in the Phase I model. The grab samples represent roughly the top 5 cm of sediment in the bed, whereas the grain size was measured in the cores to a depth of 25 cm for the Phase II study. The different sampling methods could account for the difference in sand content.

Table 3. Probability of occurrence estimated by using a Bayes network for each possible combination of the three erodibility parameters. The combinations are ranked in ascending order of their probability. The top 14 combinations were input into the model to perform a sensitivity analysis. See Table 2 for the values associated with Low, Medium, and High for each of the parameters.

Simulation ID	Dry sediment density	Critical shear stress	Erosion rate parameter	Probability, in percent
P1	Medium	Medium	Medium	13.7
P2	Low	Low	Low	9.8
P3	Medium	Medium	High	9.8
P4	Low	Low	High	7.8
P5	High	Medium	Medium	7.8
P6	Low	Low	Medium	5.9
P7	Low	Medium	High	5.9
P8	Medium	Low	Low	5.9
P9	Medium	High	Medium	5.9
P10	High	Low	Low	5.9
P11	Low	Medium	Medium	3.9
P12	Medium	High	High	3.9
P13	High	Medium	High	3.9
P14	High	High	Medium	3.9
n/a	Low	Medium	Low	2.0
n/a	Low	High	Low	2.0
n/a	Low	High	High	2.0
n/a	Medium	Low	Medium	2.0
n/a	Medium	Low	High	2.0
n/a	Medium	Medium	Low	2.0
n/a	Low	High	Medium	0.0
n/a	Medium	High	Low	0.0
n/a	High	Low	Medium	0.0
n/a	High	Low	High	0.0
n/a	High	Medium	Low	0.0
n/a	High	High	Low	0.0
n/a	High	High	High	0.0

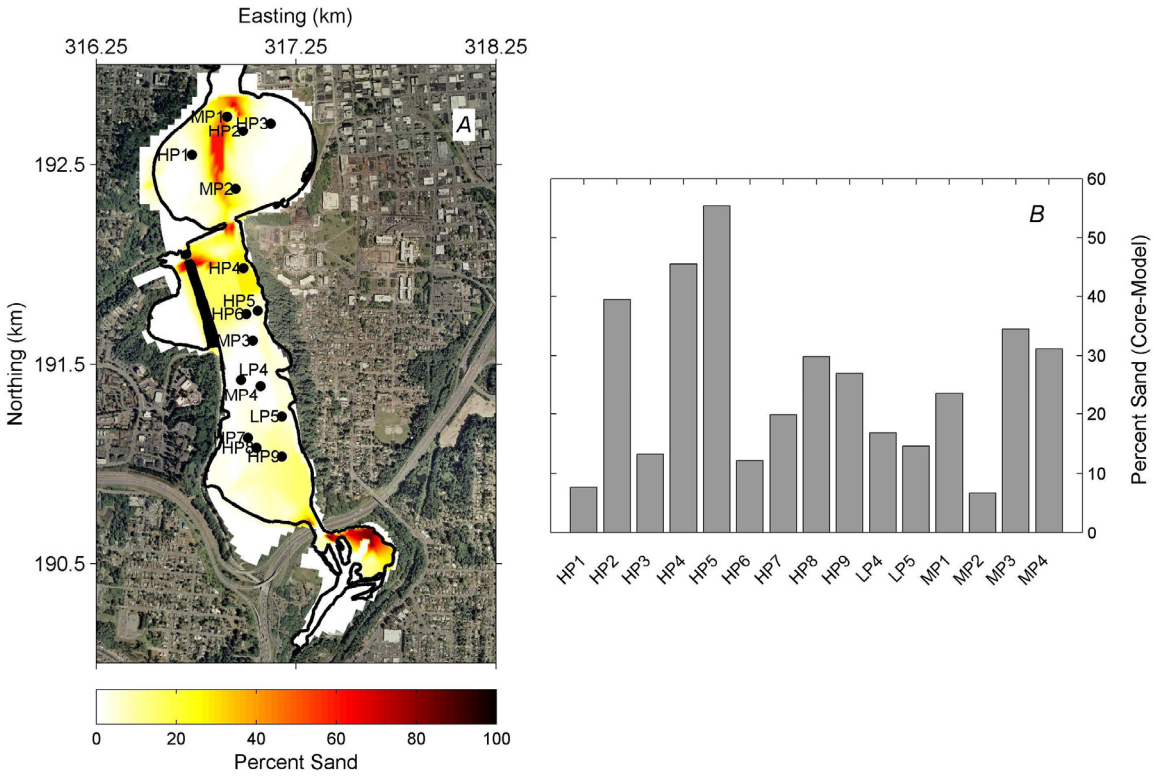

Figure 21. Sand content in bottom sediments showing *A*, map of core locations plotted on top of the percentage of sand in the Phase I model, and *B*, a graph showing the difference between mean sand content measured in the cores and in the nearest grid cell of the Phase I model.

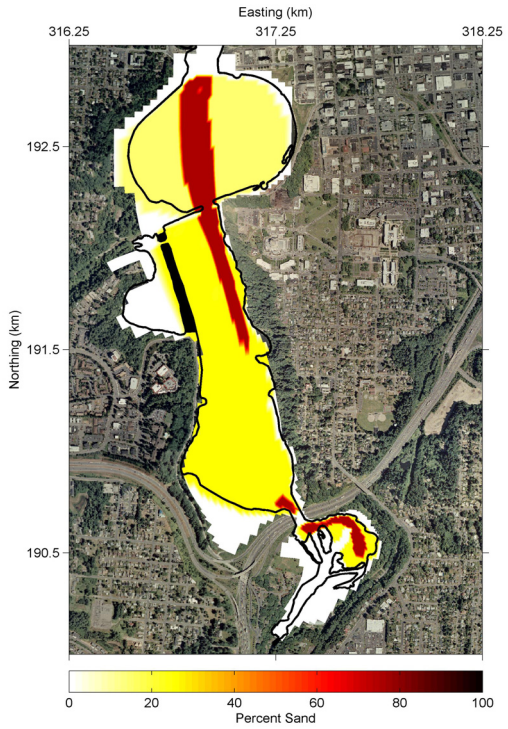

Figure 22. Map showing the sand-content schematization of bottom sediments in the Phase II model.

The distribution of sand-sized particles in the model is, therefore, changed to better reflect observations of sediment grain size from the cores collected in this study (fig. 22). The Phase II grain-size map is not as spatially complex compared to the Phase I map because it is based on only 15 cores, whereas the Phase I sediment map is based on data from 72 grab samples.

Model Results

Long-Term Morphological Change

In Phase I of the hydrodynamic and sediment transport modeling study, 4 restoration alternatives were investigated in the hydrodynamic and sediment transport model simulations. Two of the alternatives have since been dropped from consideration. In this section, we use the medium erodibility values obtained from field measurements (table 2) in model simulations to investigate postdam-removal morphological changes to the estuary for the remaining two alternatives: the estuary alternative and the dual-basin estuary alternative (fig. 23). In both restoration alternatives, a 150-m opening (red areas in fig. 23) is proposed to connect lower Budd Inlet with Capitol Lake. The dual-basin alternative additionally includes a barrier placed along a north-south axis in North Basin to preserve a portion of the current lake (blue area in fig. 23).

Morphological changes to the estuary bed occur after dam-removal in both restoration scenarios, regardless of the combination of erodibility parameters considered. In order to discuss and quantify the spatial patterns of erosion and deposition, the model domain is divided into seven regions: South Basin, Middle Basin, Percival Cove, North Basin, Port, Marina, and Budd Inlet (fig. 24). The bathymetric change in each basin is calculated over time to compare the magnitudes of erosion and deposition in different regions within a simulation and between simulations.

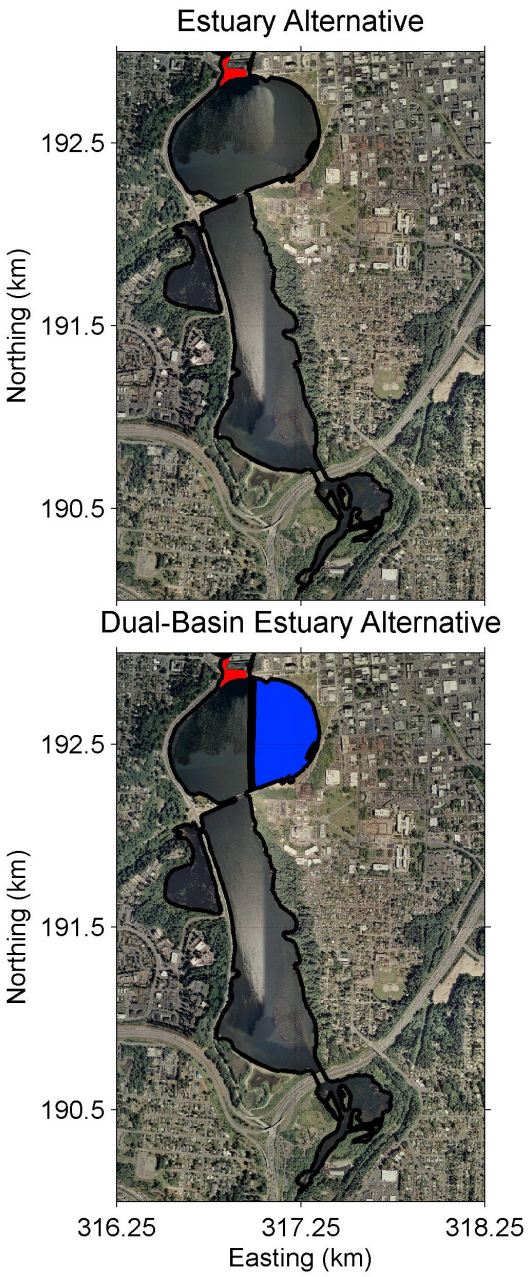

Figure 23. Map showing the two restoration alternatives: estuary and dual-basin estuary. The red lines indicate the removal of the current shoreline. In the dual-basin estuary alternative, a dike is proposed in North Basin that will retain a small portion of the current lake (shown in blue). The map coordinates are Washington State Plane South (km).

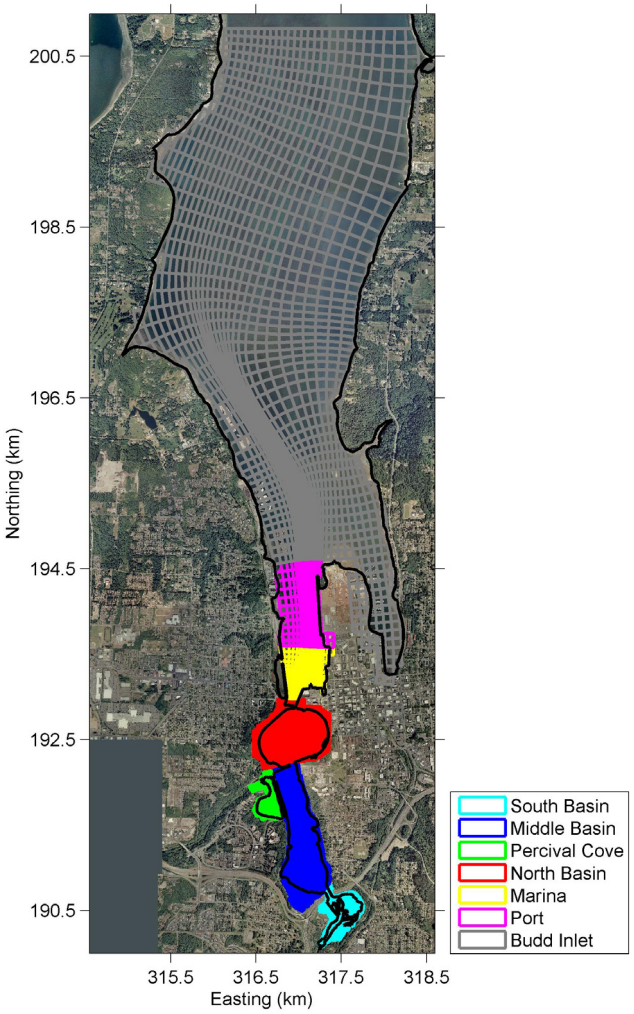

Figure 24. Model domain showing the extent of seven regions of interest: South Basin, Middle Basin, Percival Cove, North Basin, Port, Marina, and Budd Inlet.

Estuary Alternative

After dam removal, morphological changes occur in the Deschutes Estuary as a result of restored tidal processes and the unregulated flow of the Deschutes River. Considerable changes occur in the bathymetry of the estuary during the 10 years after dam removal for the estuary alternative (fig. 25). The patterns of sediment transport and associated morphological change as a result of dam removal for this alternative are broadly similar to those reported in George and others (2006).

Table 4. Sediment volume change ($\times 10^4$ m^3) for the estuary alternative in each region of interest over 10 years calculated by using medium values for each of the erodibility parameters.

Year	South Basin	Middle Basin	North Basin	Marina	Port	Budd Inlet
1	-1.45	-14.68	6.58	5.11	6.22	1.98
2	0.25	-2.70	0.78	1.89	2.94	1.30
3	0.37	-1.87	0.57	1.58	2.60	1.22
4	0.36	-1.23	0.52	1.34	2.41	1.19
5	0.34	-1.08	0.54	1.23	2.36	1.20
6	0.23	-0.97	0.60	1.12	2.39	1.24
7	0.24	-1.12	0.68	1.04	2.47	1.29
8	0.21	-0.86	0.63	0.96	2.44	1.29
9	0.19	-0.84	0.60	0.96	2.37	1.29
10	0.16	-0.54	0.49	0.91	2.37	1.30
Sum	**0.90**	**-25.89**	**12.01**	**16.12**	**28.58**	**13.31**

The most significant morphological changes to the restored estuary occur during the first year after dam removal (figs. 26-27). Large amounts of sediment erode from South and Middle Basins (Table 4). Despite the net erosion in these areas, localized deposition occurs in some portions of South Basin and north of the I-5 bridges in Middle Basin. In North Basin, a channel develops along a north-south axis from the railroad trestle to the entrance to lower Budd inlet while the deposition occurs on the channel flanks. In Middle Basin, the channel present in the lake both deepens and widens (fig. 28). A large portion of the sediment that erodes from the lake in the first year is deposited in the Port, Marina, and lower Budd Inlet areas.

The volume change in each of the basins decreases after the first year (table 4). In South Basin, initial net erosion in the first year gives way to deposition in following years. In other areas, the patterns of erosion and deposition in subsequent years resemble those observed after year one, although the magnitude of morphological change decreases. The estuary morphology continues to change 10 years after dam removal. Middle Basin continues to erode at a rate of approximately 0.5×10^4 m^3 yr^{-1}, while South Basin, North Basin, the Marina, and the Port, accumulate sediment at rates of approximately 0.2×10^4 m^3 yr^{-1}, 0.5×10^4 m^3 yr^{-1}, 0.9×10^4 m^3 yr^{-1}, and 2.4×10^4 m^3 yr^{-1}, respectively.

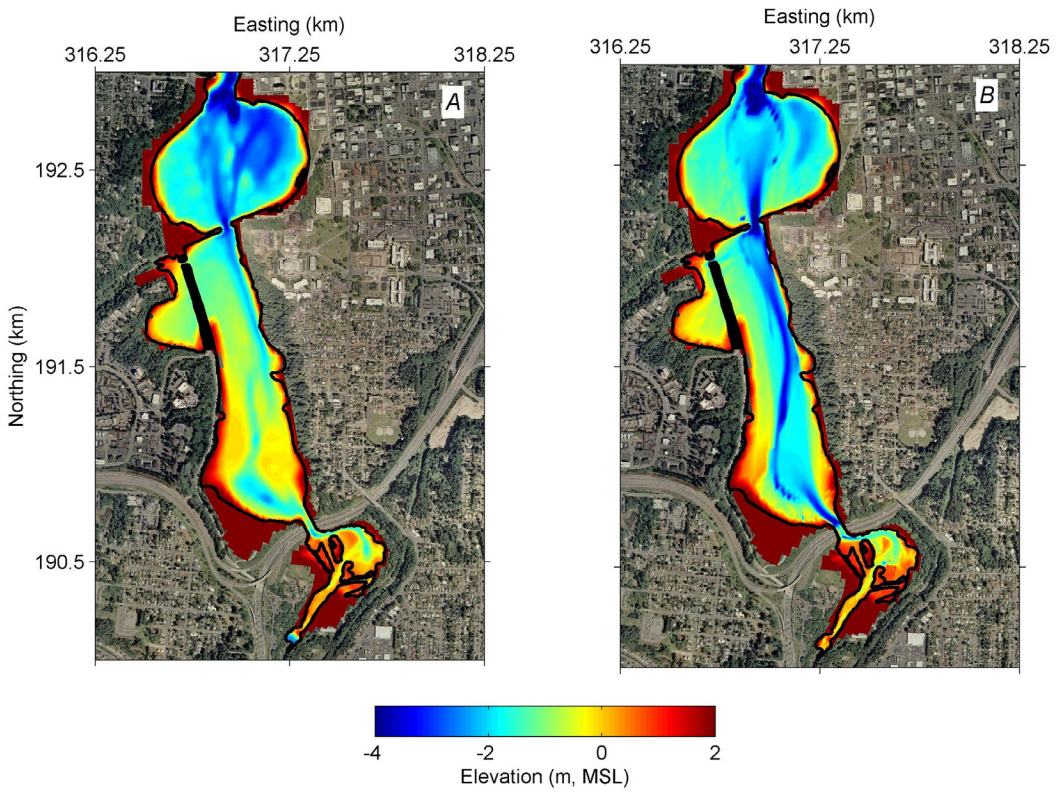

Figure 25. Maps of Capitol Lake showing long-term simulation results, *A*, initial bathymetry, and *B*, bathymetry 10 years after dam removal for the estuary restoration alternative.

The long-term model simulation suggests that the emergent estuary is not static, but will naturally continue to change, though much more slowly than initially after dam removal.

The rate of volume change within the first year is not constant (fig. 29). Rather, the rate of morphological change is associated with the flow conditions on the Deschutes river. The most rapid changes in the estuary occur during the first and largest flood event. Subsequent smaller flood events also increase the rate of morphological change in the first year. Morphological changes to the estuary bed do occur during low river-flow conditions, though at a much slower rate.

Coinciding with the patterns of erosion and deposition in the restored Deschutes Estuary are changes to the bed grain size (fig. 30). The changes in bed grain size are most dramatic in the first year after dam removal. In general, the emergent surface grain-size distributions become typical of a tidally influenced estuary. The off-channel areas become finer, and the channels become coarser. In particular, the percentage of clay sized sediment (<4 µm) increases up to 40 percent in the off channel areas of North Basin and as high as 90 percent in Percival Cove. Otherwise, the percentage of clay-sized particles within the restored estuary remains low (<25 percent). Silt-sized (4-62.6 µm) particles increase up to 90 percent in the off-channel areas of North Basin and in some areas of Middle Basin after dam removal. Sand-sized (62.5 – 2000 µm) particles dominate grain size distribution in the channel that develops in central North Basin and throughout much of Middle Basin. The increase in sand sized particles is associated with localized erosion and channel development. In subsequent years after the dam is removed, the surface grain-size distributions change more slowly.

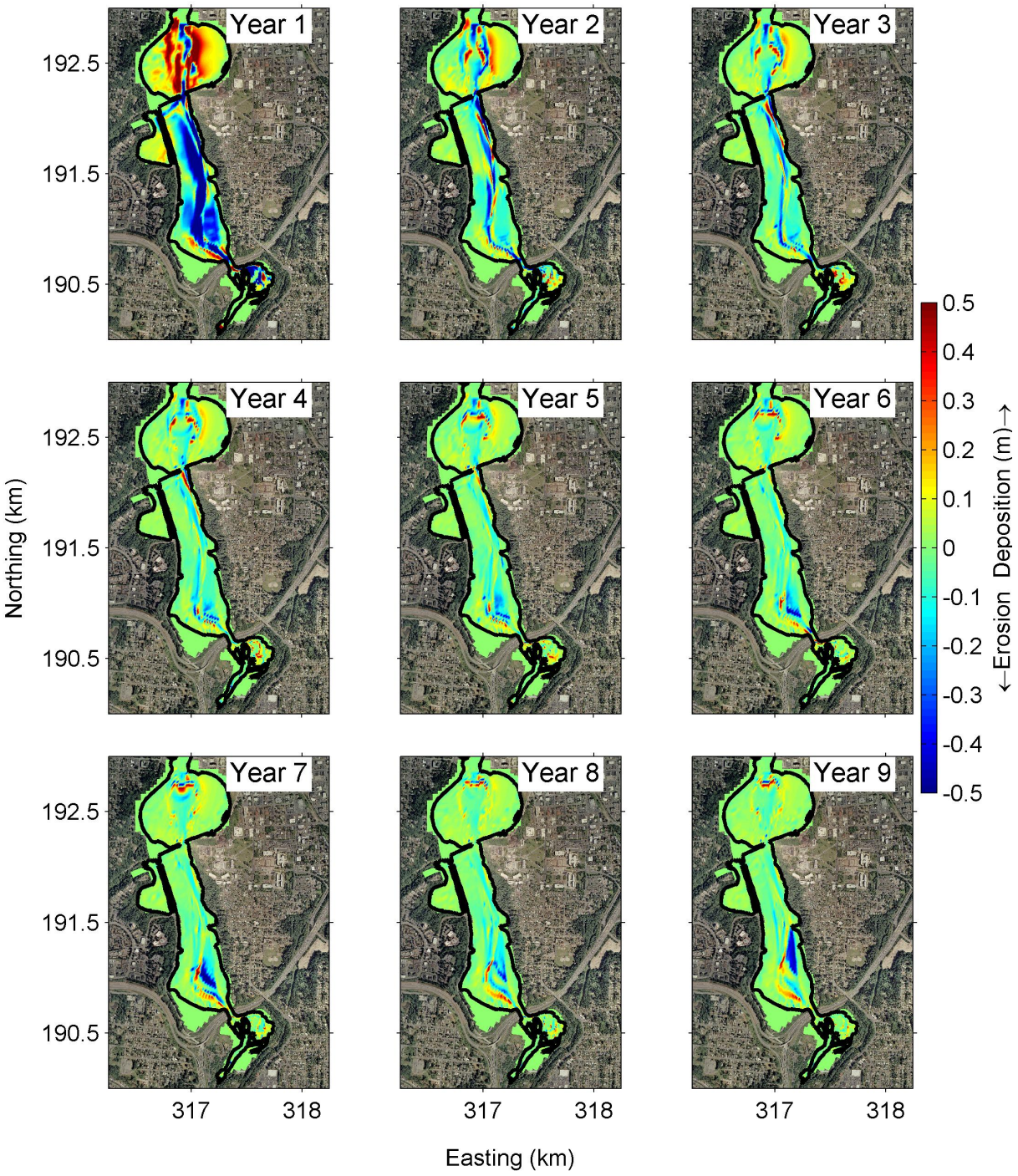

Figure 26. Maps of Capitol Lake showing yearly patterns of erosion and deposition for the long-term simulation of the estuary restoration alternative. For year 1, the erosion and deposition shown is the difference between the initial bathymetry and the bathymetry 1 year after dam removal. Subsequent years are the difference between the bathymetry of the current and the previous year.

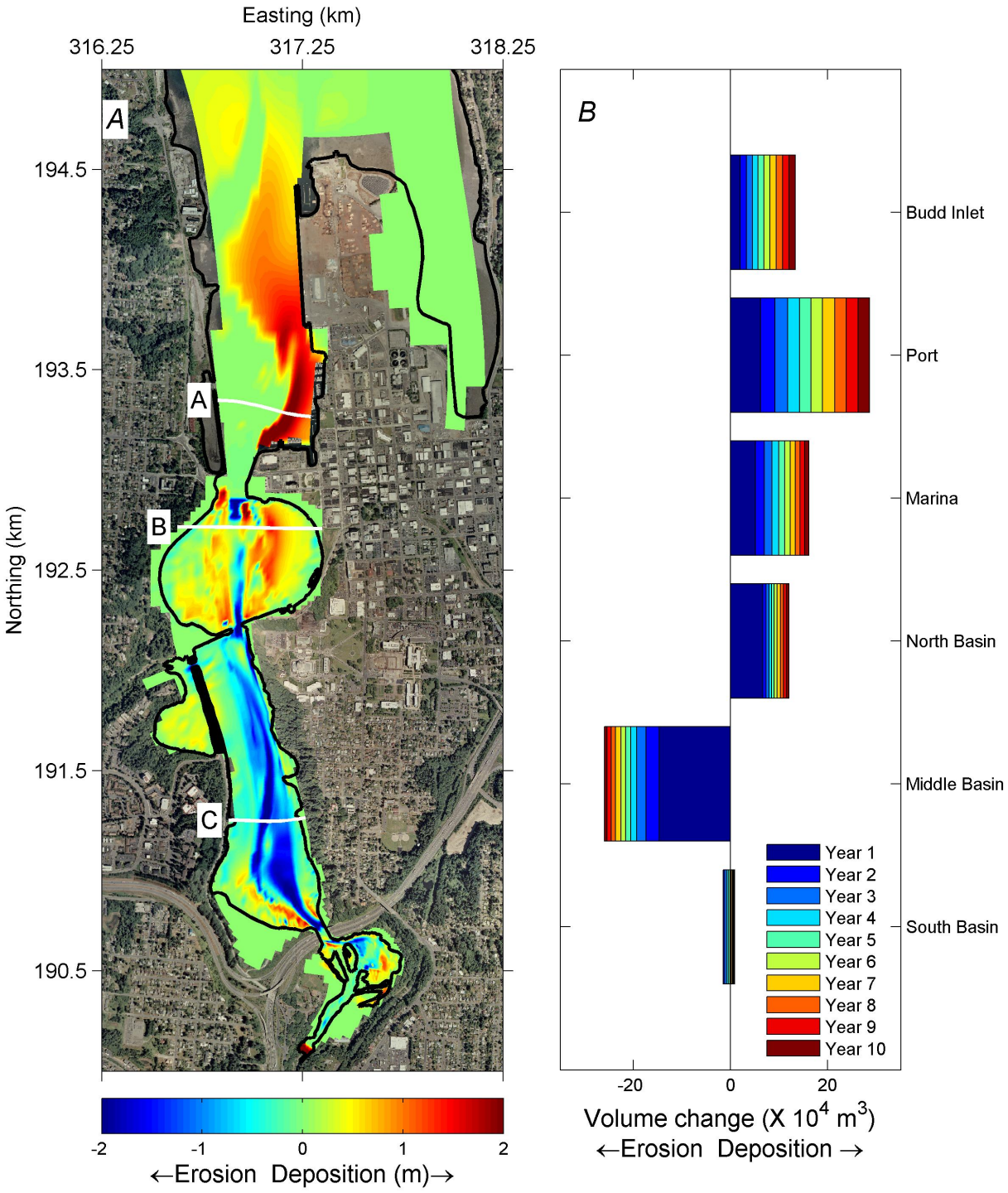

Figure 27. Results of long-term simulation with medium erodibility parameters showing, *A*, map of cumulative erosion and sedimentation. White lines in *A* show the locations of transects A, B and C shown in figure 28. *B*, Cumulative erosion or sedimentation shown for each of the regions of the model. Refer to figure 24 for the extents of each region.

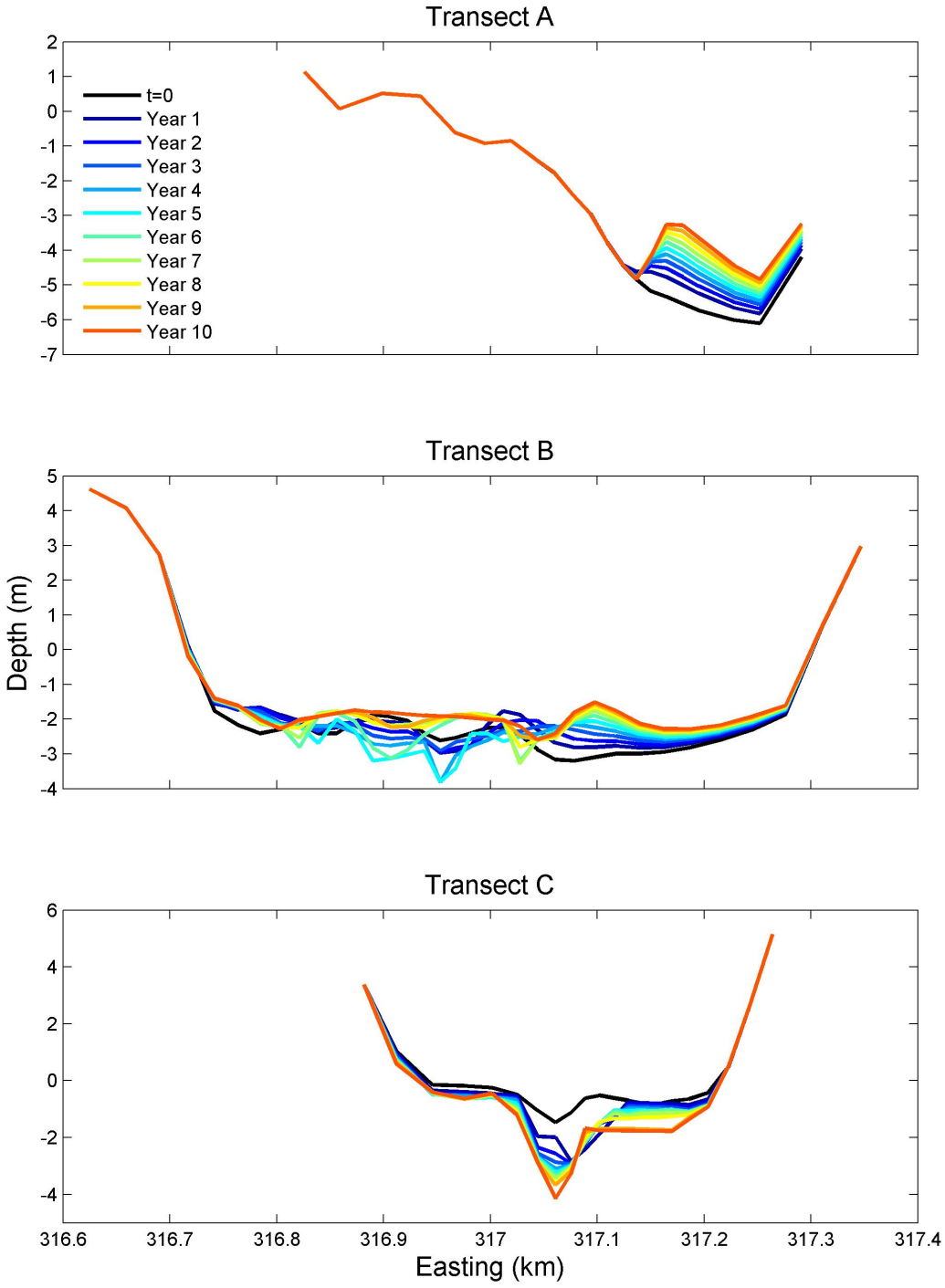

Figure 28. Cross-estuary transects at three locations (A, B, and C) showing the local changes in bottom depth over time. The locations of the transects are shown in figure 27.

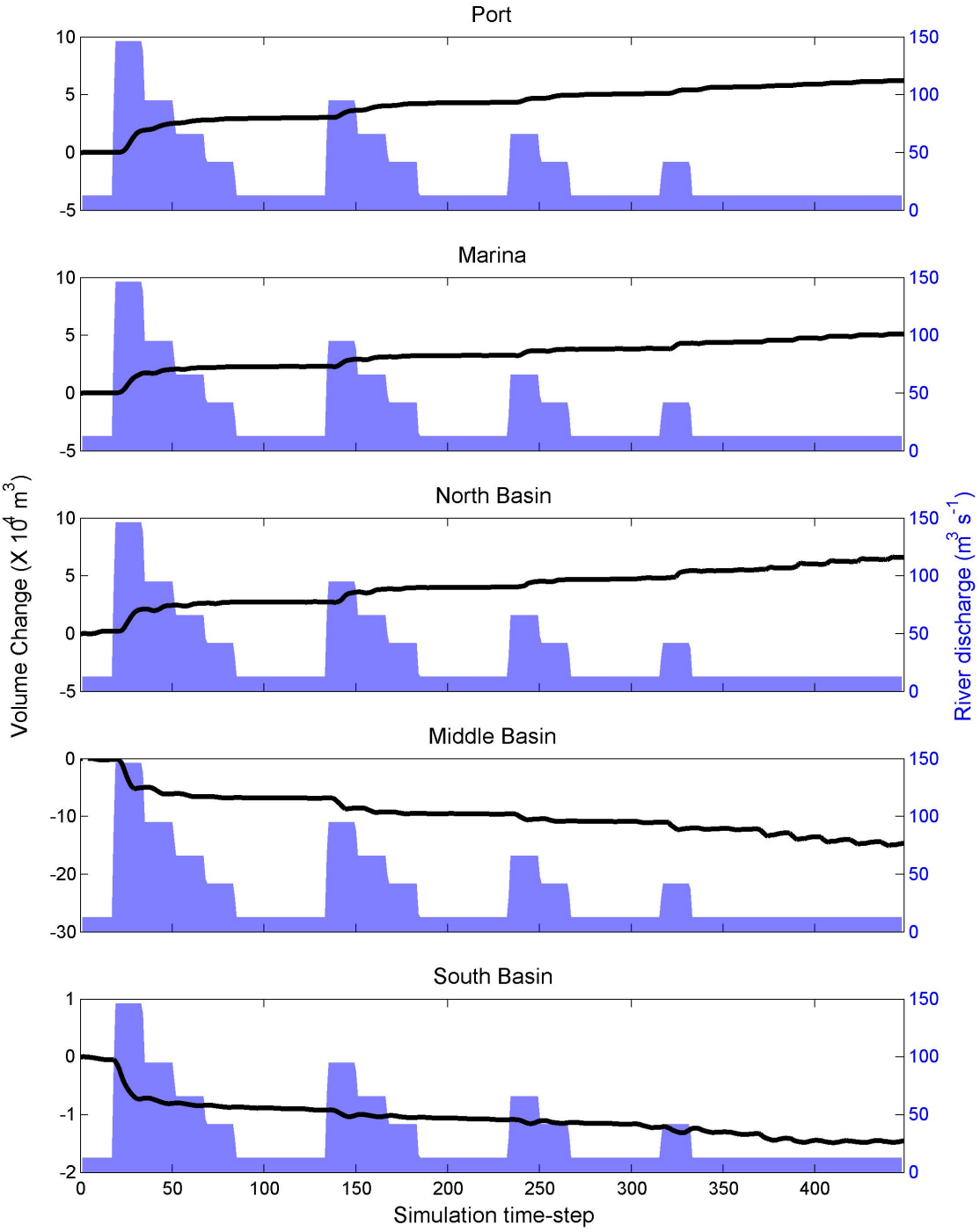

Figure 29. Time-series of cumulative erosion and sedimentation for each of the regions of interest in the model calculated for a one-year simulation with medium erodibility parameters. Negative volume change indicates erosion, and positive volume change indicates deposition. The simulated river flow throughout the year is shown in blue.

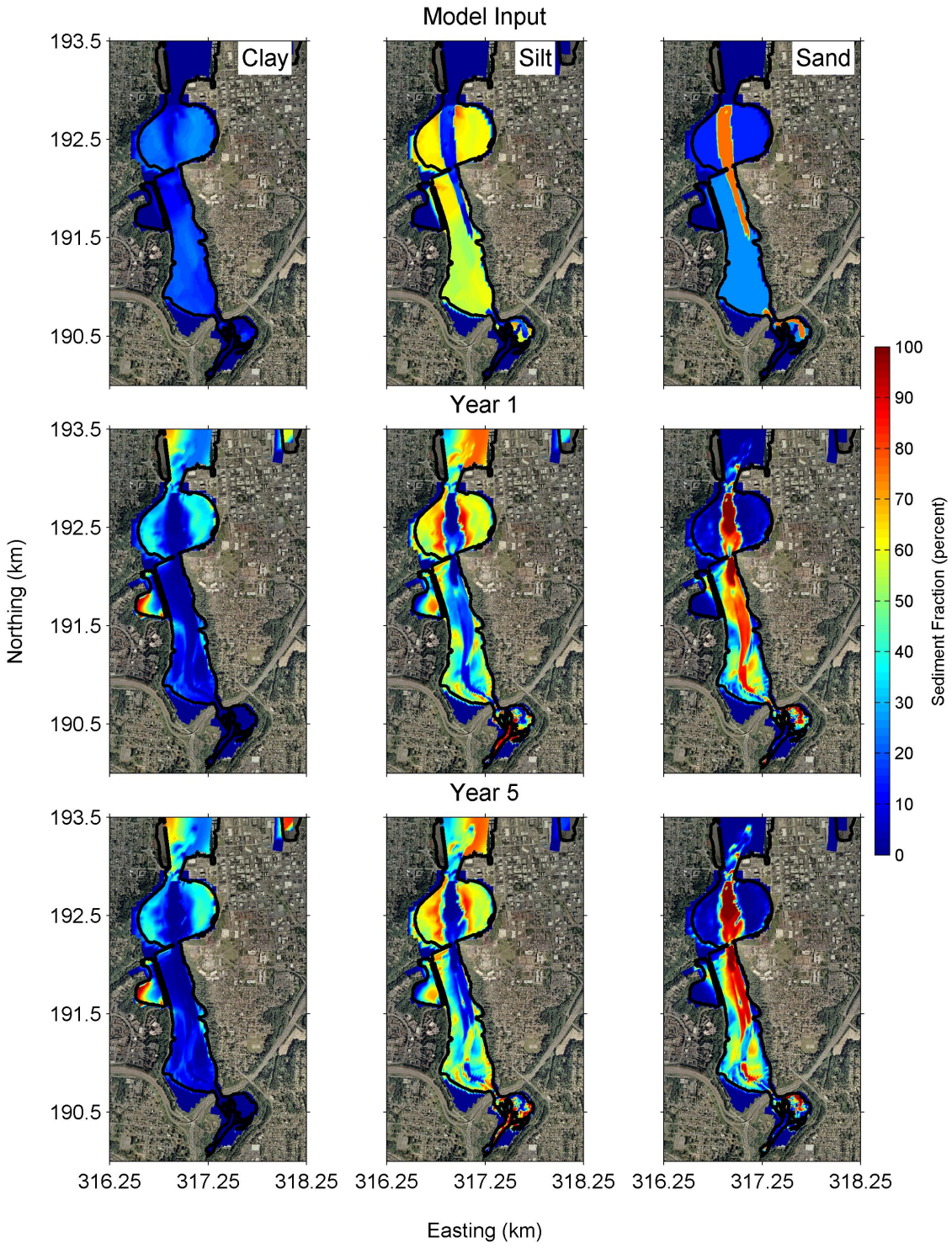

Figure 30. Maps of sediment grain size throughout Capitol Lake for the estuary alternative. The top panels show the schematization of clay-, silt-, and sand-sized particles derived from measurements of the cores collected from Capitol Lake. Subsequent panels show the simulated grain-size distributions 1 year and 5 years after dam removal.

Dual-Basin Estuary Alternative

Considerable changes occur in the bathymetry of the dual-basin estuary during the 10 years after dam removal (fig. 31). Morphological changes after 10 years are similar to those of the estuary alternative. Large amounts of sediment erode from South and Middle Basins in the first year after dam removal (figs. 32-33). In North Basin, a channel develops along a north-south axis from the railroad trestle to the entrance to lower Budd Inlet. Deposition occurs on the west side of the channel, while deposition on the east side of the channel is prevented by the dike structure. In Middle Basin, the channel present in the lake both deepens and widens (fig. 34). A large portion of the sediment that erodes from the lake in the first year is deposited in the Port, Marina, and lower Budd Inlet areas.

The morphological change in each of the basins decreases dramatically after the first year for the dual-basin estuary alternative (Table 5). In South and North Basins, initial net erosion in the first year gives way to deposition in following years. In other areas, the patterns of erosion and deposition in subsequent years resemble those observed after year one, although the magnitude of morphological change decreases. In contrast to the estuary restoration alternative, North Basin is essentially stable with little net volume change after 10 years. In the other areas, the morphology of the dual-basin estuary continues to change 10 years after dam removal. Middle Basin continues to erode at a rate of ~ 0.3×10^4 m^3 yr^{-1}, while South Basin, the Marina, and the Port, accumulate sediment at rates of approximately 0.2×10^4 m^3 yr^{-1}, 0.9×10^4 m^3 yr^{-1}, and 2.6×10^4 m^3 yr^{1}, respectively. The bottom sediment grain size changes coinciding with the patterns of erosion and deposition this restoration alternative as shown in figure 35.

Table 5. Sediment volume change ($\times 10^4$ m^3) the dual-basin estuary alternative in each region of interest over 10 years calculated by using medium values for each of the erodibility parameters.

Year	South Basin	Middle Basin	North Basin	Marina	Port	Budd Inlet
1	-1.42	-14.73	2.42	7.68	7.63	2.32
2	0.25	-2.70	-0.76	2.69	3.67	1.44
3	0.39	-1.80	-0.67	2.26	3.21	1.28
4	0.41	-1.35	-0.20	1.80	2.78	1.26
5	0.32	-1.16	-0.03	1.59	2.65	1.25
6	0.26	-1.07	-0.06	1.58	2.67	1.29
7	0.26	-1.17	0.01	1.41	2.77	1.35
8	0.23	-1.22	0.03	1.24	2.88	1.42
9	0.18	-0.91	-0.04	1.10	2.88	1.45
10	0.15	-0.30	-0.02	0.91	2.62	1.39
Sum	**1.04**	**-26.40**	**0.67**	**22.25**	**33.77**	**14.45**

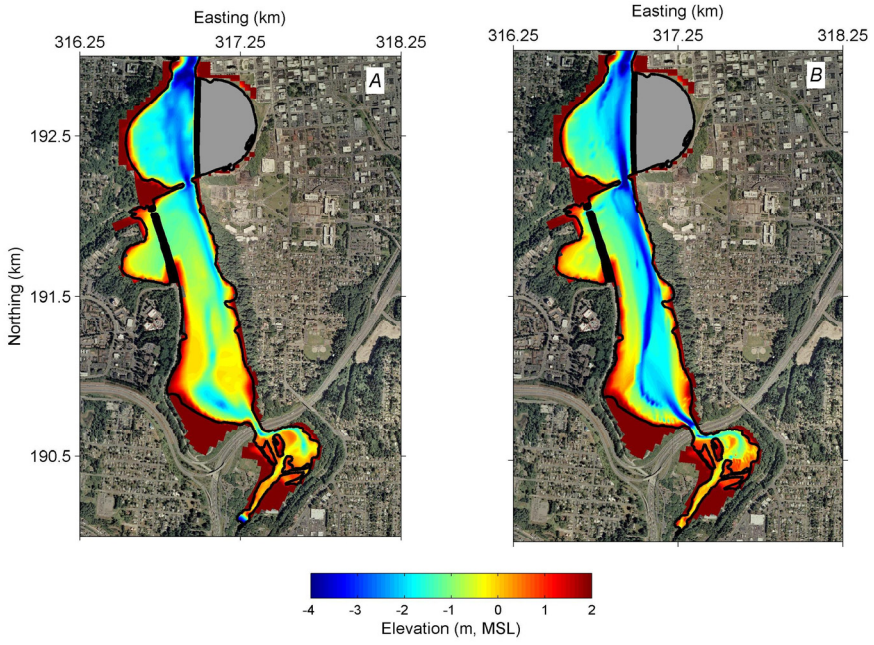

Figure 31. Maps of Capitol Lake showing long-term simulation results, *A*, initial bathymetry, and *B*, bathymetry 10 years after dam removal for the dual-basin estuary alternative.

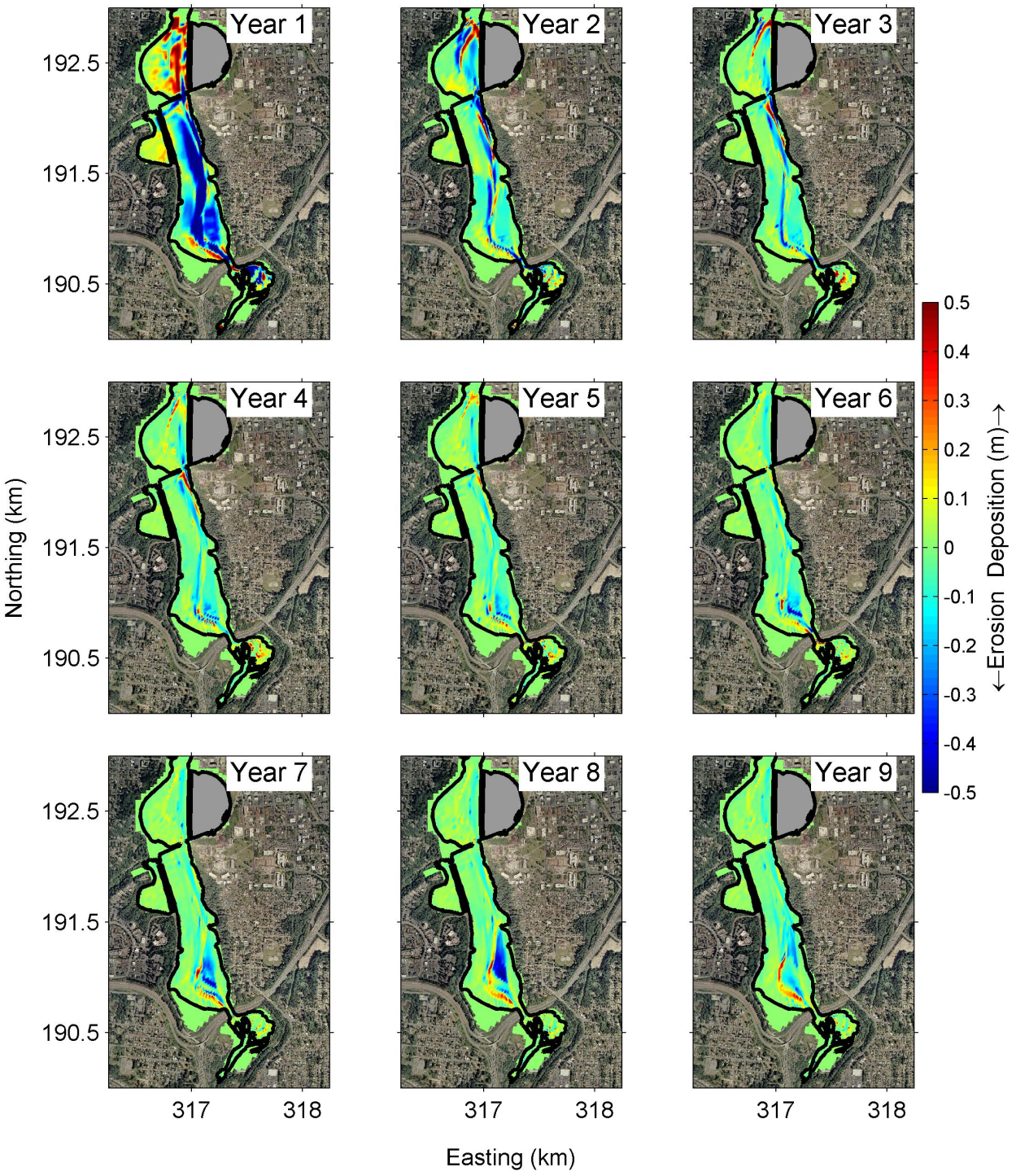

Figure 32. Maps of Capitol Lake showing yearly patterns of erosion and deposition for the long-term simulation of the dual-basin estuary alternative. For year 1, the erosion and deposition shown is the difference between the initial bathymetry and the bathymetry 1 year after dam removal. Subsequent years are the difference between the bathymetry of the current and the previous year.

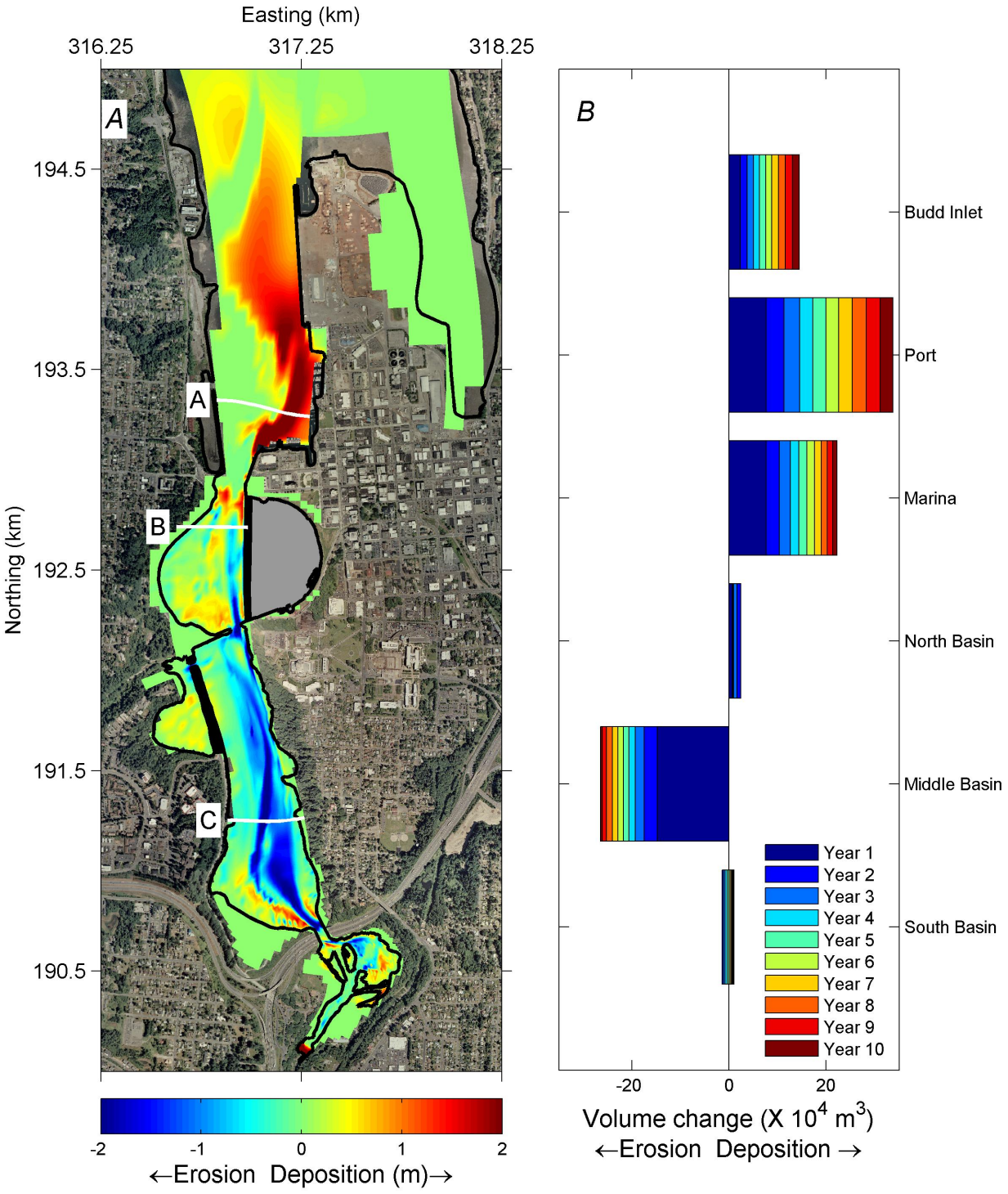

Figure 33. Results of long-term simulation of the dual-basin estuary alternative showing, *A*, map of cumulative erosion and sedimentation. White lines in *A* show the locations of transects A, B and C shown in figure 34. *B*, Cumulative erosion or sedimentation shown for each of the regions of the model. Refer to figure 24 for the extents of each region.

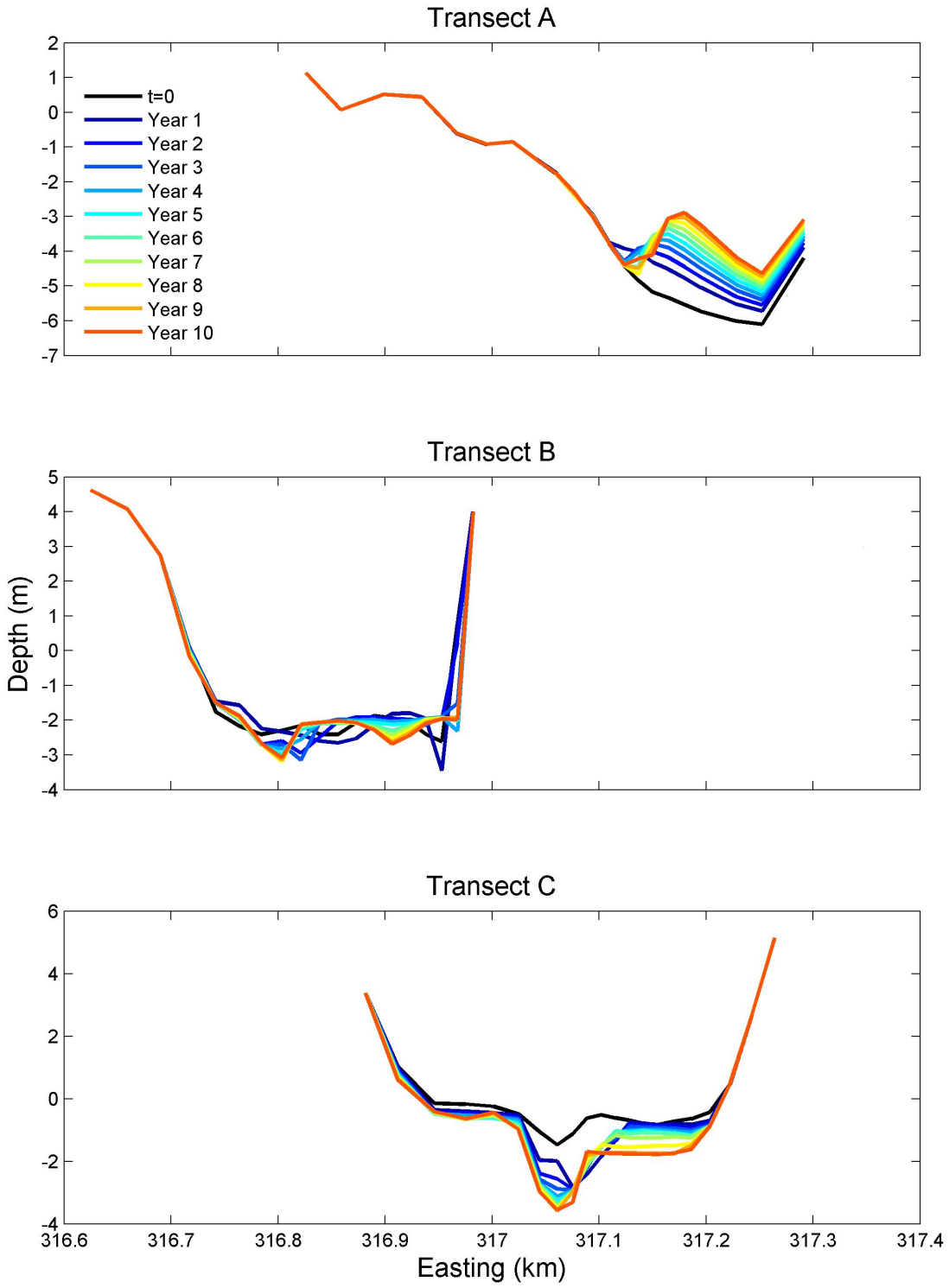

Figure 34. Cross-estuary transects at three locations (A, B, and C) showing the local changes in bottom depth over time. The locations of the transects are shown in figure 33.

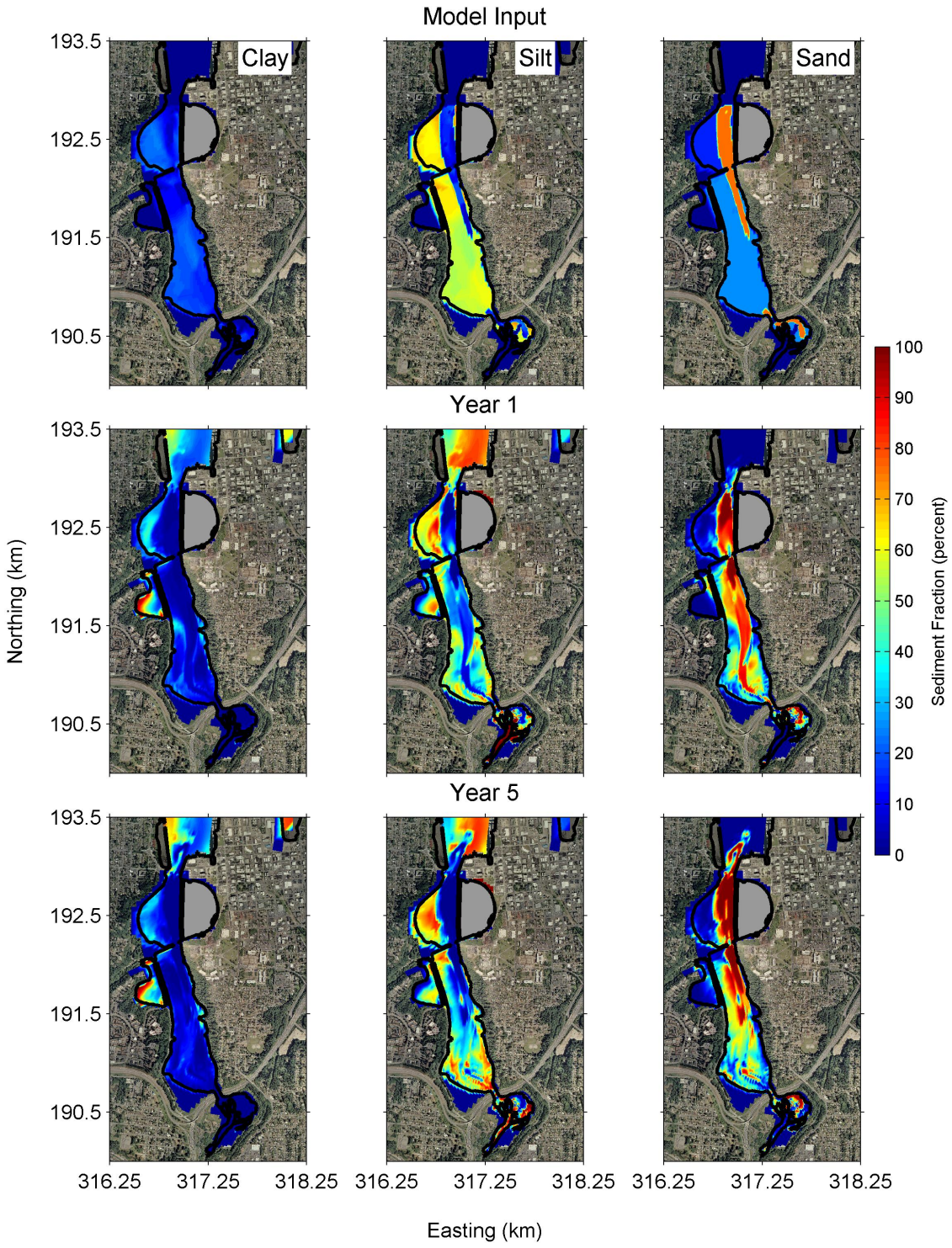

Figure 35. Maps of sediment grain size throughout Capitol Lake for the dual-basin estuary restoration alternative. The top panels show the schematization of clay-, silt-, and sand-sized particles derived from measurements of on the cores collected from Capitol Lake. Subsequent panels show the simulated grain-size distributions 1 year and 5 years after dam removal.

Comparison Between Estuary and Dual-Basin Estuary Alternatives

The evolved bathymetry that emerges after 10 years resembles that of the predam estuary for both restoration alternatives (fig. 36). The channel in Middle and North Basins becomes more pronounced compared with the current lake bathymetry. The depth distribution of the restored estuary for both scenarios more closely resembles the depth distribution of the predam estuary than of the present-day lake (fig. 37). The percentages of surface area for elevations between -5 m and 2 m show close similarities for the restored and predam estuaries, particularly for depths greater than 3 m.

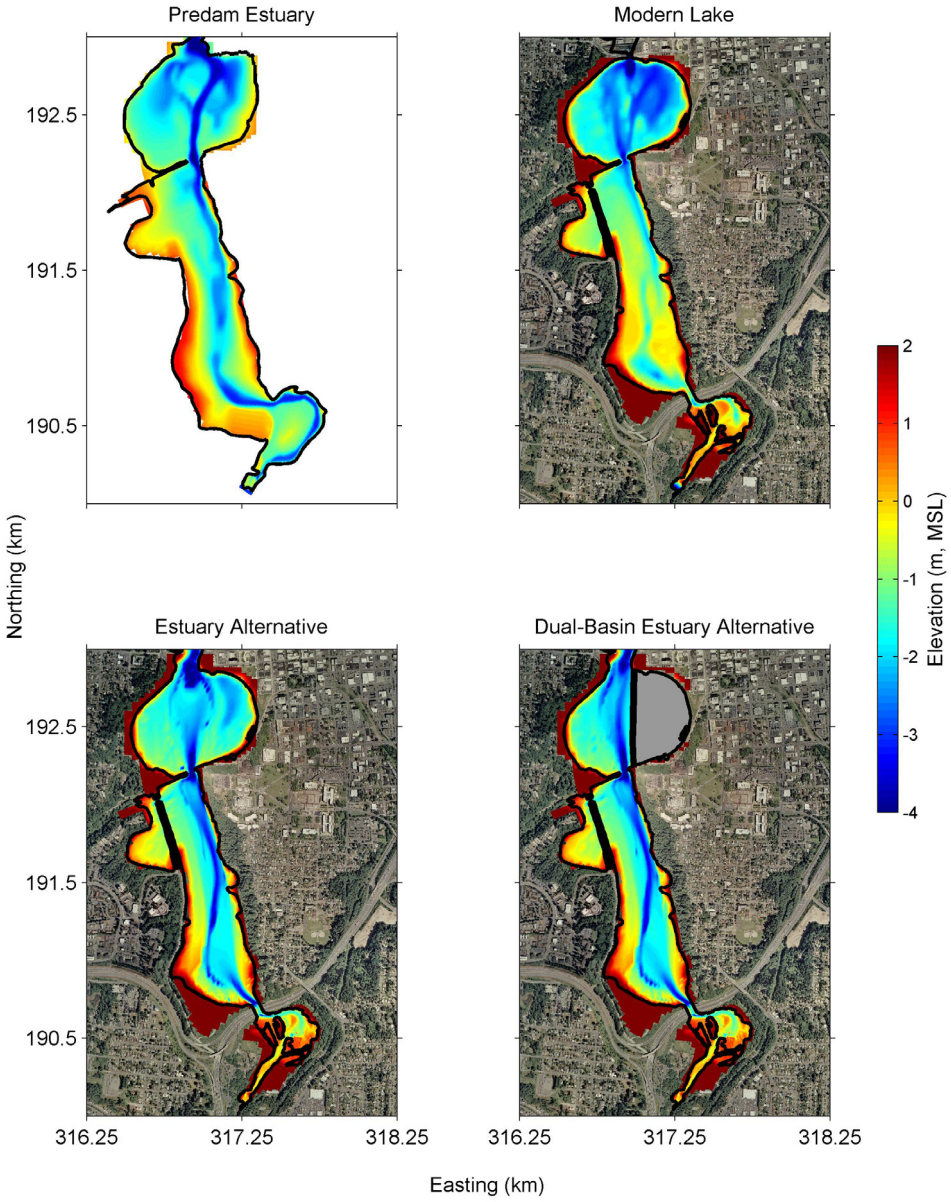

Figure 36. Maps showing comparison of predam bathymetry (top, left) and present lake bathymetry (top, right) with evolved bathymetry for the two restoration alternatives (bottom left and right) after 10-year morphological simulations.

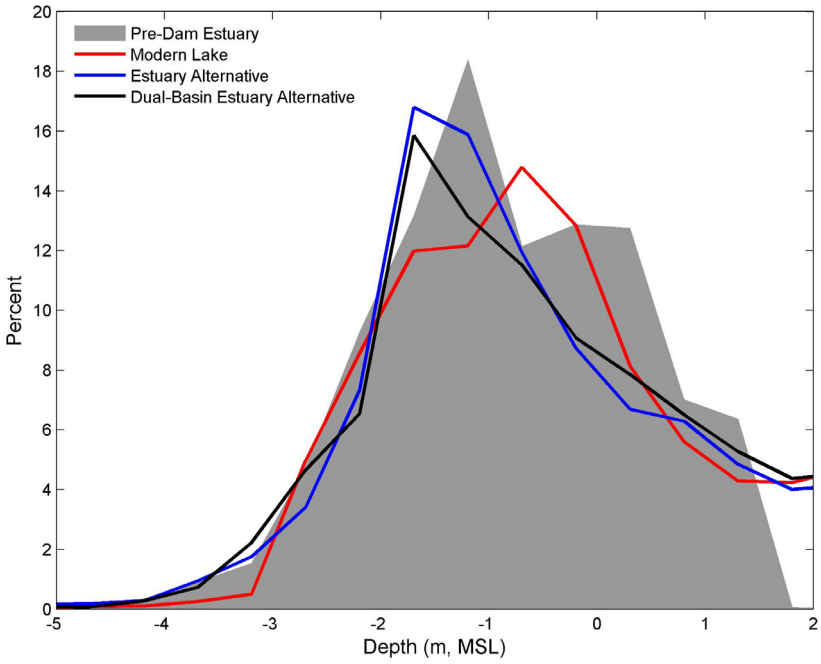

Figure 37. Comparison of the depth distributions between the predam estuary (gray area), modern lake (red line), the estuary alternative (blue line), and the dual-basin estuary alternative. For each case, the area in each depth bin shown is normalized by the total area between -5 and 2 m, mean sea level.

The volume change in Middle and South Basins is virtually identical between both restoration alternatives (fig. 38, tables 4 and 5). On the other hand, there is a marked difference in the volume change that occurs in North Basin between the two restoration alternatives. Approximately 12×10^4 m^3 of sediment accumulate in North Basin with the estuary restoration alternative, whereas less than 1×10^4 m^3 accumulate if the dual-basin estuary alternative is used. The sediment that is trapped on the eastern side of North Basin in the estuary alternative deposits in lower Budd Inlet and the Marina and Port areas in the dual-basin estuary alternative. After 10 years, the difference in volume change between the two alternatives in the Port and Marina areas is 11.3×10^4 m^3.

The differences in the patterns of erosion and deposition between the two restoration alternatives in North Basin and the Port and Marina are accompanied by differences in the bottom grain-size distributions in those areas (compare figs. 30 and 35). A greater percentage of sand-sized particles is observed in North Basin for the dual-basin estuary alternative. In the area to the north of North Basin, large areas become predominantly sandy, whereas in the estuary alternative, they do not.

Predam Removal Dredge and Fill

Dredging has been proposed in Middle and North Basins prior to dam removal in order to reduce sedimentation in the Port and Marina areas. Two model simulations were carried out to investigate the effect of dredging prior to dam removal on the volume of sediment that deposits in the Port and Marina areas. The predam removal dredge bathymetry (fig. 39) was designed by engineers based on the results of long-term morphological simulations presented above (Moffatt and Nichol, 2007). The design consists of dredging Middle and North Basins where long-term simulations suggest a channel will develop after dam removal. The dredged material would be placed along the Deschutes Parkway in Middle and North Basins. Thus, the proposed dredging is intended to resemble the natural morphology that emerges after dam removal. For the model simulations, only the bathymetry was altered for the predam removal dredge scenario. The thickness of available sediment, grain-size distributions, and the erodibility parameters were identical to the long-term morphological simulations presented above.

The patterns of erosion and deposition after three years for both restoration scenarios

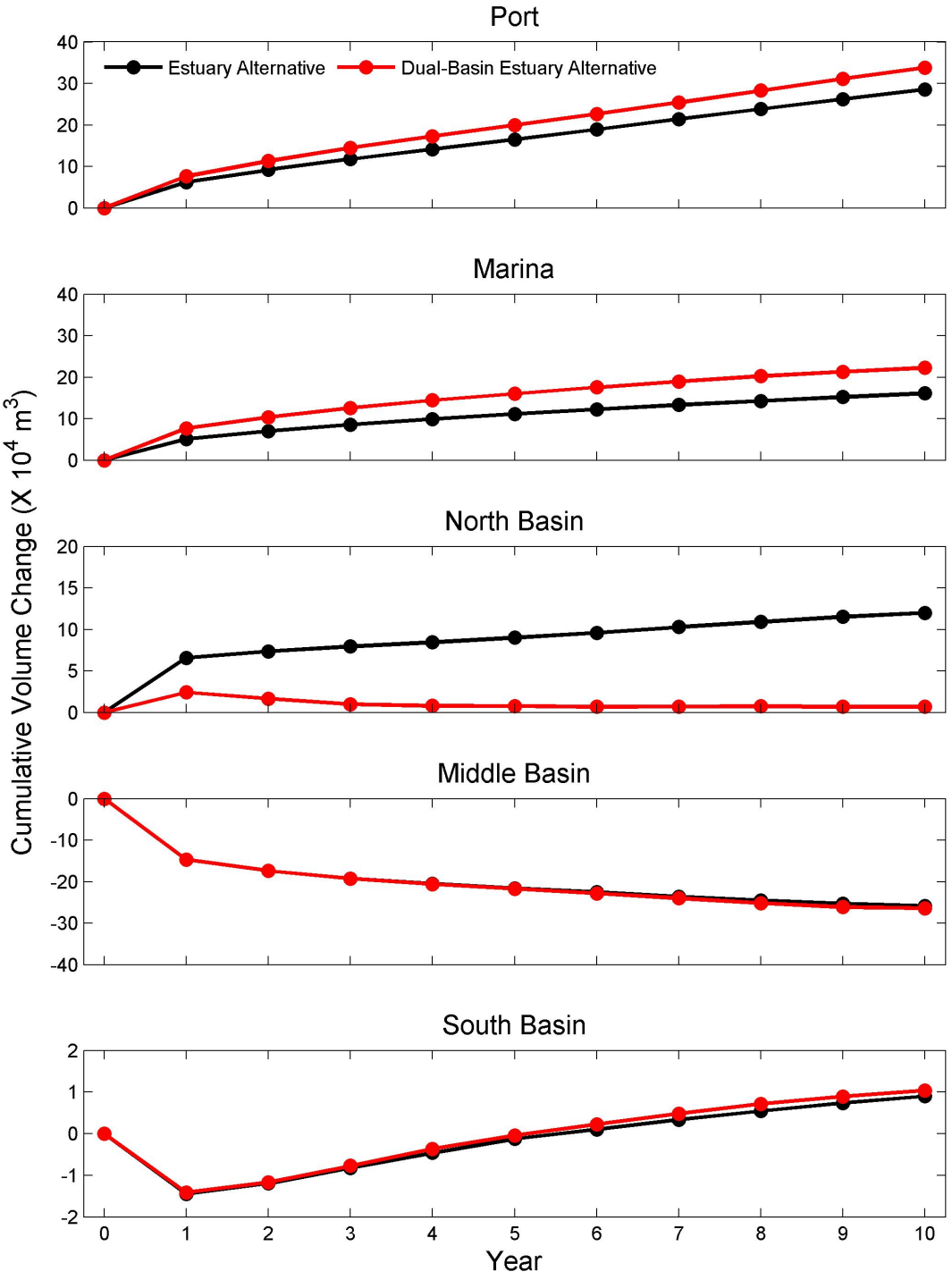

Figure 38. Time-series of cumulative erosion and sedimentation comparing the volume change in each of the regions between the estuary alternative (black line) and the dual-basin estuary alternative (red line). Negative volume change indicates erosion, and positive volume change indicates deposition.

including dredging are shown in figures 40 and 41. For the estuary restoration alternative, no net erosion occurs in Middle Basin. Only a small area of erosion occurs just north of the Interstate 5 bridge, while much larger areas are depositional. Both North Basin and the Port and Marina areas experience deposition in both restoration scenarios. However, the amount of net deposition in North Basin is much less for the dual-basin estuary alternative than for the estuary alternative. Concomitantly, the amount of sediment deposition in the Port and Marina areas is greater in the dual-basin estuary alternative compared to the estuary alternative.

Dredging Middle and North Basins prior to dam removal reduces the volume of sediment that accumulates in the Port and Marina areas (table 6). For the estuary alternative, dredging the lake prior to dam removal decreases the amount of sediment deposited near the Port and Marina from 20.3×10^4 m^3 to 8.6×10^4 m^3after 3 years.

Table 6. Sediment volume change ($\times 10^4$ m^3) in the Port and Marina areas after 3 years comparing the sediment accumulation that occurs with and without dredging prior to dam removal.

	Estuary alternative		Dual-basin estuary alternative	
Year	No dredge	Pre-dredge	No dredge	Pre-dredge
1	11.33	3.13	15.31	5.20
2	4.83	2.86	6.36	3.96
3	4.18	2.66	5.47	3.49
Sum	**20.34**	**8.65**	**27.14**	**12.66**

For the dual-basin estuary alternative, dredging the lake prior to dam removal decreases the amount of sediment deposited near the Port and Marina from 27.1×10^4 m^3 to 12.7×10^4 m^3 after 3 years. The effect of dredging prior to dam removal is largest during the first year. In subsequent years, the difference in the magnitude of morphological change due to dredging is reduced.

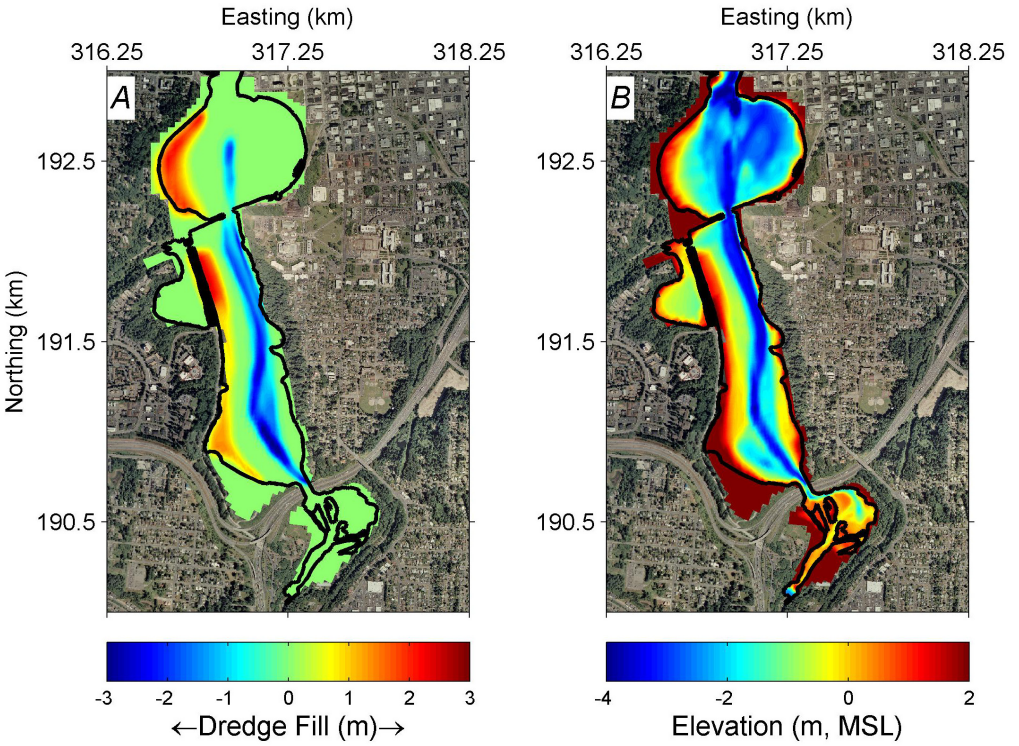

Figure 39. Predam removal dredge scenario designed by engineers (Mofatt and Nichol, 2008) showing, *A*, proposed dredge (blue) and fill (red) areas, and *B*, modified bathymetry after dredging.

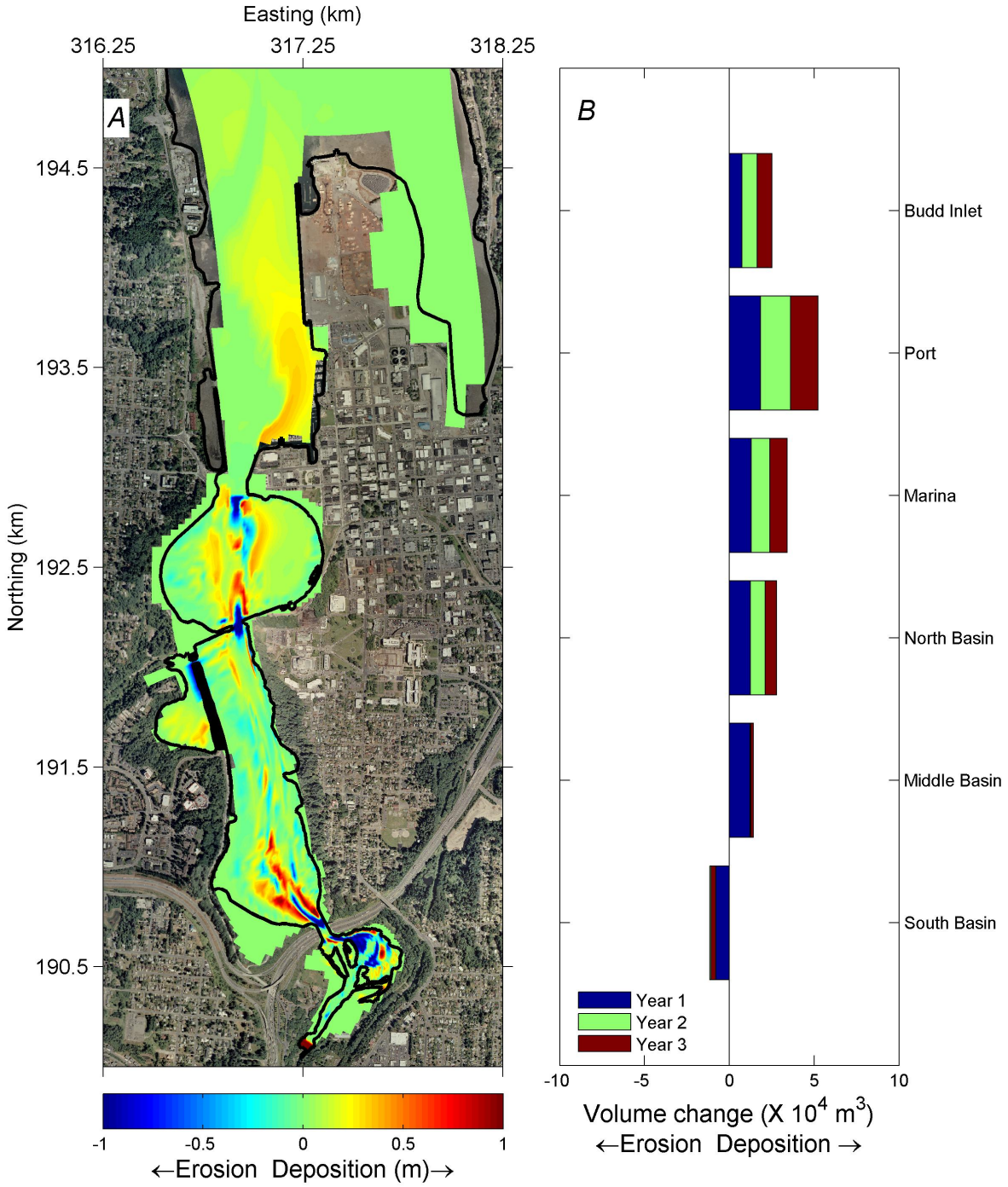

Figure 40. Results of 3-year simulation for the estuary alternative with medium erodibility parameters and predam removal dredging. *A*, Map of cumulative erosion and sedimentation. *B*, Cumulative erosion or sedimentation for each of the regions of the model. Refer to figure 24 for the extents of each region.

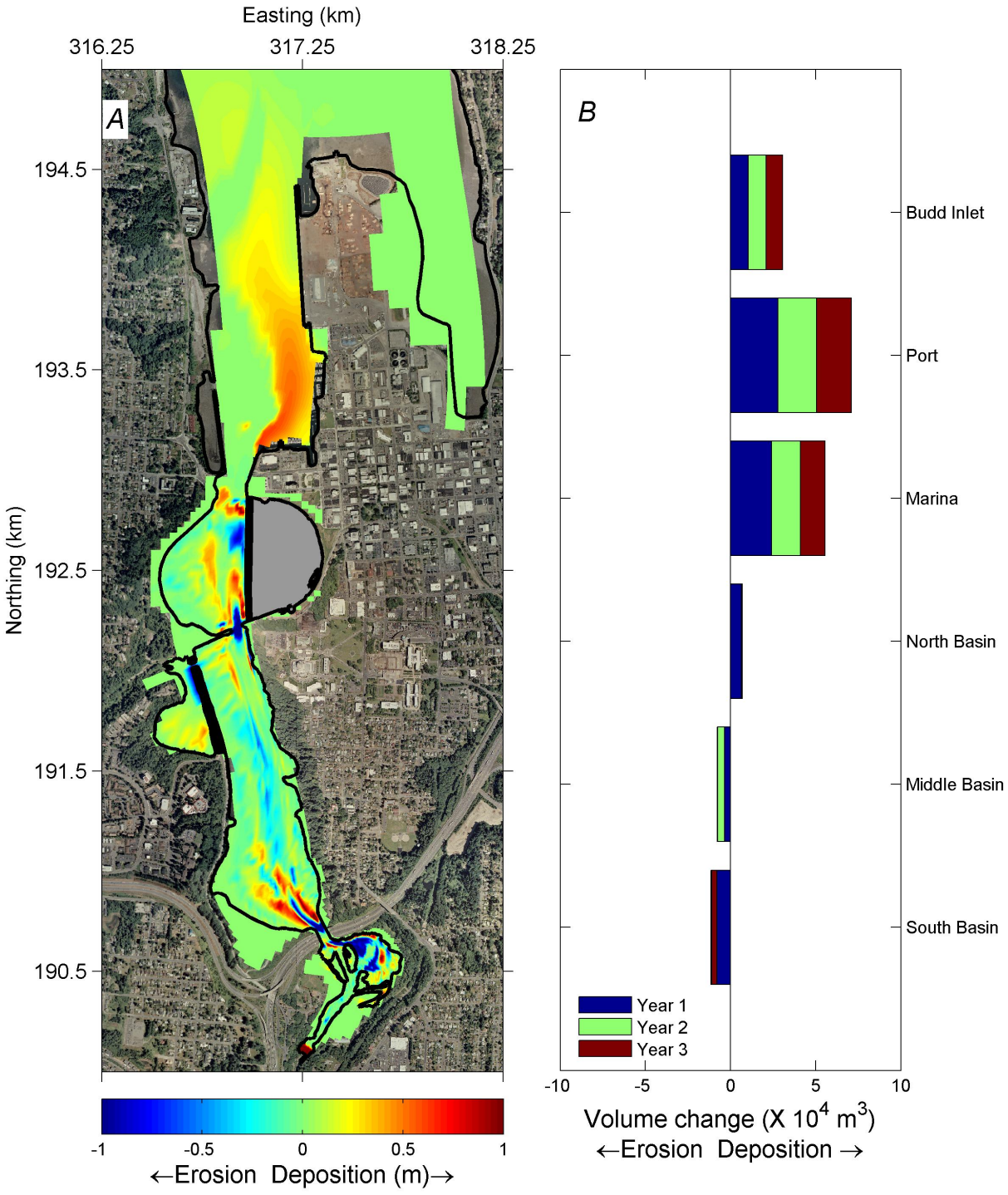

Figure 41. Results of 3-year simulation for the dual-basin estuary restoration alternative with medium erodibility parameters and predam removal dredging. *A*, Map of cumulative erosion and sedimentation. *B*, Cumulative erosion or sedimentation is shown for each of the regions of the model. Refer to figure 24 for the extents of each region.

Comparison between Phase I and Phase II

This section examines the result of changing the erodibility parameters from the Phase I values obtained from the literature (table 7) to the Phase II medium values (table 2) used in long-term simulations. The magnitude of erosion and deposition in Phase II model simulations is in between the low and high range of values reported in Phase I for both restoration alternatives (figs. 42 and 43). For instance, in the estuary alternative, the 20.3×10^4 m^3 of sediment that deposits after 3 years in the Port and Marina in Phase II is a 62-percent increase over the Phase I lower value and a 28-percent decrease from the Phase I higher value. If the lake is dredged prior to dam removal, the amount of sediment that deposits in the Port and Marina areas is 31 percent less than in the Phase I simulations with lower erodibility after 3 years. There are similar differences between Phase I and Phase II simulations in the amount of morphological change for the dual-basin estuary alternative .

Table 7. Values of the erodibility parameters used for the sensitivity analysis in Phase I.

Parameter	Lower	Higher
Dry sediment density (kg m^{-3})	1,000	1,000
Critical shear stress (Pa)	0.3	0.2
Erosion rate parameter (kg m^{-2} s^{-1})	0.00025	0.0005

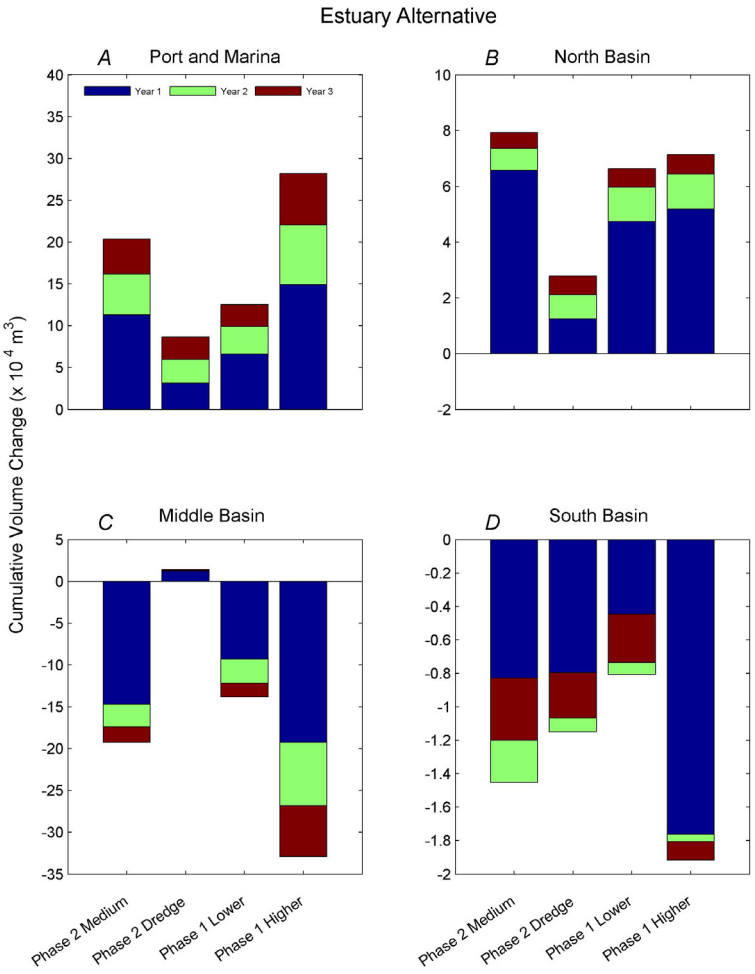

Figure 42. Cumulative volume change ($\times$ 10^4 m^3) after 3 years for the estuary alternative comparing Phase II medium erodibility values (with and without dredging prior to dam removal) and the Phase I lower and higher erodibility values in *A*, Port and Marina, *B*, North Basin, *C*, Middle Basin, and *D*, South Basin. See tables 2 and 7 for the value of each erodibility parameter used in Phase II and Phase I, respectively.

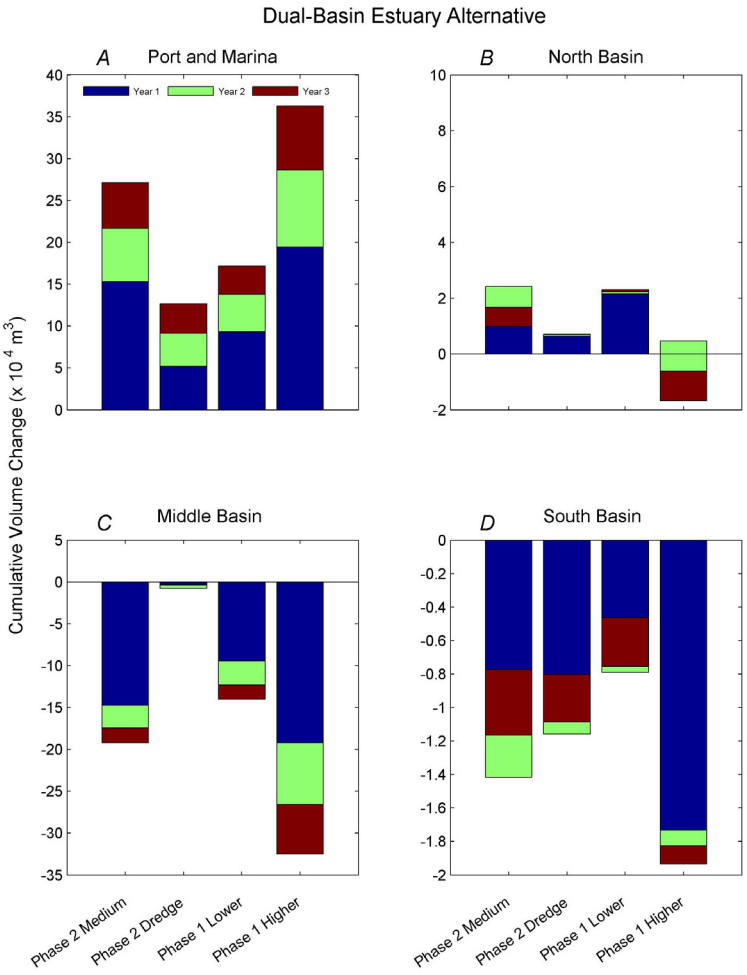

Figure 43. Cumulative volume change ($\times 10^4$ m^3) after 3 years for the dual-basin estuary alternative comparing Phase II medium erodibility values (with and without dredging prior to dam removal) and the Phase I lower and higher erodibility values in *A*, Port and Marina, *B*, North Basin, *C*, Middle Basin, and *D*, South Basin. See tables 2 and 7 for the value of each erodibility parameter used in Phase II and Phase I, respectively.

All three of the erodibility parameters, as well as the grain-size schematization, were changed from Phase I values to incorporate information obtained from the field. In order to understand how changing each parameter affected sediment transport, 6 simulations were conducted by varying each parameter one at a time (table 8). The first two simulations were run by using the lower erodibility parameters used in Phase I and a dry sediment density of 1,000 kg/m^3 and 500 kg/m^3 for simulation S0 and S1, respectively. For reference, simulation S0 is equivalent to the Phase I lower erodibility value. Erodibility parameters for simulations S3-S6 are changed one at a time towards the medium values used in Phase II long-term simulations. The spatial patterns of erosion and deposition are

Table 8. Erodibility parameters used in for simulations S0-S6 to investigate the differences between Phase I and Phase II.

Sim. ID	Dry sediment density (kg m^{-3})	Critical shear stress (Pa)	Erosion rate parameter (kg m^{-2} s^{-1})	Sediment map
S0	1,000	0.3	0.00025	Phase I
S1	500	0.3	0.00025	Phase I
S3	500	0.3	0.00025	Phase II
S4	500	0.48	0.00025	Phase II
S5	500	0.48	0.00393	Phase II
S6	421	0.48	0.00393	Phase II

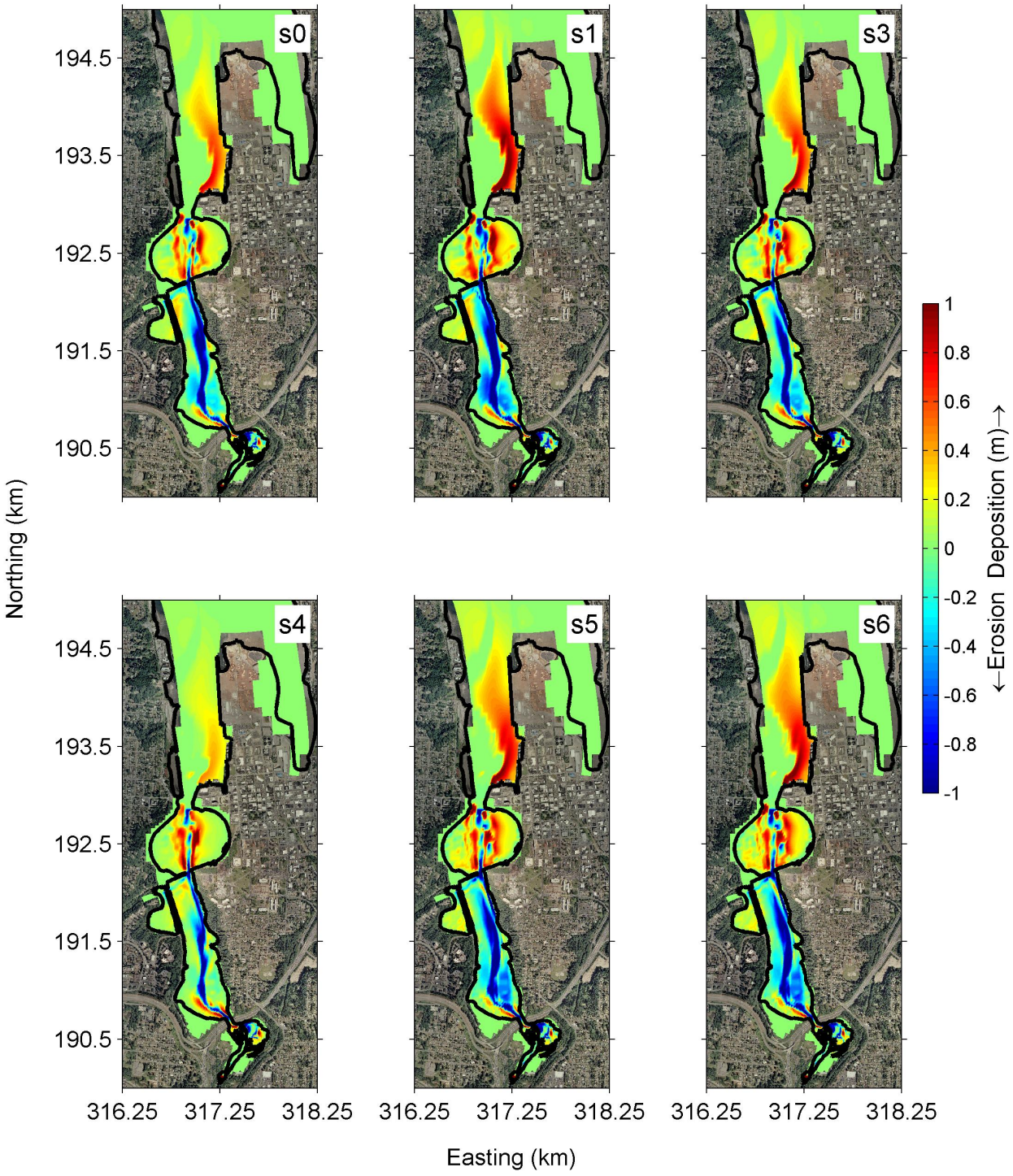

Figure 44. Maps showing erosion and sedimentation after 3 years for simulations S0-S6 for the estuary restoration alternative. The erodibility parameters used in each of these simulations can be found in table 8.

largely similar for each of the 6 simulations (fig. 44). Net erosion is predicted in Middle Basin, while the off-channel zones in North Basin and the Port and Marina areas are depositional. The main channel in Middle and North Basins deepens and widens. Despite their similarities, some differences in the spatial patterns of sediment transport are evident. The main difference between the simulations is the extent of channel widening and erosion of the shallow flats in Middle Basin. The erosion of tidal flats is limited for simulation S4 compared to S3, indicating that the critical shear stress has a strong influence over the width of the main channel. However, the erosion rate parameter also influenced the width of the main tidal channel, as evidenced by the difference between S4 and S5.

Seemingly small differences in the patterns of erosion and deposition can result in large differences in the magnitude of morphological change (fig. 45). The amount of sediment that erodes from Middle Basin and deposits in the Port and Marina after 3 years varies widely between simulations S0 through S6. For instance, the amount of sediment that deposits in the Port and Marina for simulation S6 (20.3×10^4 m^3) is more than twice the amount predicted for simulation S4 (8.9×10^4 m^3). Increasing the sand content relative to the mud content in the estuary bed, and increasing the critical shear stress, resulted in less sediment transport overall. On the other hand, increasing the erosion rate coefficient and decreasing the dry sediment density increased the magnitude of morphological change.

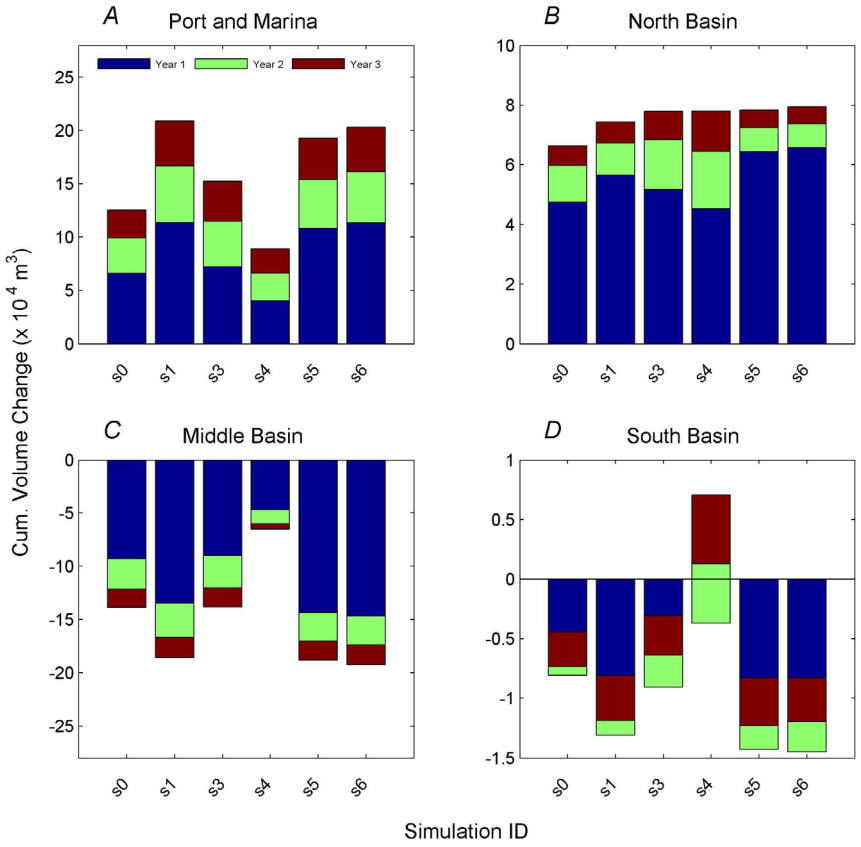

Figure 45. Cumulative volume change ($\times 10^4$ m^3) after 3 years in simulations S0 through S6 for *A*, Port and Marina, *B*, Middle Basin, *C*, North Basin, and *D*, South Basin. Negative numbers indicate erosion, and positive numbers indicate accretion in a basin. See table 8 for the erodibility parameters used in the simulations.

Sensitivity Analysis

The medium measured values represent the most-likely (table 3) and best singular approximation of the erodibility parameters that integrates the variability observed in the field data. However, a wide range in each of the parameters is observed in the data, and it is worthwhile to explore how the range of observed parameters affect the simulated sediment transport in the model. Model simulations were carried out by using 14 combinations of the high, medium and low values for each of the erodibility parameters (table 3). The morphological change that occurs in the simulations is highly variable over the range of erodibility parameters applied in the model (fig. 46). The volume of sediment that accumulates in the Port and Marina areas after 3 years ranges from 11×10^4 m^3 to 71×10^4 m^3 for simulations p14 and p6, respectively. In the Port and Marina, 6 of the 14 simulations fall within the range of sediment transport reported in Phase I (fig. 46, gray bars), while a single simulation predicts less sediment accumulation. More sediment accumulates in the Port and Marina in the remaining 7 simulations than was reported in Phase I. Similar ranges in the volume of sediment change occur in other areas in the restored estuary. These ranges constrain the sediment transport prediction over the range of observed erodibility parameters.

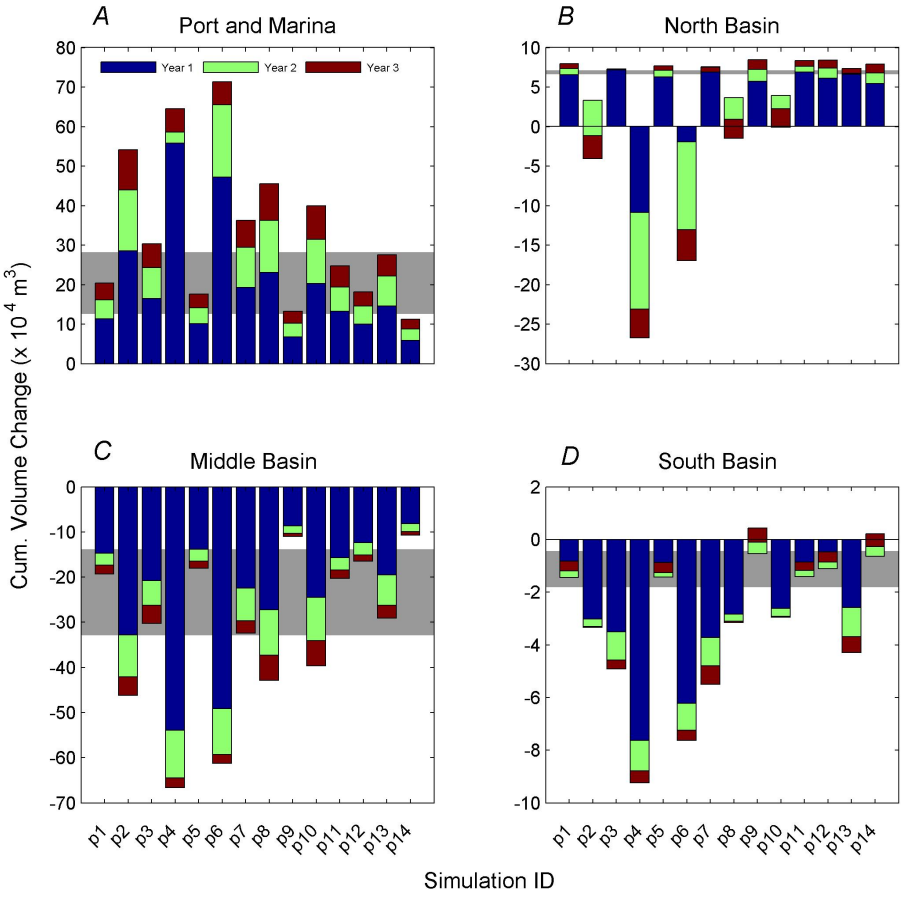

Figure 46. Cumulative volume change ($\times$ 10^4 m^3) after 3 years for the estuary alternative in simulations P1-P14 comparing various combination of low, medium, and high erodibility parameters. For each simulation the cumulative volume change is shown for *A*, Port and Marina, *B*, North Basin, *C*, Middle Basin, and *D*, South Basin. Refer to tables 2 and 3 for the values of each erodibility parameter used in the simulations.

Summary and Conclusions

Measurements were made to characterize sediment erodibility within Capitol Lake in Phase II of the hydrodynamic and sediment transport study. Fifteen cores were collected from the lake and analyzed using Sedflume. From each core, measurements of critical shear stress, erosion rates, grain size and dry sediment density were made at 5 depth intervals ranging from 0 to 35 cm in the sediment. The physical properties and erodibility of sediments in Capitol Lake varied both horizontally between cores and vertically with depth in a core. No clear spatial patterns in the erodibility data are evident in the field data.

The direct measurements of sediment erodibility were incorporated into a hydrodynamic and sediment transport model described in George and others (2006). The range of measured sediment erodibility parameters was greater than the range of values taken from the literature and used in Phase I. The most likely combination of erodibility parameters from field data was determined by using a Bayes Network. Long-term model simulations were carried out by using the most likely combination of erodibility parameters. In the long-term morphological simulations, morphological change that occurs after dam removal is not substantially different than was observed in Phase I model simulations. For both of the restoration alternatives investigated, sediment erodes from Middle Basin and deposits near the Port and Marina. The evolved bathymetry for both alternatives resembles that of the predam estuary. The volume of sediment that deposits in the Port and Marina areas in the Phase II long-term simulations is between the range of volumes given in Phase I for both restoration scenarios. Dredging Middle and North Basins prior to dam removal significantly reduces the amount of sediment that accumulates in the Port and Marina areas, especially during the first year.

Data collected in the field as a part of this study helped constrain the uncertainty associated with the erodibility of sediments in Capitol Lake. However, several other sources of uncertainty remain both in the model design and operation, as well as in the random nature of the forcing (for example, sediment delivery from the Deschutes River) that prevent certainty in the predictions presented herein.

Acknowledgments

The authors acknowledge George Tate from Sea Engineering, Inc., who helped collect the cores used in this study. Larry Kessel at General Administration facilitated use of the pontoon boat during the field data collection effort. This report was improved greatly by discussions with the Deschutes Estuary Feasibility Study Technical Committee, in particular the Tres Amigos: Curtis Tanner, Steven Morrison, and Nathaniel Jones. Nathaniel Plant (USGS) provided valuable insights into how to implement the Bayesian modeling approach. Funding for this work was provided by the State of Washington General Administration and the USGS Coastal and Marine Geology Program. An earlier version of this report was improved by thorough reviews by Chris Sherwood (USGS) and Bas Van Maren (Deltares). We thank our friends and colleagues for their support during this effort.

References

Amos, C.L., Feeny, T., Sutherland, T.F., and Luternauer, J.L, 1997, The stability of fine-grained sediments from the Fraser River delta: Estuarine, Coastal and Shelf Science, v. 45, p. 507-524.

Been, K., and Sills, G.C., 1981, Self-weight consolidation of soft soils; An experimental and theoretical study: Geotechnique, v. 31, p. 519-535.

Black, K.S., and Paterson, D.M., 1997, Measurement of erosion potential of cohesive marine sediments; A review of current in situ technology: Journal of Marine Environmental Engineering, v. 4, p. 43-83.

Blom, G., and Aalderink, R.H., 1998, Calibration of three resuspension/sedimentation models: Water Science and Technology, v. 37, p. 41-49.

Delft Hydraulics, 2006, Delft 3D Flow; Simulation of multi-dimensional hydrodynamic flows and transport phenomena, including sediments: User manual, version 3.13.

Eshleman, J., Ruggiero, P., Kingsley, E., Gelfenbaum, G., and George, D., 2006, Capitol Lake, Washington, 2004 data summary: U.S. Geological Survey Data Series 180, 35 p.

Finlayson, D.P., 2005, Combined bathymetry and topography of the Puget Lowland, Washington State: University of Washington, [http://www.ocean.washington.edu/data/pugetsound/, last accessed August 2008].

Flemming, B.W., and Delafontaine, M.T., 2000, Mass physical properties of muddy intertidal sediments; Some applications, misapplications and non-applications: Continental Shelf Research, v. 20, p. 1179-1197.

George, D.A., Gelfenbaum, G., Lesser, G., and Stevens, A.W., 2006, Deschutes estuary feasibility study; Hydrodynamics and sediment transport modeling: U.S. Geological Survey Open-File Report 2006-1318, 222 p.

Gust, G., and Müller, V., 1997, Interfacial hydrodynamics and entrainment function of currently used erosion devices; *in* Burt and others, eds., Cohesive sediments: Wiley, p. 149-174.

Hakanson, L., and Jansson, M., 2002, Principles of Lake sedimentology: Blackburn Press, 316 p.

Hill, P.S., 1998, Controls on floc size in the sea: Oceanography, v.11, p. 13-18.

Hjulstrom, F., 1939, Transportation of detritus by moving water, *in* Trask, P.D., ed., Recent marine sediments: American Association of Petroleum Geologists, p. 5-31.

Jepsen, R.A., 2006, Uncertainty in experimental techniques for measuring sediment erodibility: Integrated Environmental Assessment and Management, v. 2, p. 1-5.

Jepsen, R., Roberts, J., and Lick, W., 1997, Effects of bulk density on sediment erosion rates: Water, Air and Soil Pollution, v. 99, p. 21-31.

Jumars, P.A., and Nowell, A.R.M., 1984, Effects of benthos on sediment transport; Difficulties with functional grouping: Continental Shelf Research, v. 3, p. 115-130.

Lesser, G., Roelvink, J.A., Van Kester, J.A.T.M., Stelling, G.S., and Lakhan, V., 2004, Development and validation of a three-dimensional morphological model: Coastal Engineering, v. 51, p.883-915.

Lick, W., Chroneer, Z., Jones, C., and Jepsen, R., 1997, A predictive model of sediment transport: Estuarine and Coastal Modeling, v. 5, p. 389-399.

Maa, J.P.-Y., Wright, L.D., Lee, C.-H., and Shannon, T.W., 1993, VIMS sea carousel; a field instrument for studying sediment transport: Marine Geology, v. 115, p. 271-287.

McNeil, J., Taylor, C., and Lick, W., 1996, Measurements of erosion of undisturbed bottom sediments with depth: Journal of Hydraulic Engineering, v. 122, p. 316-324.

Mih, W., and Orsborn, J., 1974, Sediment removal and maintenance system for the upper basin of Capitol Lake Olympia, Washington—Preliminary Report; Pullman, Washington State University, 33 p.

Moffatt and Nichol, 2007, Capitol Lake alternatives analysis; Estuary dredging plan: Technical Memorandum, 8 p.

Partheniades, E., 1965, Erosion and deposition of cohesive soils: Journal of the Hydraulics Division, American Society of Civil Engineers, v. 91, p. 105–138.

Postma, H., 1967, Sediment transport and sedimentation in the estuarine environment, *in* Lauff, G.H., ed., Estuaries: American Association for the Advancement of Science, p. 158-179.

Roberts, J., Jepson, R., Gotthard, D., and Lick, W., 1998, Effects of particle size and bulk density on erosion of quartz particles: Journal of Hydraulic Engineering, v. 124, p. 1261-1267.

Roberts, J., and Jepsen, R., 2001, Development for the optical use of circular core tubes with the high shear stress flume: Sandia National Labs, SAND2001-0424.

Roelvink, J.A., 2006, Coastal morphodynamic evolution techniques: Coastal Engineering, v. 53, p. 277-287.

Sanford, L.P., and Maa, P.-Y., 2001, A unified erosion formulation for fine sediments: Marine Geology, v. 179, p. 9-23.

Spiegelhalter, D.J., Dawid, A.P., Lauritzen, S.L, and Cowell, R.G., 1993, Bayesian analysis in expert systems: Statistical Science, v. 8, p. 219-293.

Stevens, A.W., Wheatcroft, R.A., and Wiberg, P.L., 2007, Seabed properties and sediment erodibility along the western Adriatic margin, Italy: Continental Shelf Research, v. 27, p. 400-416.

Tolhurst, T.J., Black, K.S., Paterson, D.M., Mitchener, H.J., Termaat, G.R., and Shayler, S.A., 2000, A comparison and measurement standardization of four in situ devices for measuring the erosion shear stress of intertidal sediments: Continental Shelf Research, v. 20, p. 1397-1418.

van Ledden, M., van Kesteren, W.G.M., and Winterwerp, J.C., 2004, A conceptual framework for the erosion behaviour of sand-mud mixtures: Continental Shelf Research, v. 24, p. 1-11.

van Rijn, L., 1993, Principles of sediment transport in rivers, estuaries and coastal seas: Aqua Publications, 715 p.

Widdows, J., Friend, P.L., Bale, A.J., Brinsley, M.D., Pope, N.D., and Thomsen, C.E.L., 2007, Inter-comparison between five devices for determining erodibility of intertidal sediments: Continental Shelf Research, v. 27, p. 1174-1189.

Appendix A. Sediment Properties and Erodibility Parameters from Sedflume Analysis

Appendix A provides the sediment properties and erodibility parameters measured with Sedflume on cores collected from Capitol Lake. For each core, five erosion cycles were performed. For each erosion cycle, the depth interval, dry sediment density, mean grain size, percent sand, percent silt, critical shear stress, and the erosion rate parameter are provided (table A1). Figures A1 through A15 show the location of each core and down-core profiles of mean grain size, dry sediment density, critical shear stress and erosion rate parameter.

Table A1. List of sediment properties and erodibility parameters for each core analyzed with Sedflume. See Table 1 for locations of cores.

Core ID	Cycle	Start depth (mm)	End depth (mm)	Dry sediment density (kg m^{-3})	Mean grain size (μm)	Sand (%)	Silt (%)	Clay (%)	Critical shear stress (Pa)	Erosion coefficient (kg m^{-2} s^{-1})
HP1	1	0	55	257.8	18.0	15.6	79.4	5.0	0.12	0.011005
HP1	2	55	101	274.7	15.5	11.1	84.0	4.8	0.64	0.040288
HP1	3	101	157	301.1	14.7	8.5	85.6	5.8	0.48	0.014144
HP1	4	159	194	406.7	15.1	10.2	84.1	5.7	0.52	0.004440
HP1	5	200	237	455.3	14.6	13.3	79.8	6.8	0.84	0.009226
HP2	1	0	59	388.6	19.1	22.7	72.0	5.4	0.48	0.000990
HP2	2	59	135	490.1	27.7	26.2	69.8	3.9	0.21	0.000977
HP2	3	148	196	1315.6	578.5	88.7	9.9	1.4	0.24	0.121787
HP2	4	198	231	1192.6	42.6	44.6	50.0	5.4	0.22	0.001116
HP2	5	251	301	805.7	34.2	43.1	48.5	8.4	0.22	0.000598
HP3	1	0	43	253.1	20.0	19.5	74.7	5.8	1.04	0.001567
HP3	2	56	110	309.7	21.1	15.3	81.1	3.6	0.21	0.000364
HP3	3	115	143	415.7	16.8	10.9	83.1	5.9	0.24	0.000286
HP3	4	149	218	393.1	14.9	11.4	82.6	6.1	1.61	0.000000
HP3	5	223	289	365.2	15.8	10.5	84.5	5.0	0.72	0.023376
HP4	1	0	55	1034.1	207.5	60.4	36.7	2.9	0.41	0.231078
HP4	2	56	106	1297.5	367.4	96.3	3.2	0.5	0.23	0.189905
HP4	3	106	165	927.7	109.9	67.7	30.1	2.2	0.21	0.009577
HP4	4	166	216	549.5	40.0	38.3	57.9	3.7	0.12	0.000122
HP4	5	270	305	1304.5	254.4	98.6	1.2	0.2	0.21	0.092401
HP5	1	0	48	554.8	33.7	40.4	55.4	4.2	0.23	0.066409
HP5	2	51	90	1263.0	451.2	91.1	7.8	1.2	0.16	0.137435
HP5	3	90	128	1374.7	419.9	93.0	6.1	1.0	0.20	0.135414
HP5	4	130	219	719.2	150.3	72.3	25.4	2.2	0.22	0.005010
HP5	5	219	260	640.3	20.1	12.2	82.3	5.5	0.26	0.000566
HP6	1	0	45	273.3	19.3	15.3	79.9	4.8	0.26	0.008570
HP6	2	45	105	435.1	22.7	18.7	76.9	4.4	0.26	0.048483
HP6	3	105	158	577.5	39.9	36.9	59.4	3.7	0.52	0.013941
HP6	4	158	201	434.4	18.6	15.7	79.6	4.8	0.64	0.012996
HP6	5	202	255	448.8	21.0	14.9	80.5	4.7	1.28	0.002993
HP7	1	0	60	296.5	23.5	17.6	78.9	3.4	0.16	0.000435
HP7	2	60	117	435.0	20.3	18.1	77.6	4.2	0.43	0.002261
HP7	3	117	162	594.3	27.9	22.2	73.9	3.9	0.48	0.002691
HP7	4	162	219	476.3	24.4	19.9	75.9	4.2	0.52	0.005201
HP7	5	219	279	672.6	41.3	36.6	59.5	3.9	0.22	0.001224

Table A1. List of sediment properties and erodibility parameters for each core analyzed with Sedflume—Continued.

Core ID	Cycle	Start depth (mm)	End depth (mm)	Dry sediment density (kg m^{-3})	Mean grain size (μm)	Sand (%)	Silt (%)	Clay (%)	Critical shear stress (Pa)	Erosion coefficient (kg m^{-2} s^{-1})
HP8	1	0	52	224.7	24.0	21.1	75.0	4.0	0.16	0.003118
HP8	2	52	101	554.1	35.4	33.5	63.2	3.3	0.45	0.018246
HP8	3	104	150	617.8	28.7	32.5	63.4	4.1	0.64	0.005456
HP8	4	150	185	668.2	35.4	50.0	46.9	3.2	1.28	0.004456
HP8	5	195	255	770.6	40.9	38.2	58.3	3.5	1.04	0.004772
HP9	1	0	51	355.2	25.3	25.7	70.6	3.7	0.13	0.003883
HP9	2	52	98	644.7	35.0	36.2	60.3	3.5	0.46	0.050786
HP9	3	103	152	674.2	34.4	36.6	59.5	3.9	1.04	0.004175
HP9	4	153	200	836.8	44.4	40.8	56.0	3.2	0.92	0.007549
HP9	5	239	270	759.5	73.5	54.7	41.8	3.5	0.26	0.040061
LP4	1	0	53	248.8	19.0	12.3	83.3	4.4	0.13	0.003136
LP4	2	53	109	355.2	20.8	12.9	83.2	3.9	0.32	0.016085
LP4	3	110	151	411.0	22.0	15.1	80.9	4.0	0.46	0.008429
LP4	4	151	202	566.5	27.2	21.8	73.7	4.5	0.64	0.003777
LP4	5	207	251	608.3	32.5	28.4	67.5	4.1	0.64	0.003399
LP5	1	0	50	443.7	20.4	14.4	81.7	3.9	0.24	0.004297
LP5	2	66	118	440.8	23.9	20.3	75.3	4.5	0.45	0.000699
LP5	3	149	210	612.1	26.6	19.2	76.3	4.4	0.22	0.001357
LP5	4	216	267	686.0	30.3	23.6	71.5	4.9	0.43	0.012686
LP5	5	275	331	686.0	30.3	27.6	67.6	4.8	0.43	0.005169
MP1	1	0	50	516.7	89.5	55.9	40.2	3.9	0.16	0.001749
MP1	2	51	109	858.5	62.3	49.7	46.7	3.6	1.84	0.000000
MP1	3	111	157	672.5	46.3	43.7	53.4	2.9	0.22	0.061672
MP1	4	157	206	875.8	68.4	50.9	46.4	2.7	0.24	0.001088
MP1	5	209	262	955.3	100.8	56.0	40.3	3.8	0.48	0.002433
MP2	1	0	50	290.6	13.8	16.2	76.6	7.2	0.16	0.001019
MP2	2	50	97	402.5	21.9	20.1	75.5	4.4	0.64	0.002684
MP2	3	100	160	323.2	18.5	17.8	77.4	4.8	0.24	0.001932
MP2	4	170	210	510.7	23.8	24.1	71.8	4.2	0.87	0.007076
MP2	5	210	246	463.8	22.5	22.4	73.0	4.6	1.28	0.003093
MP3	1	0	53	346.6	20.7	15.0	80.3	4.6	0.23	0.008272
MP3	2	65	96	1097.4	140.6	63.7	33.9	2.4	0.21	0.163460
MP3	3	98	130	1000.5	93.0	59.1	38.4	2.5	0.26	0.000778
MP3	4	149	210	408.7	21.9	18.4	77.6	4.1	0.52	0.003540
MP3	5	213	277	560.1	24.5	20.9	74.6	4.5	0.85	0.009522
MP4	1	0	52	328.7	16.2	13.0	81.4	5.6	0.06	0.001224
MP4	2	52	103	409.0	20.1	19.7	75.8	4.5	0.48	0.018239
MP4	3	104	155	574.6	53.3	56.1	40.8	3.1	0.52	0.033071
MP4	4	155	205	504.6	24.6	24.7	71.2	4.0	0.64	0.006638
MP4	5	208	254	764.8	44.6	42.2	54.3	3.6	0.44	0.002145

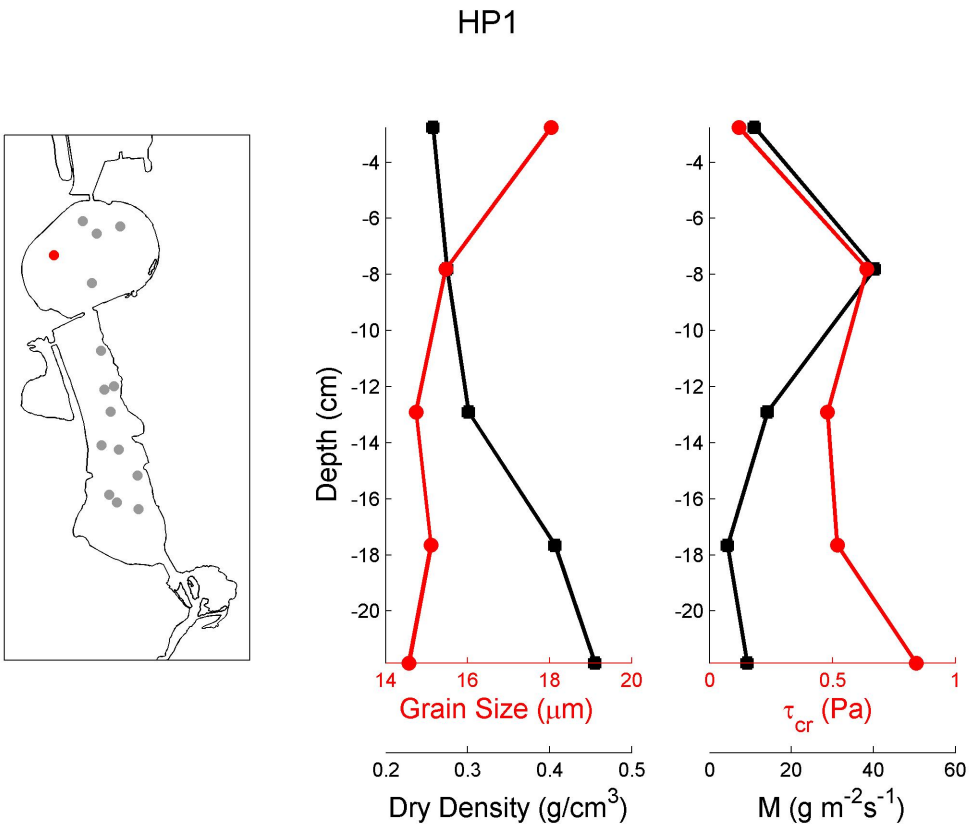

Figure A1. Data for core HP1 from Sedflume analysis showing the core location (red dot, left panel), mean grain size and dry sediment density (middle panel), and critical shear stress and erosion rate parameter (right panel).

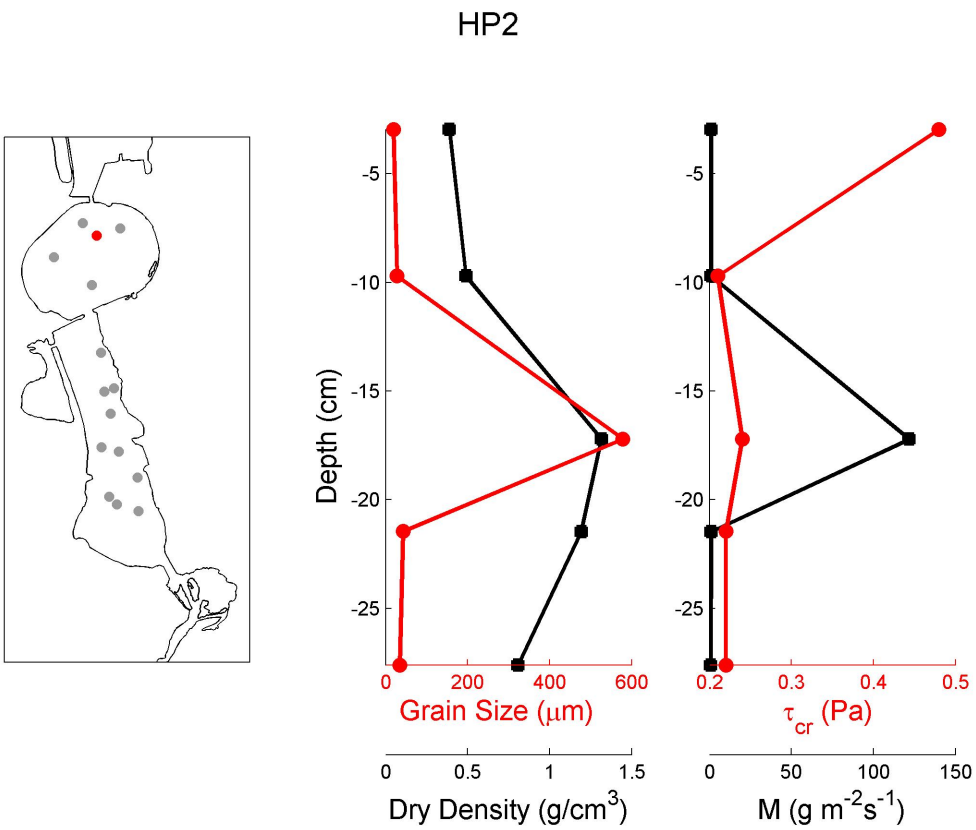

Figure A2. Data for core HP2 from Sedflume analysis showing the core location (red dot, left panel), mean grain size and dry sediment density (middle panel), and critical shear stress and erosion rate parameter (right panel).

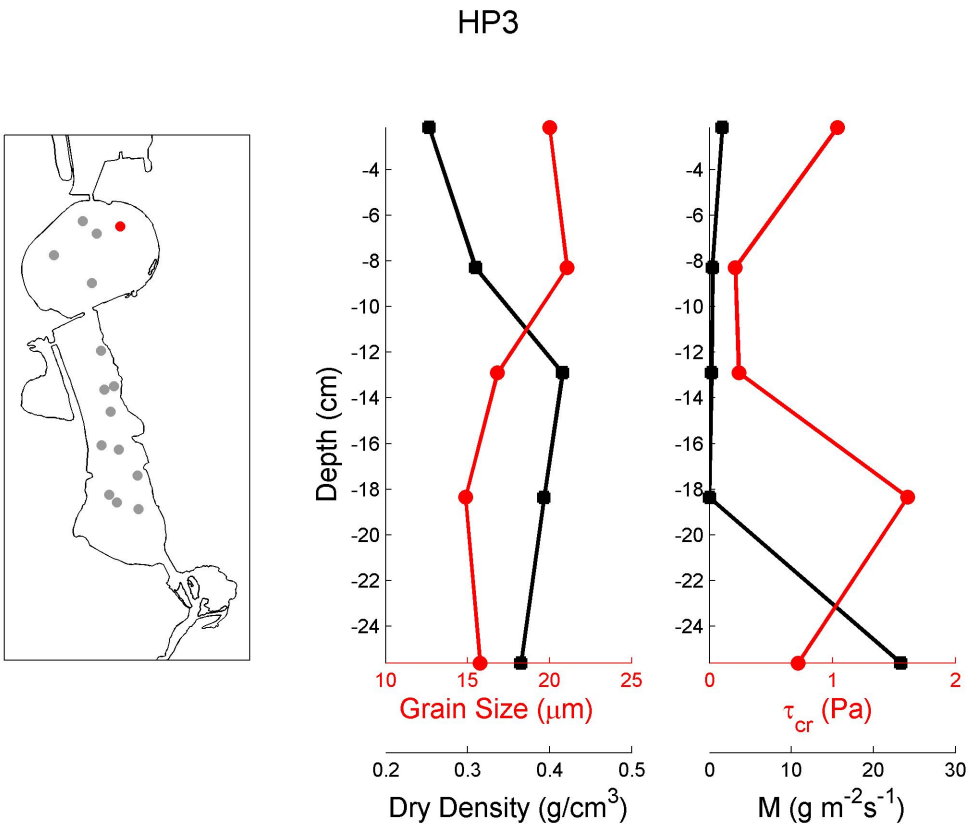

Figure A3. Data for core HP3 from Sedflume analysis showing the core location (red dot, left panel), mean grain size and dry sediment density (middle panel), and critical shear stress and erosion rate parameter (right panel).

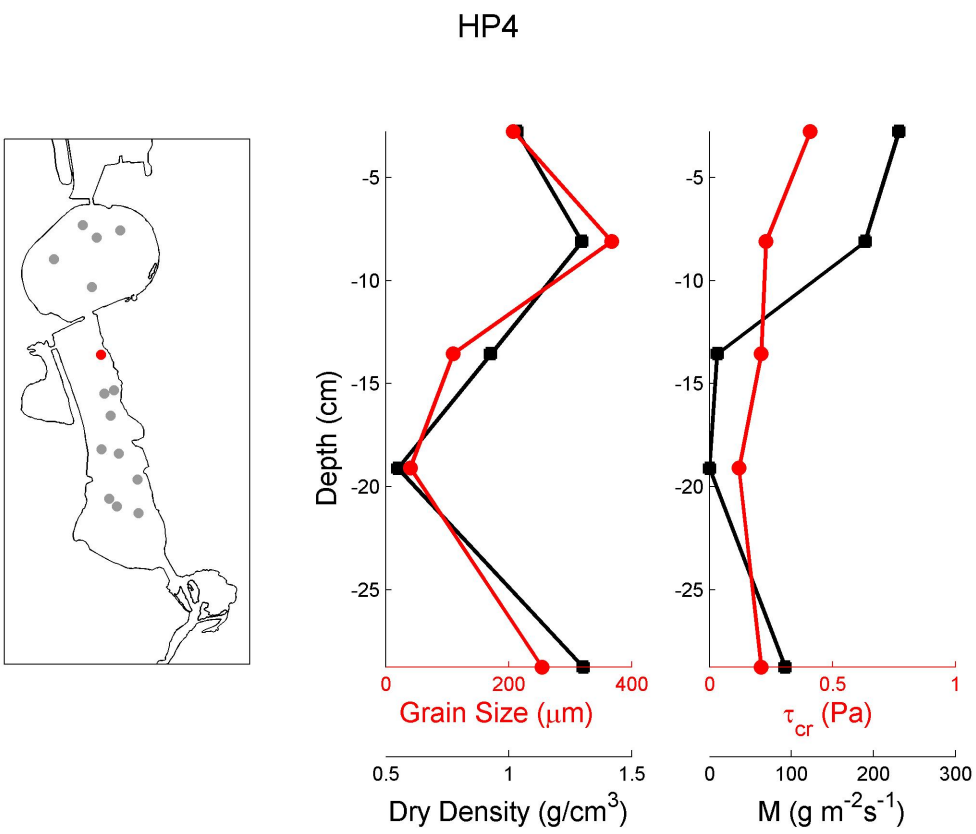

Figure A4. Data for core HP4 from Sedflume analysis showing the core location (red dot, left panel), mean grain size and dry sediment density (middle panel), and critical shear stress and erosion rate parameter (right panel).

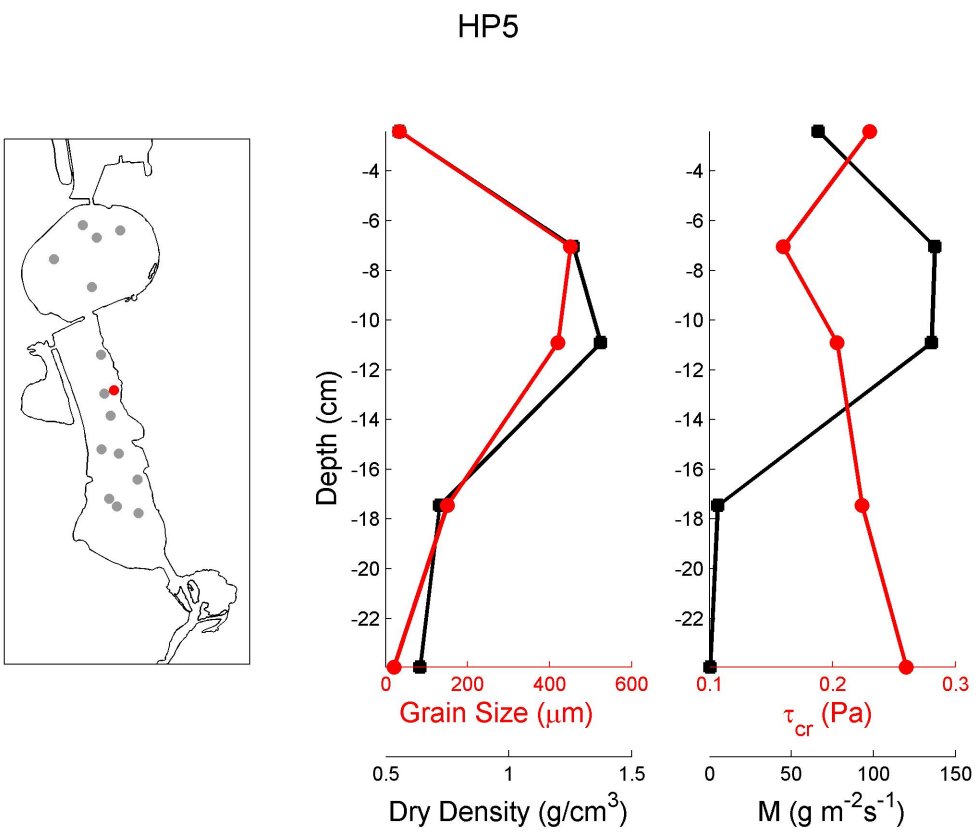

Figure A5. Data for core HP5 from Sedflume analysis showing the core location (red dot, left panel), mean grain size and dry sediment density (middle panel), and critical shear stress and erosion rate parameter (right panel).

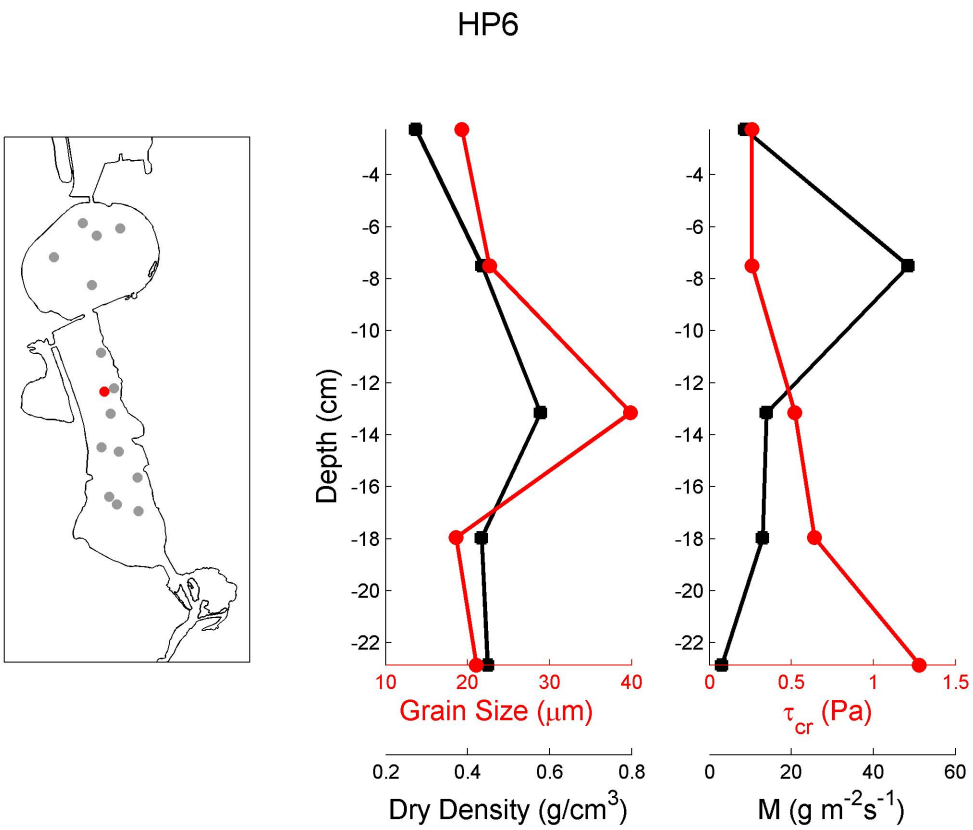

Figure A6. Data for core HP6 from Sedflume analysis showing the core location (red dot, left panel), mean grain size and dry sediment density (middle panel), and critical shear stress and erosion rate parameter (right panel).

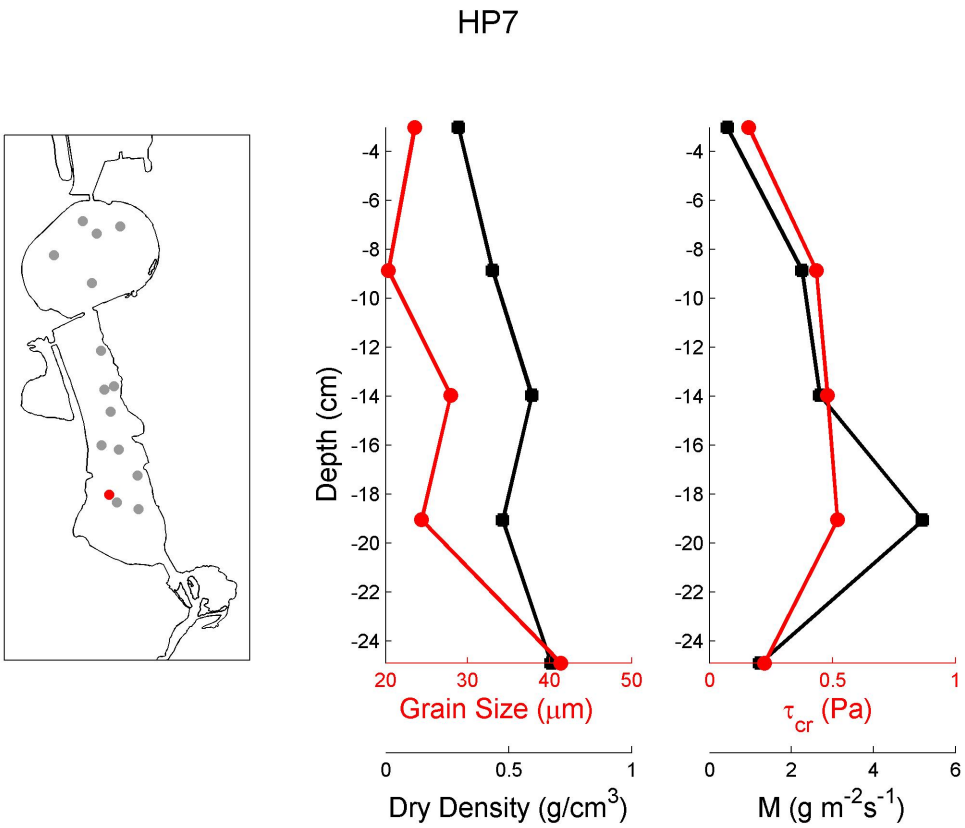

Figure A7. Data for core HP7 from Sedflume analysis showing the core location (red dot, left panel), mean grain size and dry sediment density (middle panel), and critical shear stress and erosion rate parameter (right panel).

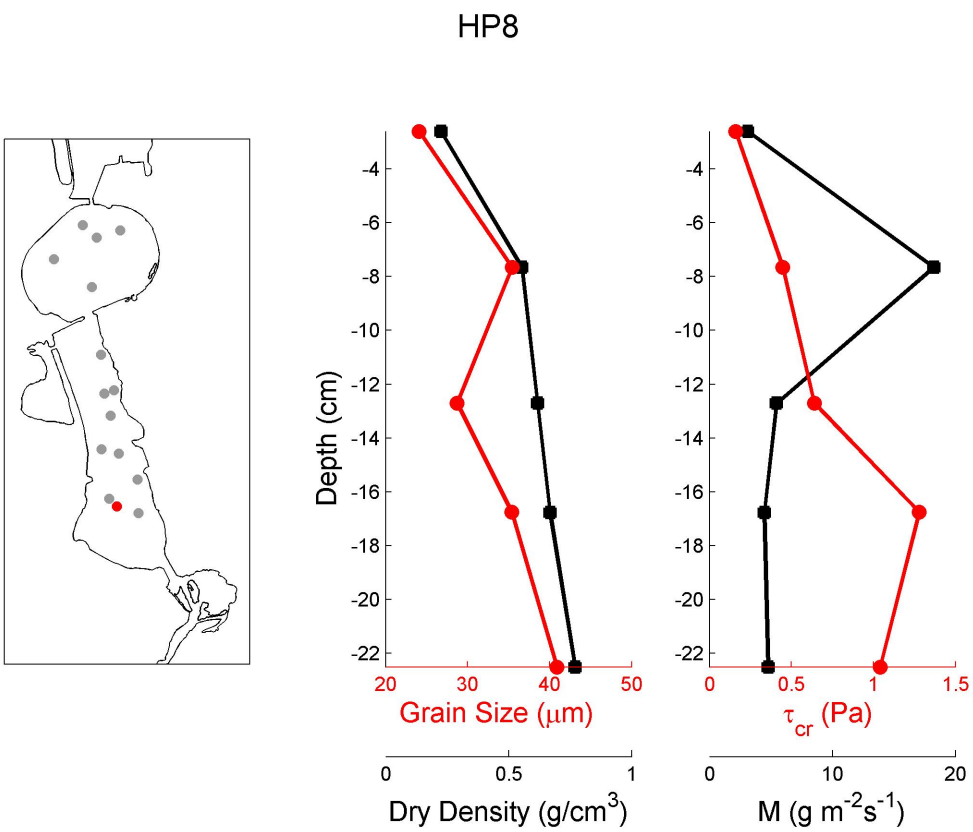

Figure A8. Data for core HP8 from Sedflume analysis showing the core location (red dot, left panel), mean grain size and dry sediment density (middle panel), and critical shear stress and erosion rate parameter (right panel).

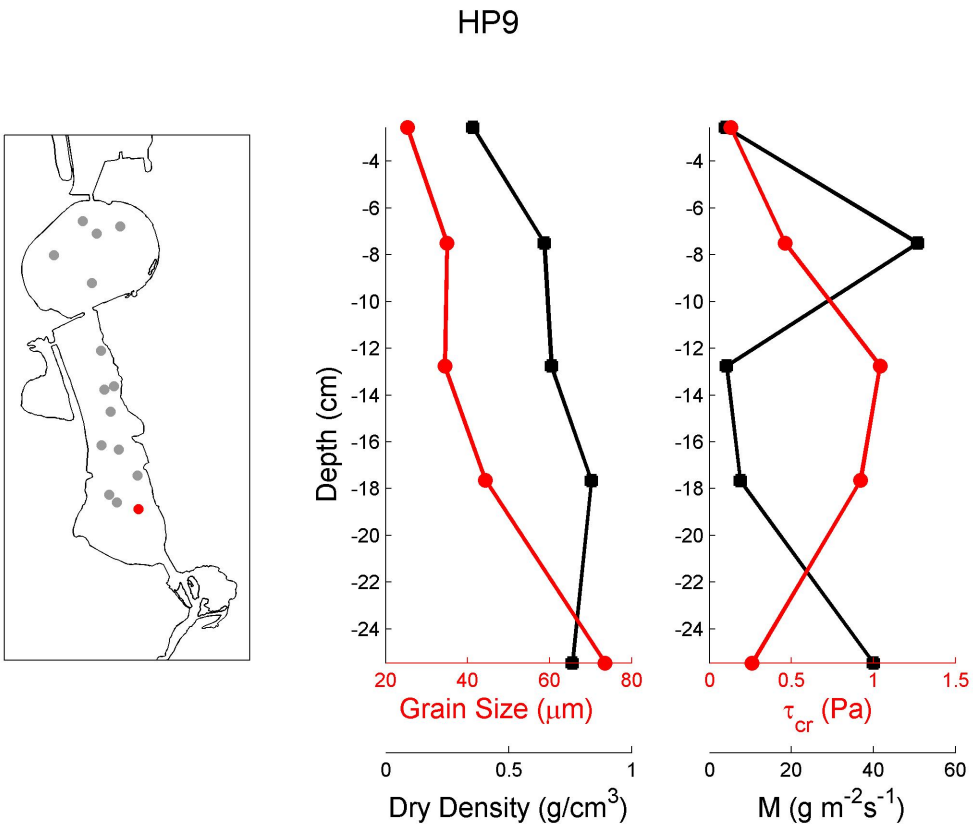

Figure A9. Data for core HP9 from Sedflume analysis showing the core location (red dot, left panel), mean grain size and dry sediment density (middle panel), and critical shear stress and erosion rate parameter (right panel).

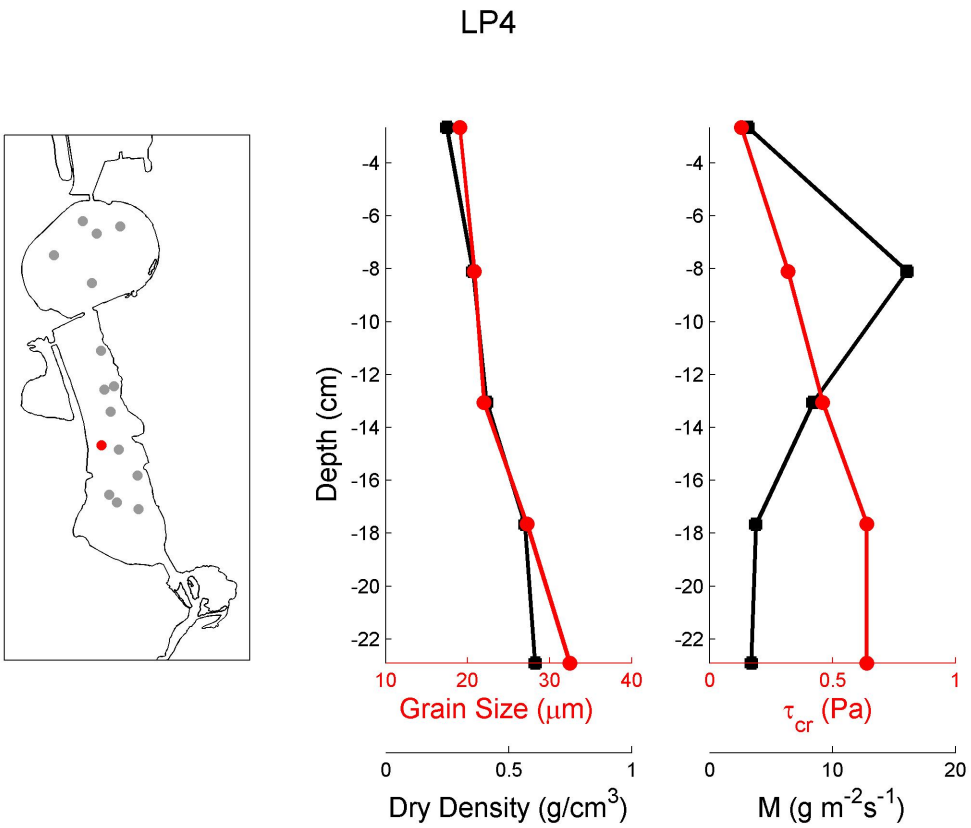

Figure A10. Data for core LP4 from Sedflume analysis showing the core location (red dot, left panel), mean grain size and dry sediment density (middle panel), and critical shear stress and erosion rate parameter (right panel).

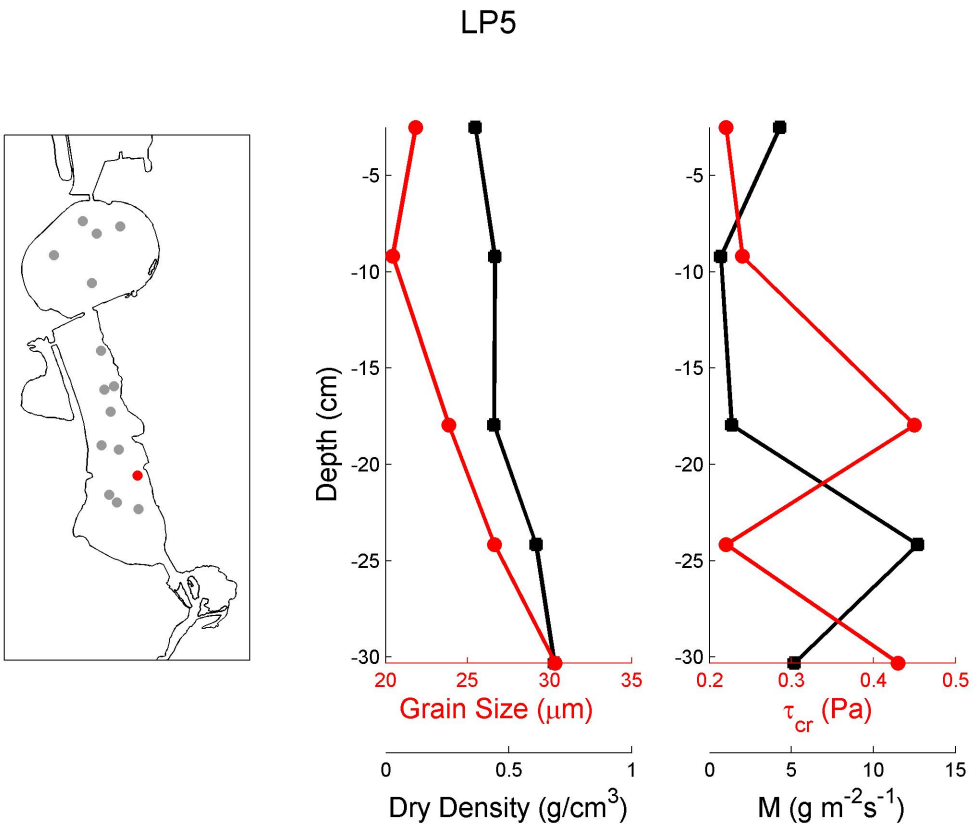

Figure A11. Data for core LP5 from Sedflume analysis showing the core location (red dot, left panel), mean grain size and dry sediment density (middle panel), and critical shear stress and erosion rate parameter (right panel).

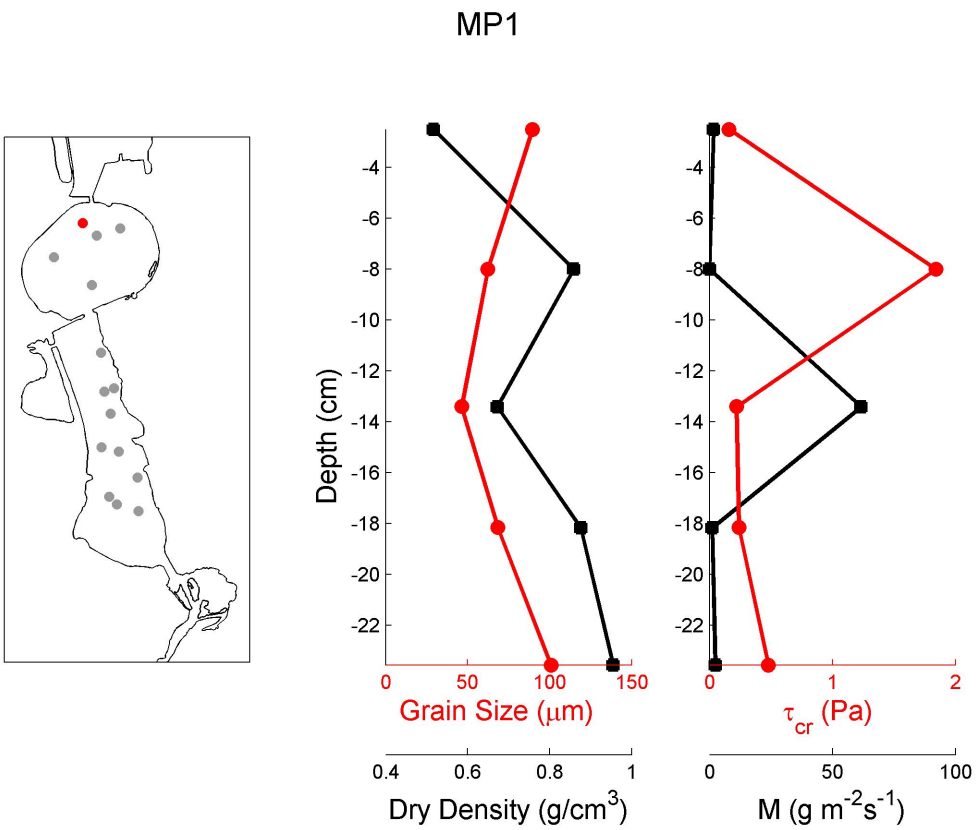

Figure A12. Data for core MP1 from Sedflume analysis showing the core location (red dot, left panel), mean grain size and dry sediment density (middle panel), and critical shear stress and erosion rate parameter (right panel).

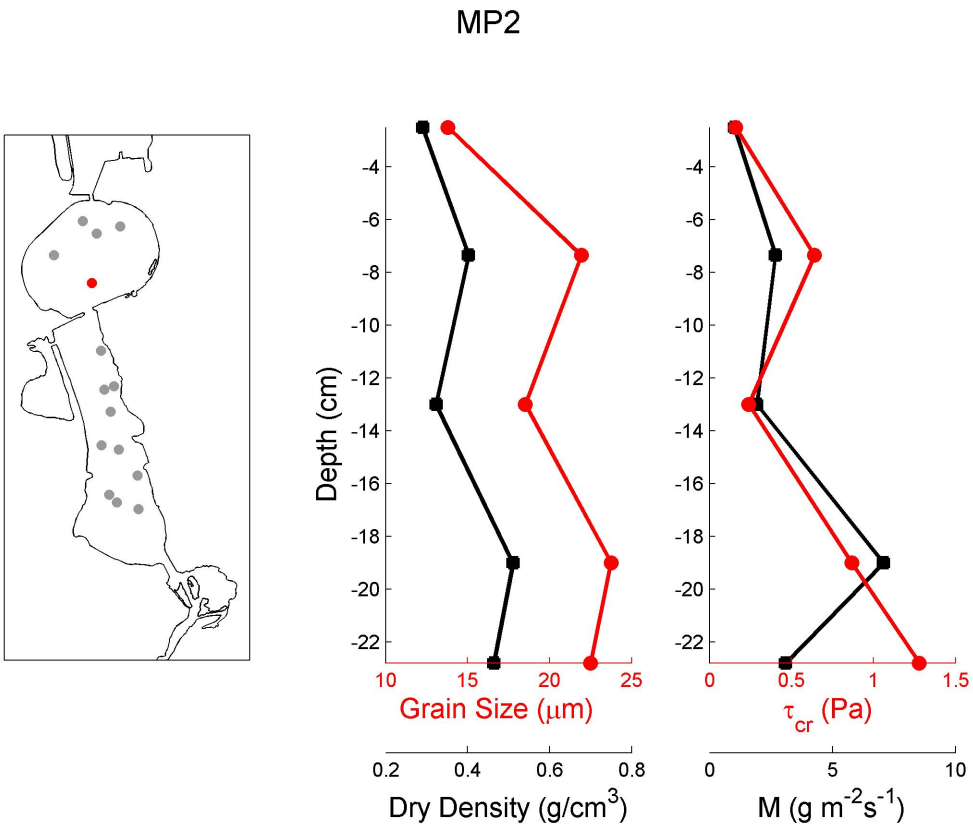

Figure A13. Data for core MP2 from Sedflume analysis showing the core location (red dot, left panel), mean grain size and dry sediment density (middle panel), and critical shear stress and erosion rate parameter (right panel).

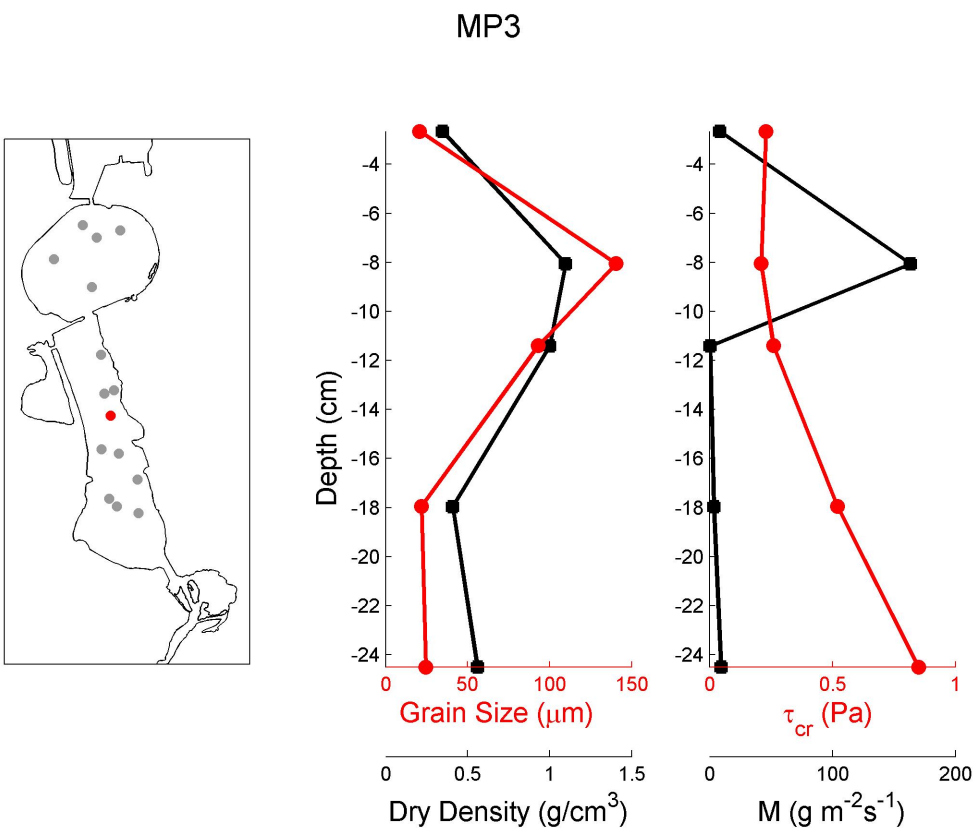

Figure A14. Data for core MP3 from Sedflume analysis showing the core location (red dot, left panel), mean grain size and dry sediment density (middle panel), and critical shear stress and erosion rate parameter (right panel).

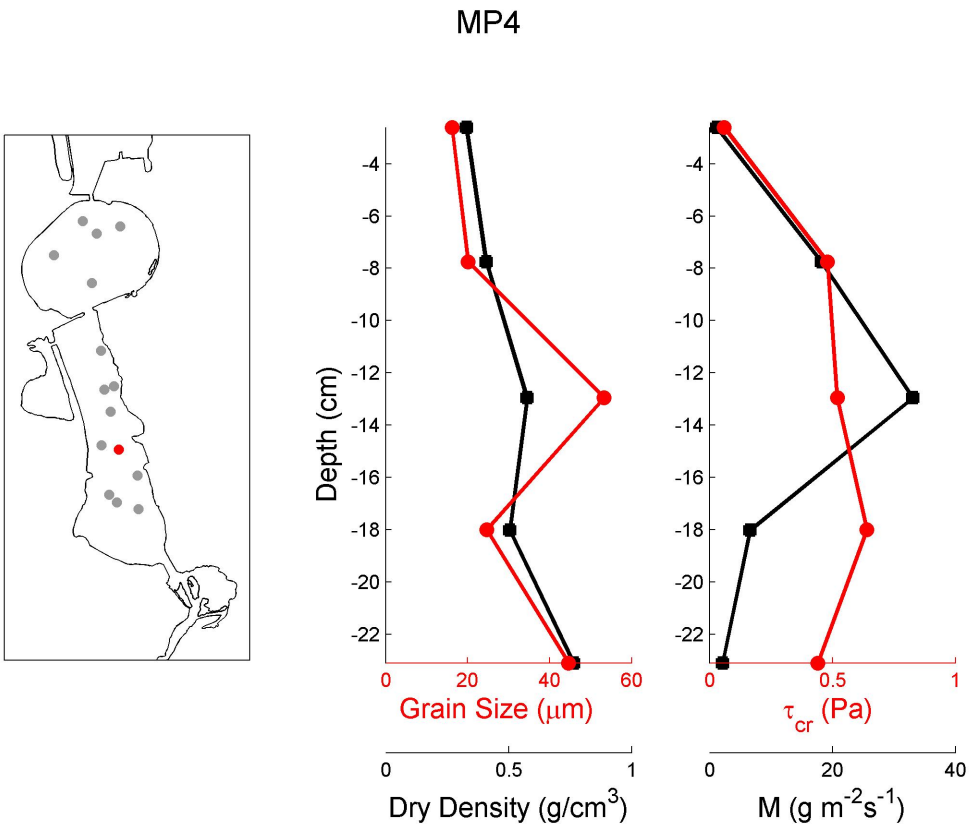

Figure A15. Data for core MP4 from Sedflume analysis showing the core location (red dot, left panel), mean grain size and dry sediment density (middle panel), and critical shear stress and erosion rate parameter (right panel).

Appendix B. Grain-size Data from Samples Collected in Lower Budd Inlet

Appendix B provides grain-size data from grab samples collected in lower Budd Inlet. Grain-size distributions were determined by using standard techniques in the U.S. Geological Survey Coastal and Marine Geology lab. Samples were sieved to separate coarser particles from the silt and clay. The coarse fraction (>2 mm) was separated, and gravel fractions were determined with sieves. The sand fractions (2–63 μm) were quantified by using a 2-m settling tube, and fine fractions (<63 μm) were quantified by using a Beckman Coulter Model LS230 laser-diffraction particle analyzer. Figure B1 shows the location of the samples in lower Budd Inlet, and figures B2 and B3 show the particle-size distribution for each sample.

Table B1. List of sample identification numbers, locations, date collected, percent gravel (>2 mm), percent sand (63 μm-2 mm), percent silt (4 μm-63 μm), percent clay (< 4 μm), and mean grain size for each grab sample collected from lower Budd Inlet.

Sample ID	Longitude, degrees west	Latitude, degrees north	Collection date and time	Gravel, percent	Sand, percent	Silt, percent	Clay, percent	Mean grain size, millimeters
B10	122.9076	47.0476	01-Nov-2007 13:52:23	0.1	88.1	7.1	4.7	0.1412
B11	122.9110	47.0490	01-Nov-2007 13:57:03	0.0	41.4	39.8	18.9	0.0313
B12	122.9096	47.0489	01-Nov-2007 14:00:39	0.0	68.2	23.1	8.7	0.0536
B13	122.9085	47.0490	01-Nov-2007 14:04:43	0.0	69.5	21.5	9.0	0.0609
B14	122.9075	47.0489	01-Nov-2007 14:08:41	0.0	41.4	40.5	18.0	0.0248
B15	122.9067	47.0489	01-Nov-2007 14:12:51	0.0	17.6	54.4	28.0	0.0108
B16	122.9056	47.0490	01-Nov-2007 14:16:49	0.0	11.9	56.2	31.9	0.0086
B17	122.9113	47.0502	01-Nov-2007 14:23:10	0.0	18.5	59.1	22.4	0.0144
B18	122.9099	47.0504	01-Nov-2007 14:28:00	0.0	31.2	52.5	16.3	0.0221
B20	122.9075	47.0503	01-Nov-2007 14:37:10	0.0	44.0	40.3	15.8	0.0285
B21	122.9060	47.0502	01-Nov-2007 14:44:10	0.0	12.6	56.4	31.0	0.0089
B3	122.9103	47.0463	01-Nov-2007 13:21:41	0.0	34.5	48.5	17.0	0.0227
B4	122.9095	47.0463	01-Nov-2007 13:26:34	0.1	92.3	5.2	2.5	0.2215
B5	122.9083	47.0463	01-Nov-2007 13:30:56	2.2	66.4	19.4	12.0	0.0999
B6	122.9106	47.0475	01-Nov-2007 13:38:17	0.0	42.5	44.0	13.5	0.0305
B7	122.9095	47.0475	01-Nov-2007 13:42:25	0.0	88.7	7.1	4.2	0.1383
B8	122.9088	47.0475	01-Nov-2007 13:45:24	0.0	56.1	29.1	14.8	0.0428
B9	122.9084	47.0475	01-Nov-2007 13:49:07	0.0	89.0	7.4	3.7	0.1584

Figure B1. Locations of grab samples collected from lower Budd Inlet. The red box in the left panel shows the extent of the map in the right panel. Map projection is Universal Transverse Mercator (UTM), zone 10, kilometers.

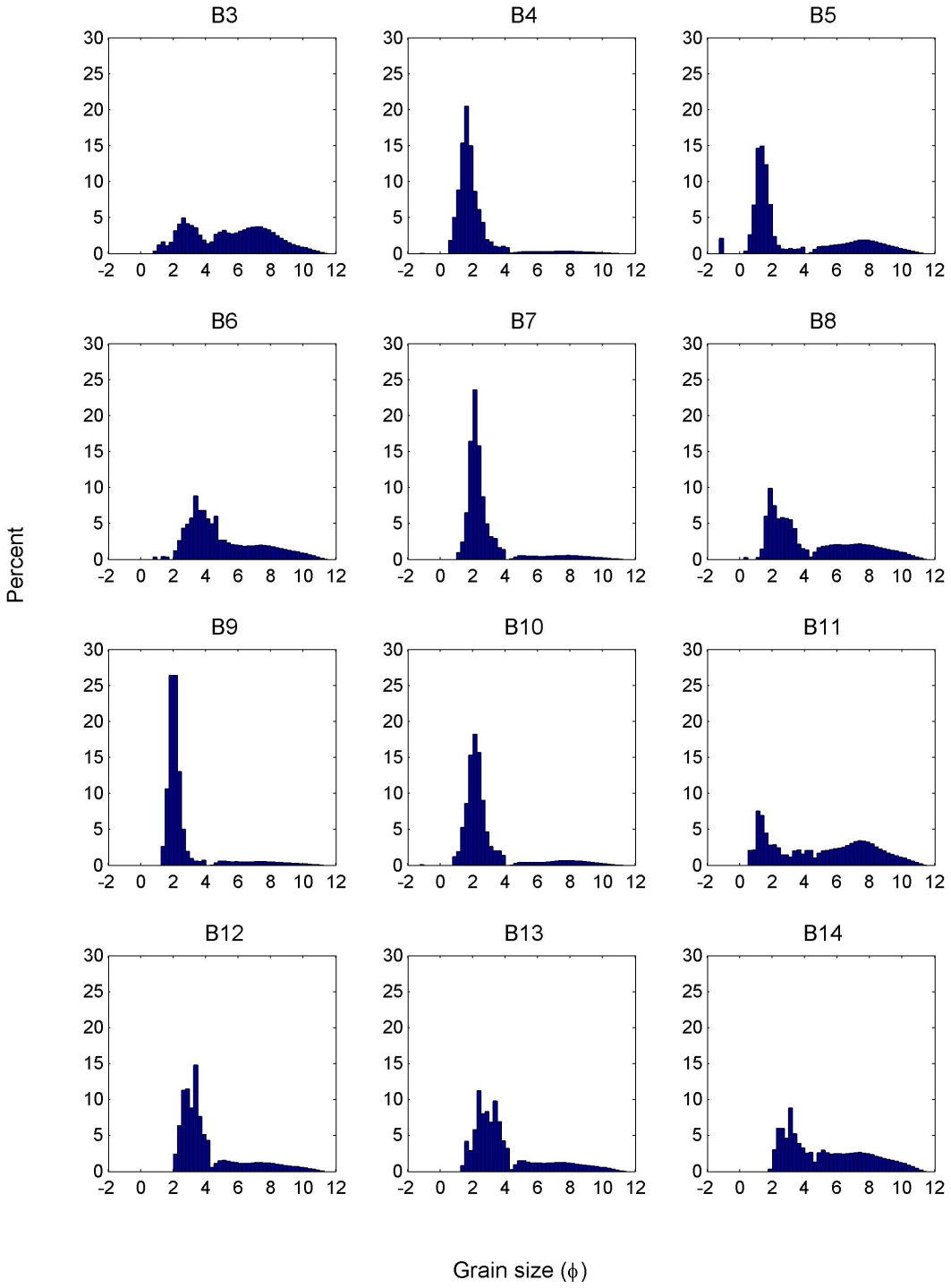

Figure B2. Sediment grain-size distribution (weight percent) for samples B1-B14 from lower Budd Inlet. The grain size is given in phi units. Phi units are related to mm by, $mm = 2^{-phi}$. See table B1 for locations of samples.

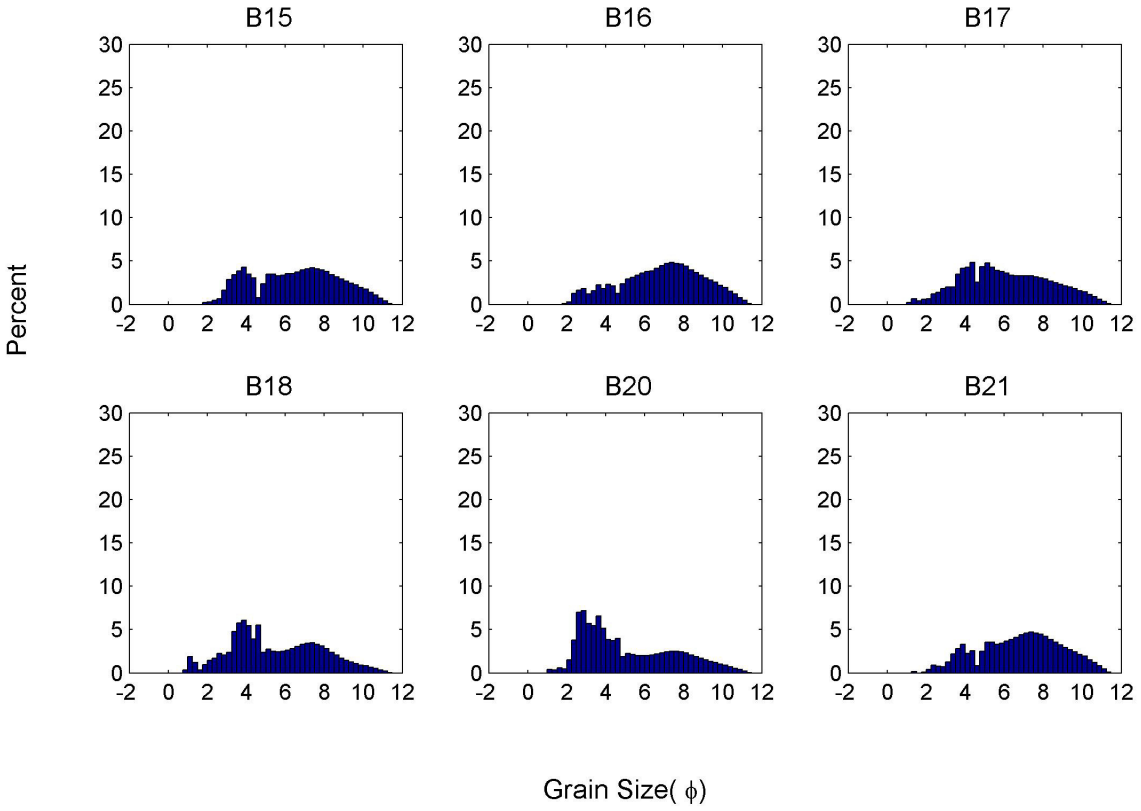

Figure B3. Sediment grain-size distribution (weight percent) for samples B15 through B21 from lower Budd Inlet. The grain size is given in phi units. Phi units are related to mm by, $mm = 2^{-phi}$. See table B1 for locations of samples.